Freeze Casting: From Low-Dimensional Building Blocks to Aligned Porous Structures-A Review of Novel Materials, Methods, and Applications

Gaofeng Shao, Dorian Hanaor, Xiaodong Shen, Aleksander Gurlo

ADVANCED MATERIALS
www.advmat.de

Freeze Casting: From Low-Dimensional Building Blocks to Aligned Porous Structures—A Review of Novel Materials, Methods, and Applications

Gaofeng Shao, Dorian A. H. Hanaor, Xiaodong Shen, and Aleksander Gurlo*

Freeze casting, also known as ice templating, is a particularly versatile technique that has been applied extensively for the fabrication of well-controlled biomimetic porous materials based on ceramics, metals, polymers, biomacromolecules, and carbon nanomaterials, endowing them with novel properties and broadening their applicability. The principles of different directional freeze-casting processes are described and the relationships between processing and structure are examined. Recent progress in freeze-casting assisted assembly of low dimensional building blocks, including graphene and carbon nanotubes, into tailored micro- and macrostructures is then summarized. Emerging trends relating to novel materials as building blocks and novel freeze-cast geometries—beads, fibers, films, complex macrostructures, and nacre-mimetic composites—are presented. Thereafter, the means by which aligned porous structures and nacre mimetic materials obtainable through recently developed freeze-casting techniques and low-dimensional building blocks can facilitate material functionality across multiple fields of application, including energy storage and conversion, environmental remediation, thermal management, and smart materials, are discussed.

1. Introduction

The presence of anisotropic structures across multiple scales is one of the distinctive features of biological systems. The synthesis of bioinspired materials mimicking such structures has emerged as a valuable approach for the fabrication of high-performance structural and functional materials in diverse application fields. The fabrication of bioinspired structures with biomimetic features across multiple length-scales can be realized using a variety of techniques that have been established over recent decades. These techniques, which include additive manufacturing, laser etching and electrospinning, have established the feasibility of realizing structured materials comprising nano- and microscale features. Advances in tomographic techniques, predominantly micro-CT, have provided valuable new insights into the multiscale structures of porous natural materials and have facilitated the establishment of structure–property relationships necessary for porous materials design.

As a means towards the realization of synthetic bioinspired porous materials, freeze casting, known also as ice-templating, is a particularly versatile technique, which has been applied extensively in recent years for the fabrication of well-controlled porous materials based on ceramics, metals, polymers, biomacromolecules, and carbon materials, endowing them with novel properties and broadening their applicability. As in natural systems, the cellular templating resulting from freeze casting processes can endow structures with distinct physico/mechanical attributes. Consequently, freeze casting is a logical route toward the design of synthetic materials inspired by nature. By altering parameters of freeze casting processes, the morphology of obtained structures can be tailored, drawing inspiration from functional biological systems that have emerged in the plant and animal kingdoms.

Freeze casting gained much attention in the early 2000s as a processing route for polymer and ceramic biomaterials with aligned pores, as well as hybrid organic–inorganic composites.[1] In the following decade, the number and diversity of potential applications for these materials grew considerably. In parallel, the use of carbon materials for biological applications emerged as a promising approach, in particular the use of carbon nanotube scaffolds.[2] The diverse applications of porous nanomaterials have also driven the rapid development of freeze cast scaffolds based on graphene and biomacromolecules in recent years. In addition to the diversification of the building blocks used to produce freeze cast scaffolds, much attention has been paid to the variation of the micro- and macrostructures through the control of freeze casting processes as well as the combination of freeze casting with other

Prof. G. Shao
School of Chemistry and Materials Science
Nanjing University of Information Science & Technology
Nanjing 210044, China
Prof. G. Shao, Dr. D. A. H. Hanaor, Prof. A. Gurlo
Fachgebiet Keramische Werkstoffe/Chair of Advanced Ceramic Materials
Technische Universität Berlin
Hardenbergstr. 40, Berlin 10623, Germany
E-mail: Dorian.hanaor@ceramics.tu-berlin.de
Prof. X. Shen
College of Materials Science and Engineering
Nanjing Tech University
Nanjing 211816, China
The ORCID identification number(s) for the author(s) of this article can be found under https://doi.org/10.1002/adma.201907176.

DOI: 10.1002/adma.201907176

processing technologies. Recent developments in composition and processing have resulted in intriguing multifunctional materials geometries with promising properties for emerging applications. To date, a number of excellent review articles and books on freeze casting have been published.[3] Among the first, Devile[3a] provided a review of freeze-cast porous ceramics in 2008, with particular attention being paid to the underlying principles of the structure formation mechanisms and the influence of processing parameters. Recently, Scotti and Dunand[3f] established an indexed repository for freeze-casting experimental data, which is available through the web interface: FreezeCasting.net.

In the present review, we discuss contemporary developments in the field of freeze cast materials. As outlined in **Figure 1**, first, a basic principle of the freeze casting process is described. Subsequently we summarize recent progress in freeze-casting assisted assembly of various low dimensional building blocks into targeted micro- and macrostructures. We present emerging trends relating to 1) novel materials as building blocks: carbon nanotubes, graphene sheets, ceramic nanowires, nanofibers and plates, metallic nanowires, polymer chains and macromolecules, 2) novel freeze cast geometries: beads, fibers, films, complex macrostructures, and nacre-mimetic composites, and 3) emerging functional applications: structural materials, energy storage, and conversion, environmental remediation, thermal insulation, thermal management materials, electronic materials, biomaterials and bioinspired smart materials. Last, challenges and future prospects are briefly discussed.

2. Principles of Freeze Casting

Freeze casting involves the controlled solidification of a solution, suspension, sol or gel, followed by the sublimation of the solvent (mostly commonly water) under reduced pressure, and subsequent densification by posttreatment.[1a,3a–f,4] During the controlled solidification process, as the solvent solidifies, phase separation takes place, with the resulting solid phase (usually ice) serving as a template. For this reason, freeze casting is also commonly referred to as ice-templating. Afterwards, the solidified solvent template is removed by sublimation while the structural framework is retained, eventually yielding a well-shaped monolith. A key advantage of freeze-casting is its applicability to a wide range of materials, with diverse assembly units, or building-blocks, being utilized in such methods including nanoparticles, nanotubes, nanowires, nanofibers, nanosheets, nanoplatelets, polymer chains and macromolecules, so long as these can be stably dispersed. Another advantage is that various alterations to processing conditions may produce drastic changes in the obtained micro- and macrostructures of freeze-cast scaffolds. Microstructural properties of scaffolds, in terms of porosity and pore morphology (lamellar, honeycomb, cellular, radial etc.) can be tailored by chemical and physical methods, while diverse scaffold geometries at the macroscale can be achieved by combining freeze casting with other processing and shaping routes.[5]

2.1. Single-Particle Model

For freeze casting processes to yield aligned or otherwise tailored porous structures, it is essential that solid particles are rejected by the solidification front. Otherwise ice-templating does not occur, as particles will be distributed homogeneously throughout the frozen system. A key to interpreting freeze-casting processes, is the thermodynamic free energy of the system, as illustrated

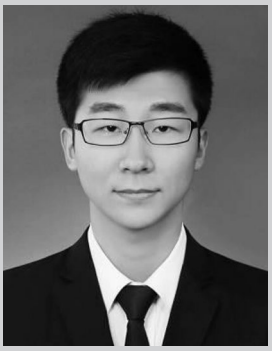

Gaofeng Shao obtained his B.S. (2013) and Ph.D. (2018) degrees from Nanjing Tech University (NJTech) under the supervision of Prof. Xiaodong Shen. He joined Prof. Aleksander Gurlo's group at Technische Universitaet Berlin (TU Berlin) as a visiting Ph.D. student in 2017. After working as a postdoctoral researcher in the same group (2018–2019), he joined Nanjing University of Information Science & Technology (NUIST) as a School Professor. His current research interests focus on macroscopic assembly of low-dimensional building blocks and their structural, functional, and smart applications.

Dorian A. H. Hanaor has been bridging multiple disciplines of engineering through roles in research, consulting, and teaching since completing his B.E. in materials science and engineering with first class honors at UNSW in Australia in 2006. Following a Ph.D. in ceramic science and technology (2012) from UNSW, he worked on several high-value Australian engineering projects before joining the School of Civil Engineering at the University of Sydney as a research fellow. Since 2017 Dr. Hanaor has been based in Germany and is working as a lecturer and research group leader at TU Berlin.

Aleksander Gurlo obtained his Ph.D. in chemistry from the Belarusian State University (Minsk, Belarus) in 1998 and his Habilitation in Materials Science in 2010 from the Technische Universitaet Darmstadt (Darmstadt, Germany). Since 2014 he has been a Full Professor and Head of the Chair of Advanced Ceramic Materials at the Technische Universitaet Berlin. His research focus is on advanced ceramics, with emphasis on the design, synthesis, and characterization of different material classes and the fabrication of functional devices by various methods including additive manufacturing techniques and in situ and in operando characterization.

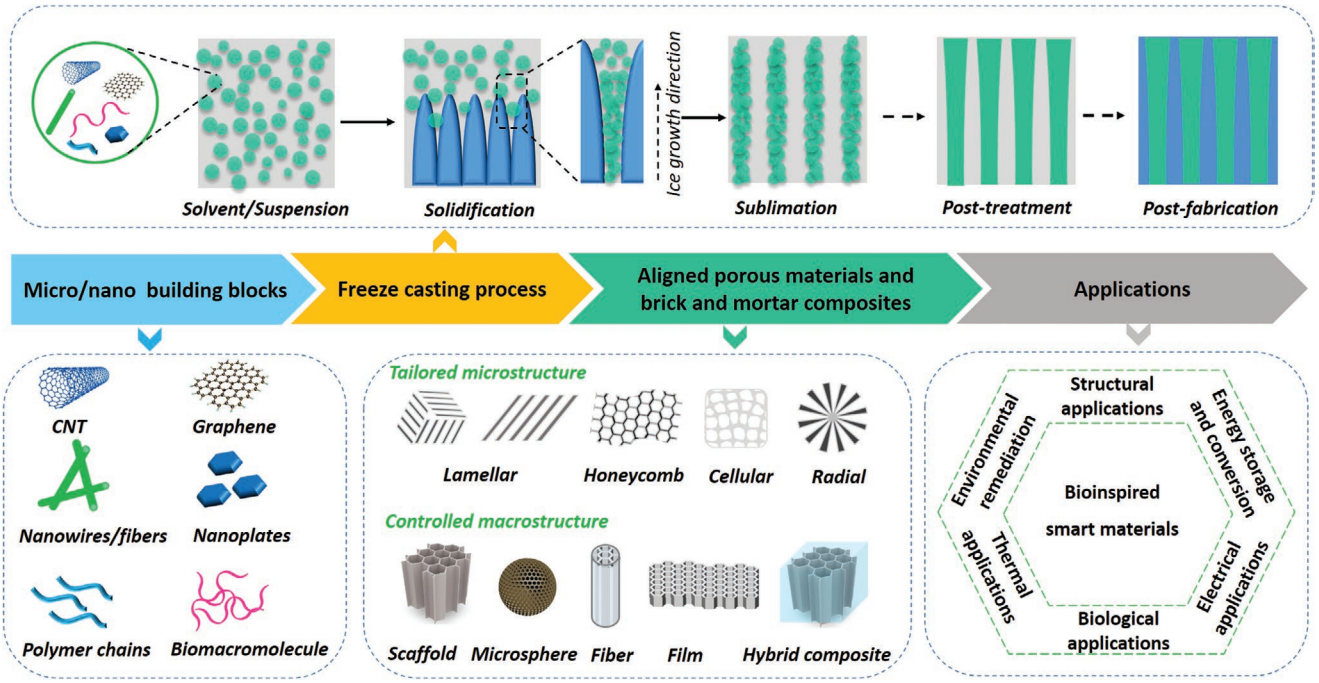

Figure 1. An overview of the themes discussed in this review, from the macroscopic assembly of micro/nano building blocks to emerging applications.

using a single-particle model in **Figure 2**A. During the solidification step, the thermodynamic condition for a suspended "particle" to be rejected by the solidification front is that the interfacial free energies satisfy this following criterion:[3a,c]

$$\Delta\gamma_0 = \gamma_{ps} - (\gamma_{pl} + \gamma_{sl}) > 0 \quad (1)$$

where γ_{ps}, γ_{pl} and γ_{sl} are the interfacial free energies associated with the particle–solid, particle–liquid, and solid–liquid interfaces respectively. This energy balance facilitates the analysis of systems where suspended particles experience both repulsive, F_R, and attractive, F_A, forces with respect to the advancing freezing front arising due to interparticle van der Waals

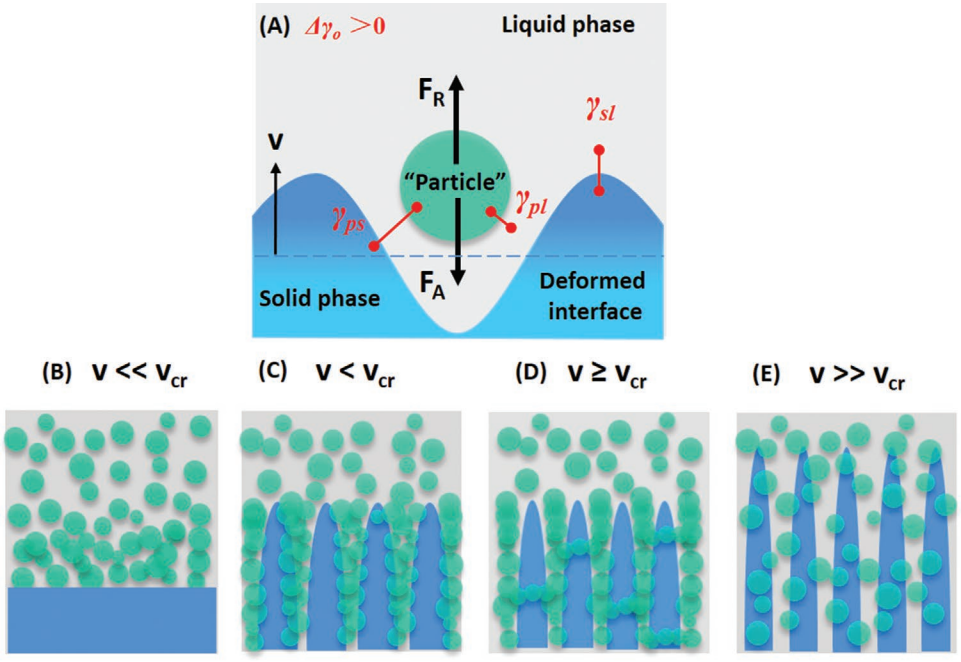

Figure 2. A) Illustration of the forces acting on a suspended particle in the vicinity of a freezing front. B–E) four cases of freezing front progression at different velocities.

interactions at the liquid-solid interface and viscous drag, respectively.

$$F_R = 2\pi r \Delta\gamma_0 \left(\frac{\alpha_0}{d}\right)^n \quad (2)$$

$$F_A = \frac{6\pi\eta v r^2}{d} \quad (3)$$

where r is the radius of the solid particle, v is the freezing front velocity, α_0 is the mean distance between molecules in the liquid phase, d is the thickness of the liquid layer between the solid–liquid interface and the particle (i.e., the distance between the ice front and the particle), η is the dynamic viscosity of the liquid and n is an empirical correction factor for the repulsive forces that generally ranges from 1 to 4.[3c]

Equating F_R and F_A and solving for the ice front velocity, v, results in an expression for the critical freezing front velocity, v_{cr}.

$$v_{cr} = \frac{\Delta\gamma_0 d}{3\eta r}\left(\frac{a_0}{d}\right)^n \quad (4)$$

As illustrated in Figure 2B–E, at very low solidification velocities ($v << v_{cr}$), the ice-growth proceeds as a planar front, displacing particles and increasing the solids loading of the unfrozen region. For $v < v_{cr}$, particles will generally be rejected and will form lamellar walls within the final freeze-cast scaffold and for $v \geq v_{cr}$, a certain fraction of particles will generally be entrapped by the solid phase, creating bridges between lamellar walls, yielding fine-scale porosity throughout the resulting freeze cast structure.[3c,6] Another freeze-cast structure occurs when particles are given insufficient time to segregate from the suspension, resulting in complete encapsulation of the particles within the ice front. This occurs when the freezing rates are rapid ($v >> v_{cr}$).

This force balance, derived from the original F_R and F_A terms, is related to the nature of the liquid phase, the solid particles, and the interactions between the particles and the approaching freezing front. As indicated by Equation 4, particle entrapment and rejection can be both chemically and physically manipulated by changing the suspension constituents (solvents, additives and solids) and freezing conditions (temperature, velocity, direction, external force fields), resulting in finely-tuned pore morphologies and microstructural features.

2.2. Multiple-Particle Model

Most mechanistic studies of structure formation in freeze casting focus on the interaction of individual particles with the solidification front. However, to include interactions between particles, single-particle analytical models can be extended to multiple particles by taking into account viscous friction in the compacted particle layer, which has been addressed in recent research.[7] The force acting on a particle close to the solidification front can be separated into three components (**Figure 3**A). In the compacted particle layer, viscous friction on the particle matrix and the associated fluid pressure drop induce an additional trapping force (F_P) on particles. At the level of a particle entering the front, a so-called lubrication force (F_L) leads to a reduction of the film that separates particle and front with a corresponding rise of the repelling thermomolecular force (F_T) exerted by the front on particles.[7b]

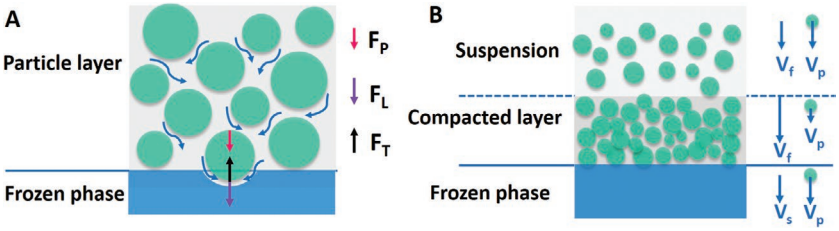

Figure 3. A) Forces acting on a particle entering the frozen phase. B) Cross section of the multiple-particle system: the suspension, the compacted layer of particles, and the frozen phase.

The mean velocities of the fluid, particles, and of the solid with respect to the solidification front are denoted V_f, V_s, and V_p, respectively.[7b,d] Velocities of the suspension and the frozen phase both equal the solidification velocity in the opposing direction. However, in the compacted layer of particles, they differ following the rise of particle volume fraction. The thickness of the compact accumulated layer thus increases, until the equilibrium is reached. In a steady-state regime, particles are then encapsulated as the interface moves, maintaining a compact layer of constant thickness ahead of the interface.

2.3. Suspension Preparation

The successful preparation of precursor suspensions for freeze casting processes involves components of solids, suspension media, and additives and is fundamental to the achievement of scaffold structures. The solid phase is in the form of suspended particles, which serve as building blocks in the freeze-casting process. In addition to the nature of these building blocks, the inclusion of solvents, to modify freezing behavior and surfactants to modify interparticle forces governs the obtained porous structure arising from freeze casting, as described by the force balances in Equations 2 and 3. Similar to conventional suspensions, the use dispersible particles is required and the homogeneous dispersion of 1D and 2D building blocks is often achieved using macromolecular or polymeric additives as dispersants and binders.[8] Freeze casting can be applied not only to particulate suspensions but also to colloidal sols and gels, which can be achieved, as with conventional sol–gel processing, through surface grafting or functionalization to control the formation of open networks.[9]

Pores of freeze cast structures are significantly affected by solvent chemistry. Four solvents generally used in freeze casting are water, camphene, camphor-naphthalene, and *tert*-butyl alcohol, which due to their different crystallization morphologies tend to impart lamellar, cellular, dendritic and prismatic pore morphologies, respectively. The formation of crystalline ice structures in terms of nucleation, growth and recrystallization is further controlled through the use of ice structuring agents, generally in the form of alcohols or salts.[10] Through the control of crystallization, the final pore morphologies of freeze cast materials can be tailored.

2.4. Solidification

In freeze-casting processes, the solidification (freezing) stage can be altered in terms of its velocity,[11] temperature and direction[12] as well the application of additional external force fields.[13] Manipulating the freezing-front velocity and temperature gradient of the solutions changes the spacing and thickness of resulting scaffold walls. Lower freezing temperatures lead to a higher degree of undercooling and higher solidification velocity, which, consequently results in the formation of narrower pore channels with thinner walls.

The application of unidirectional freezing, bidirectional freezing,[12a,14] radial freezing,[15] radial-concentric freezing,[16] freezing under flow,[17] dynamic freezing,[18] random freezing,[19] or freeze–thawing[20] have been explored as means toward the control of porosity and microstructure for functional freeze cast scaffolds. In the case of conventional unidirectional freezing, the suspension starts freezing under a single temperature gradient, causing the nucleation of ice to occur randomly on the cold finger surface (**Figure 4**A). As a result, the solidified suspension media consists commonly of microscale crystallites oriented preferentially along the direction of freezing, and resulting scaffolds with small-scale (multiple-domain) lamellar structures (Figure 4B). In bidirectional freezing (Figure 4C,D), solid phase building blocks (ceramic particles,[12a] platelets,[21] boron nitride (BN) nanosheets,[12b] graphene sheets[8g,22]) assemble into a large-size single-domain (centimeter-scale) aligned lamellar structures. This is achieved through the controlled nucleation and growth of ice crystals under dual temperature gradients generated by modified freeze-casting configurations, which allow the ice to grow both vertically and horizontally. Radial freeze casting is implemented using a copper mold in lieu of a polymer mold, with the suspension subjected to two temperature gradients, one along the *Z*-axis of the copper mold and the other in the radial direction, resulting in both longitudinally and radially aligned porosity (Figure 4E,F). Drawing inspiration from the efficient capillary transport of water in trees, radial freeze casting was used in a recent study to produce porous biomimetic structures analogous to cellular tracheid structures in conifers, to yield highly optimized fluid transport.[15b,23]

In addition to the engineering of freeze cast structures by controlled thermal gradients, external magnetic,[24] electric,[25] and acoustic[26] fields, as well as light irradiation[27] can serve to further control the chemical states of suspension media or solid particles in colloidal suspensions during or after solidification. Magnetic fields generated by permanent magnets arranged in a variety of spatial orientations can produce scaffolds with different microstructural patterns when used in the freeze casting of magnetic particles or other building blocks functionalized with magnetic nanoparticles. As an example, a continuous core–shell structure consisting of radially aligned lamellae and core can be formed under a radial magnetic field. By applying an axial field parallel to the solidification direction, scaffolds were formed presenting three banded regions of low-density and high-density core–shell architectures. A scaffold consisting of two primary structural features: lamellar walls and mineral bridges, illustrated in Figure 4G,H, can be achieved under transverse magnetization. This magnetic uniformity produced scaffolds with uniform architectures rather than gradient architectures similar to those formed under the radial and axial magnetic fields. Recent research into magnetic freeze casting has demonstrated the utility of diverse types of magnets and magnet positioning techniques, including rotating magnets, to control field strength and produce freeze cast structures of

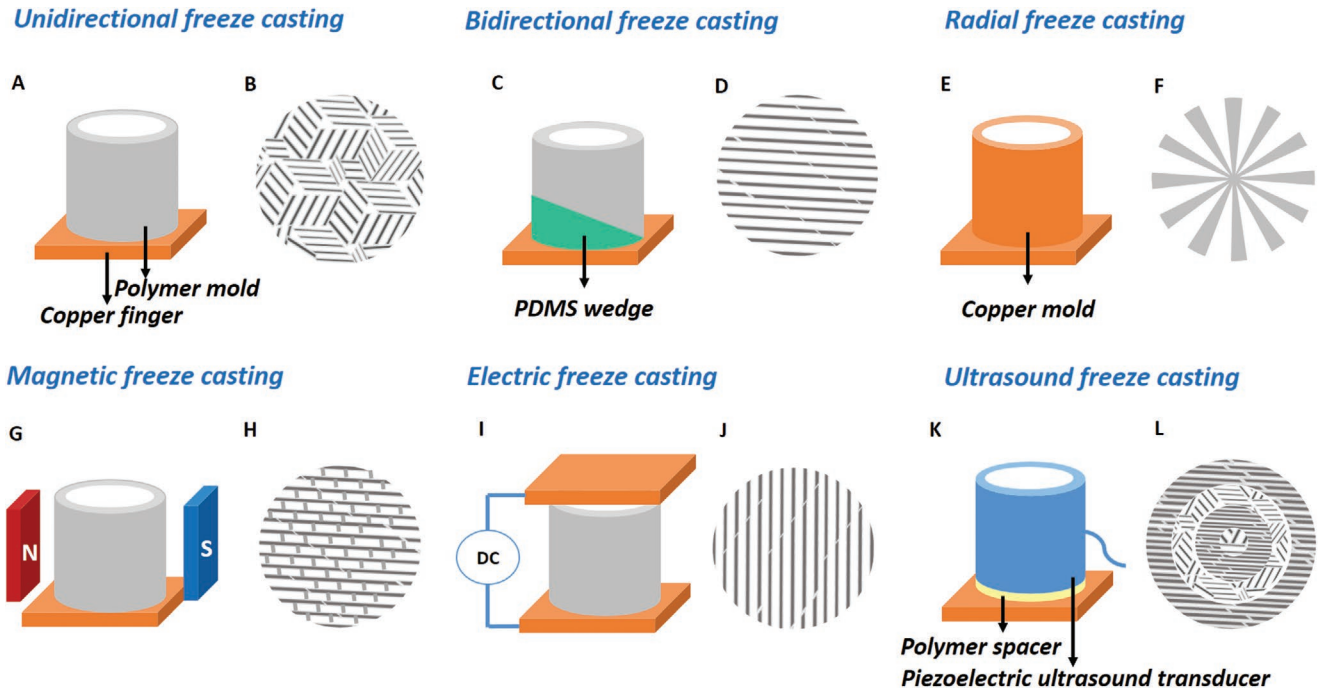

Figure 4. Schematics of freeze casting techniques and corresponding top-view microstructures of resulting scaffolds. A,B) unidirectional, C,D) bidirectional, E,F) radial, G,H) magnetic, I,J) electric and K,L) ultrasound freeze casting.

various tailored forms including helical scaffolds, uniform scaffolds, and functionally graded materials.[24a-c,e] Compared with permanent magnets, the magnetic fields generated by Helmholtz coils are more uniformly distributed with no or minimal field gradients, and lamellar wall alignment can be achieved through the various applied magnetic field directions.[24a,e]

In another approach, the application of an electric field can be used to impart a temperature gradient, thus controlling the growth path of ice crystals. As shown in Figure 4I,J, electric fields oriented perpendicular to the freezing direction produce long-range alignment of lamellar walls through the formation of angled ice crystals.[25c] In contrast, applying electric fields parallel to the solidification direction, producing scaffolds with bilayered dense/porous regions.[25b] By employing a standing ultrasonic wave field (Figure 4K),[26] whereby the acoustic radiation force creates a standing pressure wave, regions of high and low pressure can be imparted in freeze-casting processes. As particles are driven to low pressure regions of the standing wave, the resulting scaffolds exhibit a distribution of alternating dense/porous rings (Figure 4L). A further novel approach to assisted freeze casting is the use of light irradiation to drive reactions and rearrangement between polymeric building blocks in the obtained frozen state.[28] As will be discussed in a subsequent section of this review, the incorporation of light driven cross-linking into freeze-casting processes is playing an increasingly important role in the development of novel techniques for the fabrication of aligned porous polymers and polymer-based materials.

Of further note, in addition to monolithic freeze-cast scaffolds, macrostructures such as beads/microspheres,[29] fibers,[8f,30] meshes,[10b,31] films,[32] membranes[10c,33] and other complex morphologies[34] with aligned porous microstructures can be achieved by combining freeze-casting with other materials processing or shaping routes such as electrospraying,[29e] electrospinning,[30b,35] extrusion,[8f] tape-casting,[36] or additive manufacturing[37] during the solidification process. As the adoption of freeze casting techniques progresses, these forming techniques are the subject of growing interest towards diverse applications as discussed in a subsequent section of this review.

2.5. Recrystallization

When a solvent is held for a prolonged duration in its frozen state, Ostwald ripening may occur, in which large crystals grow at the expense of smaller ones, resulting in an increase in the mean crystal size and a decrease in the total number of crystals. The grain size that emerges from this process can be readily adjusted by the addition of ionic solutes and the control of freezing time and temperature.[38] Thus recrystallization can be exploited as a templating approach for the fabrication of various 2D and 3D porous materials based on nanoparticles,[10d] Ag nanowires (AgNWs),[10b] graphene oxide (GO) nanosheets,[39] and polymers with tunable pore sizes.

2.6. Sublimation

Freeze drying (lyophilization) is the most commonly used method for sublimation of the solidified solvent (suspension media) template after the solidification process. Freeze drying parameters have not been found to significantly impact the final microstructure of freeze-cast samples. More recently, freeze substitution (whereby samples are rapidly frozen and solidified fluids are dissolved) and supercritical drying were reported for the removal of solidified solvents containing nonvolatile cryoprotectants, such as glycerol or ethylene glycol, which cannot be effectively removed by freeze-drying. This method enables the use of high concentrations of cryoprotectants to control the pore forms and yields highly uniform, crack-free aerogels with a finer pore texture.[40]

2.7. Posttreatment

To impart desired structural and physical properties to aligned porous materials formed by freeze-casting, posttreatment processes such as densification, pyrolysis, thermal reduction, and carbonization are applied to dried scaffolds. Densification processes are required to impart adequate mechanical properties to porous scaffolds, particularly those consisting of ceramic or metallic building blocks. High temperature sintering is the most common method for densification. Through high temperature processing, binders are removed and particles sinter together. Additionally, in nanowire-based systems, high temperature processes promote chemical bonding between glass binders and 1D building blocks.[8b,c,41] In other recent studies into novel freeze cast systems, high temperature pyrolysis under inert atmospheres is adopted for ceramization of freeze cast preceramic polymer precursors. For the freeze casting of novel assembled graphene scaffolds, thermal reduction processes are used to remove the functional group of graphene oxide units and reconstruct graphene structures, further improving the electrical and mechanical properties of 3D graphene based scaffolds.[8f,42] Additionally, lightweight carbon materials can be derived from biomacromolecular based scaffolds through carbonization process.[8d,22,43]

2.8. Postfabrication

Infiltration freeze-cast skeletons with a secondary phase allows for fabrication of aligned composites, hydrogels, and nacre-mimetic hybrids. While not part of the freeze casting process, postfabrication infiltration serves to impart new functionality to freeze cast structures and broaden the range of systems that can be achieved through this synthesis approach. To date, a variety of infiltration techniques have been established, including polymer/metal melt immersion,[1b,44] in situ polymerization,[21,45] and deposition approaches such as chemical/physical vapor deposition,[46] electrochemical deposition,[29f,47] atomic layer deposition.[48]

Through control of suspension components and subsequent processing, as outlined above, freeze casting serves as a versatile and inexpensive approach toward materials fabrication. It can be extended to a wide range of materials combinations with different building blocks and offers valuable pathways to high-performance materials in applications including energy dissipation, storage and conversion, environmental remediation, thermal insulation and biological applications.

3. Recent Trends in Freeze-Casting Materials

3.1. Carbon Nanotubes as Building Blocks

Since pioneering works by Iijima in 1991, carbon nanotubes (CNTs) have received significant attention due to their attractive electrical, mechanical, chemical, and thermal properties. The assembly of CNTs is achievable in diverse macroscopic forms, including 1D fibers/yarns, 2D films and 3D scaffolds/sponges/aerogels through various methods such as spinning, vacuum filtration, template and self-assembly.[49] The freeze casting of CNTs is an interesting approach to the fabrication of functional porous materials as such structures offer attractive properties in terms of biocompatibility, conductive, high surface area combined with good mechanical strength. These characteristics make CNT scaffolds particularly valuable towards tissue regeneration and electrodes in microbial fuel cells.

Pioneering work in the fabrication of 3D aligned porous CNT scaffolds by freeze-casting was conducted by Gutiérrez and co-workers,[2,8a,47,50] who developed a series of aligned porous multiwall CNTs (MWCNT) based scaffolds with a chamber-like architecture in the form of interconnected chitosan bound MWCNT sheets arranged in parallel layers, with a view toward biological applications (**Figure 5**A,B). The relative content of chitosan, which functions both as a binder and a dispersion agent, is critically important for achieving homogeneous suspensions before freezing. In these freeze cast scaffolds, densely networked MWCNTs form parallel layers separated by orthogonal struts. This distinct structure was shown to confer favorable mechanical properties, while serving to facilitate cell growth.[8a] As an alternative to chitosan, CNT scaffolds can also be assembled with the aid of silk fibroins as binders.[51] In related work, a hybridization process was conducted in which 3D aligned porous CNTs scaffolds were homogeneously mineralized by a flow-through electrodeposition process to realize remarkable biocompatibility with human osteoblast cells (Figure 5C).[47]

Novel freeze cast CNT based structures have further been achieved through the use of heterogeneous building blocks, which include unzipped or partially exfoliated MWCNTs.[52] This approach results in altered structures of the ice templated material. The honeycomb nanocarbon aerogels with leaf-like structures can be achieved. The tailoring of scaffolds in such ways is an active field of research in recent years. As one example, these structures are of interest owing to their attractive performance in vibration damping. Further applications of porous CNT monoliths are emerging in the field of electrochemical energy storage. Ordered CNT-based scaffolds were applied as electrodes in Li–S batteries. Through the use of freeze-cast CNTs, a conductive scaffold with regular spacing can be produced whereby a large amount of sulfur can be reversibly accommodated with minimal expansion stresses and performance deterioration.[53]

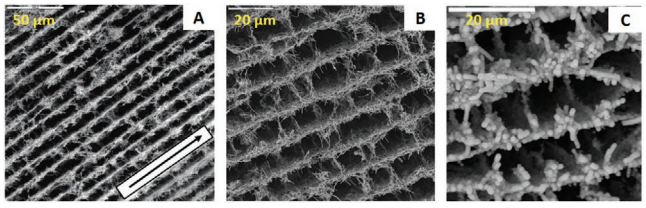

Figure 5. SEM micrographs of A) longitudinal section and B) transverse section of monolithic MWCNT/ chitosan architectures. Reproduced with permission.[8a] Copyright 2007, American Chemical Society. C) Transverse section of CNT scaffolds after mineralization. Reproduced with permission.[47] Copyright 2012, Wiley-VCH.

3.2. Graphene Sheets as Building Blocks

As synthesis methods for graphene continually evolve, the freeze casting of porous structures assembled from graphene sheets is of rapidly growing interest. Graphene, a 2D layered nanomaterial that consists of sp^2-bonded carbon atoms, has piqued the interest of scientists worldwide, due to its unique physical and chemical properties, driving the exploration of their potential applications in catalysis, sensors, electronic devices, and energy storage. 2D graphene based materials include single- and multilayer graphene, graphene oxide and reduced graphene oxide (rGO). In recent years, the development of grapheme-based nanocomposites has been the subject of extensive research across numerous disciplines. From a survey of contemporary literature, it is clear that a broad range of functionalized composites are being intensively investigated. These composites include graphene-based materials coupled with metal or metal oxide nanoparticles, 1D structures such as nanowires or nanotubes, polymers, and other 2D nanosheets. It is therefore evident that the development of freeze-casting techniques applied to graphene-based building blocks constitutes a promising avenue of research toward functional porous 3D systems.

The most common strategies for the assembly of graphene building blocks into 3D forms rely on mechanisms of (I) self-assembly, whereby hydrothermal/chemical reduction promotes the partial overlapping or coalescing of graphene sheets to one another (II) cross linking where metal ions or polymers cross-link with the functional oxygen groups on graphene oxide and promote the formation of 3D structures through primary and secondary bonding and (III) interfacial assembly, where an existing 3D scaffold, such as a metal foam, silica aerogel, or polymeric sponge, serves as a template on which graphene is grown or deposited, with porous graphene structures formed upon removal of the template. These approaches result in random porous scaffolds.[54] More controlled scaffolds formed by graphene and graphene-based materials have been achieved through additive manufacturing processes based on direct ink writing.[37e,55] This method imparts macroscopic structural control, while microscale pores structures remain random. Finer tuning of structural features in additively manufactured graphene-based materials was recently achieved using a microstereolithography technique.[56] However, this process suffers from low throughput and high costs.

The rationale for the development of freeze casting methods toward structured porous graphene based systems stems from the ability of this approach to yield structures with well-controlled pore geometries across multiple length scales. Illustrating the versatility of this approach, various graphene scaffolds with tailored microstructures and controlled macrostructures obtained through freeze casting of graphene oxide suspensions are shown in the timeline of **Figure 6**.

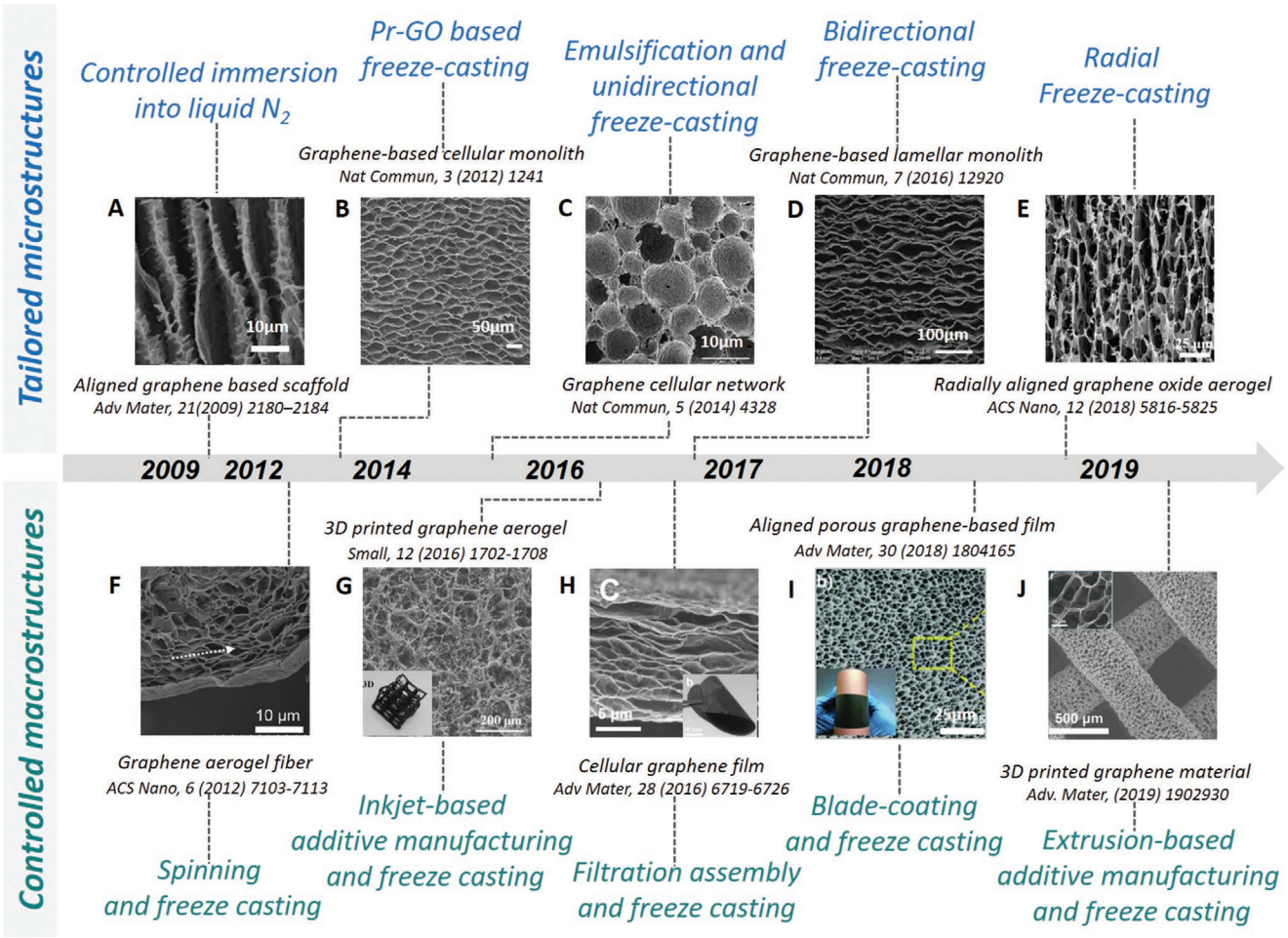

Figure 6. Timeline of the development of aligned porous graphene structures by freeze casting. Tailored microstructures: A) Reproduced with permission.[57] Copyright 2009, Wiley-VCH. B) Reproduced with permission.[58] Copyright 2012, Springer Nature. C) Reproduced under the terms of the Creative Commons CC-BY license.[8f] Copyright 2014, Springer Nature. D) Reproduced under the terms of the Creative Commons CC-BY license.[22] Copyright 2016, Springer Nature. E) Reproduced with permission.[15b] Copyright 2018, American Chemical Society. Controlled macrostructures: F) Reproduced with permission.[30a] Copyright 2012, American Chemical Society. G) Reproduced with permission.[37a] Copyright 2016, Wiley-VCH. H) Reproduced with permission.[32a] Copyright 2016, Wiley-VCH. I) Reproduced with permission.[32b] Copyright 2018, Wiley-VCH. J) Reproduced with permission.[59] Copyright 2019, Wiley-VCH.

The freeze casting of porous graphene-based materials has been realized using both unidirectional freeze-casting and bidirectional freeze-casting.[8g,15b,22,60] Unidirectional freeze-casting has been applied for the ice templating of GO by means of controlled immersion in liquid nitrogen,[57,61] or by the more conventional cold-substrate approach.[42a,c,43b,c,44a,45a,62] The porous microstructures achieved from freeze-casting are shown in **Figure 7**. It can be seen that the unidirectional freeze-casting tends to result in a cellular structure, akin to a honeycomb morphology, with equiaxed cells in the transverse direction and elongated cells seen in a longitudinal orientation. In contrast, bidirectional freeze-casting is conducive to the formation of templated GO in a lamellar structure. As with other freeze casting processes, the design of process parameters and geometry, including radial freeze casting, can be implemented to fine-tune the obtained microstructures.[57,61]

In general, as with most freeze-casting processes, freezing induced phase separation results in the rejection of GO sheets from the solidification front, which then accumulate between the growing ice crystals. Templated GO forms a continuous 3D network after the sublimation of the ice, generating a porous GO aerogel. Often this takes the form of well-ordered microchanneled GO structures oriented along the freezing direction.[57,61b,d] The objective of ice templating GO suspensions is often the achievement of rGO-based scaffolds. Often these porous materials are referred to as 3D graphene structures, however the ubiquitous presence of residual oxidation means that final materials are more correctly termed rGO aerogels or scaffolds. Reduction of GO is particularly important towards achieving electrical conductivity and realizing the unique mechanical responses offered by graphene scaffolds, such as superelasticity. Consequently, a physical or chemical reduction step is generally required to convert GO to rGO or graphene. One approach applied in various research efforts toward the formation of assembled graphene structures, illustrated in Figure 7A,B, involves the ice templating of partially

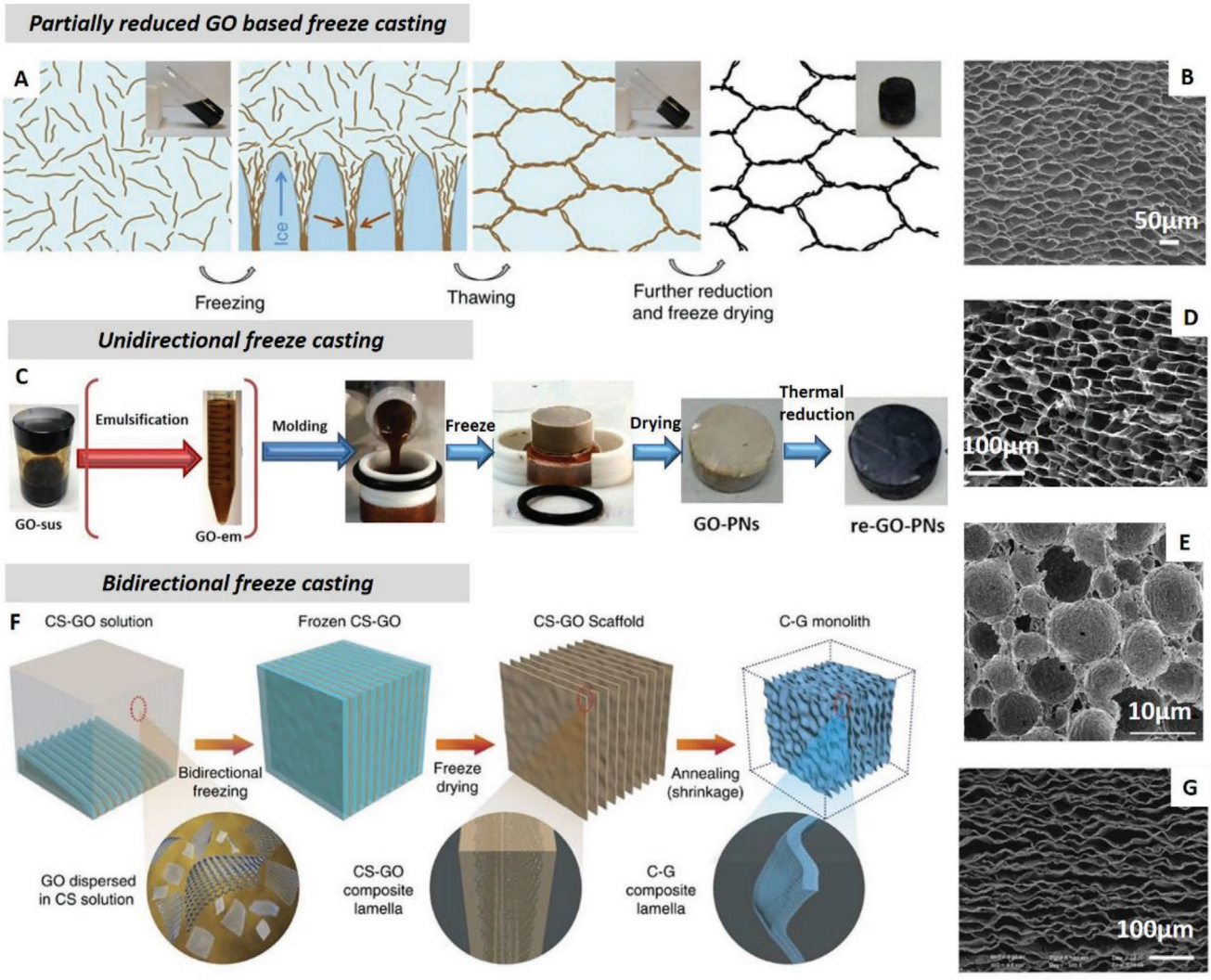

Figure 7. A) Formation mechanism and B) transverse section morphology of a cork-like graphene elastomer. Reproduced with permission.[58] Copyright 2012, Springer Nature. C) Processing strategy of the porous graphene networks. Reproduced with permission.[62e] Copyright 2015, Springer Nature. D) Transverse section morphology of honeycomb graphene network. Reproduced with permission.[42a] Copyright 2017, Springer Nature. E) Transverse section morphology of cellular graphene network. Reproduced with permission.[8f] Copyright 2014, Springer Nature. F) Schematic illustration of the fabrication and G) transverse section morphology of carbon–graphene monolith. Reproduced with permission.[22] Copyright 2016, Springer Nature.

reduced GO (pr-GO) to form an ordered network, followed by thawing. In one such study, a porous biomimetic structure inspired by cork was fabricated, showing a superelastic response at high strains (up to 80%).[58] In such processing, the initial partial reduction of GO inhibits agglomeration and facilitates microgelling, thus allowing the cellular structure to be retained through thawing.[32a] In subsequently obtained hydrogels, templated prereduced GO interspersed with liquid water is further reduced by the use of chemical reduction agents (such as ascorbic acid). The resultant graphene (or rGO) hydrogel is then subjected to freeze drying. A more common approach to the reduction of assembled GO involves thermal treatment under reducing atmospheres after sublimation of the solidified solvent. In the absence of a prereduction step, the use of directional freeze casting coupled with polymer or surfactant additives as structure directing agents is essential in order to impart cellular alignment and avoid a brittle scaffold with random pore orientations.

Showing the role of directionality in the freeze casting of GO, unidirectional freezing of GO with a polymeric binder gives rise to a fine microhoneycomb structures, which can subsequently be thermally reduced to form functional rGO scaffolds (Figure 7C,D). Initially reported by Saiz,[8f] this approach, coupling unidirectional freeze-casting, polymeric binders and thermal reduction is widespread. Through the integration of emulsification with the suspension preparation step, closed-cellular structure can be achieved (Figure 7E). With both closed and open structures, pore morphologies obtained through unidirectional freeze-casting of GO suspensions can be controlled by adjusting suspension parameters. Reducing the freezing temperature results in finer pore structures and higher strength to weight characteristics.

In contrast to the cellular or honeycomb-type structures produced by unidirectional freeze-casting, the lamellar structures produced by bidirectional freezing confer distinct mechanical and transport properties to freeze cast GO systems.[8g,15b,22,60,63] Dual temperature gradients used in bidirectional freeze-casting can be achieved through different processing methods. In a technique used by several researchers, in-plane and out-of-plane heat gradients are simultaneously produced using a single base plate that is asymmetrically cooled, for example, by the immersion of one side of the plate in liquid nitrogen.[22,60c] Figure 7F,G shows a bidirectional freezing process and the resulting monolithic carbon–graphene composite comprising a large number of multiarch microscale structures arranged into parallel stacks.[22] In a second approach, an insulating polymer of varying thickness can be placed on top of a uniformly cold surface to modify the cooling rate in the in plane direction. This is similar to the method illustrated in Figure 4B, realized using a polydimethylsiloxane (PDMS) wedge.[8g] Finally, the use of radial-concentric freeze casting offers a third approach to bidirectional freezing of graphene oxide suspensions.[15b]

A different strategy involves the freezing of GO liquid crystals with a high aspect ratios.[64] This concept could be extended to other materials that can form liquid crystals, and further controlling the orientation of the liquid crystals during freeze could be an approach for the construction of more complex structures.

Porous graphene based structures are particularly attractive as the basis for the fabrication of composite materials. These can be realized through the hybridization of the initial suspension prior to freeze casting by adding secondary building blocks such as nanoparticles,[61c,d,62a,65] 1D nanomaterials (CNTs,[66] ceramic nanofibers/nanowires,[62i] metal nanowires[32b]), polymers,[29f,57,61e,62h] macromolecules,[9b,22,29c,g,43b,c,60c,61a,62d,67] 2D nanosheets (BN,[44b] $Ti_3C_2T_x$ MXene[68]) by freeze casting process. Alternatively, composite structures can be produced by modifying a graphene based scaffold postsynthesis through infiltration or deposition. Such hybrid structures, which tend to comprise a highly conductive cellular phase with an inserted secondary phase are attractive in energy materials, where a balance of electronic and mass transport is often of great importance.[29c,36c,69] The unique structure of graphene aerogels is key to achieving new levels of performance in such composites and represents a promising avenue of research towards further design and development of functional materials as discussed further in Section 4 of this work.

3.3. Ceramic Nanofibers and Nanosheets as Building Blocks

A wide variety of inorganic materials, such as ceramic or metallic particles have been assembled into aligned porous structures by freeze casting for structural and biomedical applications. The relationships between process parameters, microstructures and physical properties have been comprehensively investigated among conventional inorganic material systems. In recent year, novel 1D and 2D inorganic build blocks, such as ceramic nanofibers/nanosheets or metallic nanowires emerge out, providing the opportunity for the construction of aligned porous structures (**Figure 8**) with unique physical and functional properties such as lightweight, elasticity, thermal and electrical conductivity.

Ceramic aerogels based on SiO_2,[74] Al_2O_3,[75] SiC,[76] and BN[77] have been widely investigated due to their light weight, low thermal conductivity, high refractoriness, and corrosion resistance. As a well-known example, thermal insulation systems of extraordinarily high performance have been achieved on the basis of silica aerogels and emerging as the first significantly commercialized aerogel materials. However their poor fracture toughness and relatively high production costs limit the rapid uptake of these materials, motivating further process optimization.

In general, most existing processes for the fabrication of ceramic aerogels are based on the assembly of nanoparticles using sol–gel processing and supercritical drying, which yields disordered pore structures.[78] Freeze casting offers a versatile new approach to the production of ceramic aerogels having aligned porosity. Ordered freeze cast pore structures impart enhanced mechanical properties to ceramic aerogels, without increasing thermal conductivity through the use of a reinforcing phase. An attractive approach toward the fabrication of ceramic aerogels of enhanced toughness involves the use of 1D ceramic nanostructures as assembly units in freeze casting processes. As an example of this approach, in several studies, SiC fibers were assembled, using various dispersion and binding additives, into highly aligned porous networks by unidirectional freeze-casting,[8b] resulting in a structure analogous to that produced of CNTs in earlier work.[8a] The mechanical properties of freeze cast SiC fiber- based scaffolds can further be enhanced through liquid phase sintering, resulting in a supporting oxide phase.[8b] Through a similar approach (**Figure 9**A), SiO_2 nanofibers were used to produce cellular ceramic nanofiber aerogels (CNFAs), which when combined with a glassy phase yielded robust superelastic materials.[41] CNFAs produced by freeze casting tend to exhibit porous heterostructures, resembling various natural systems, with a clear network of cells and struts formed by the ice templating process, and a finer structure formed by the interweaving of the fibrous constituents. Drawing inspiration from natural structures, through the adjustment of composition and freezing conditions, specific biomimetic CNFA microstructures can be achieved. As another example of this, Knöller et al. reported the ice-templated fabrication of a ceramic-based scaffold comprising V_2O_5 nanofibers, mimicking the structure of cuttlebone, with good compressive properties at very low densities.[9a,71] Due to their very high void ratio, CNFA heterostructures, when infiltrated with water, can form unusual hydrogels. A CNFA structure formed by alginate bonded SiO_2 nanofibers was in recent work used to produce hydrogel materials accommodating high elastic deformations with strain sensitive conductivity.[79]

Further to the templating of 1D ceramic nanostructures, 2D ceramic structures can be used as building blocks in freeze-casting processes. In recent years BN sheets[12b,44b,70,80] and MXenes flakes,[9c,81] have been used in conjunction with ice templating to achieve scaffolds with high levels of thermomechanical performance. Several recent research efforts have examined the fabrication of boron nitride aerogels by freeze-casting methods using polymer cross linking

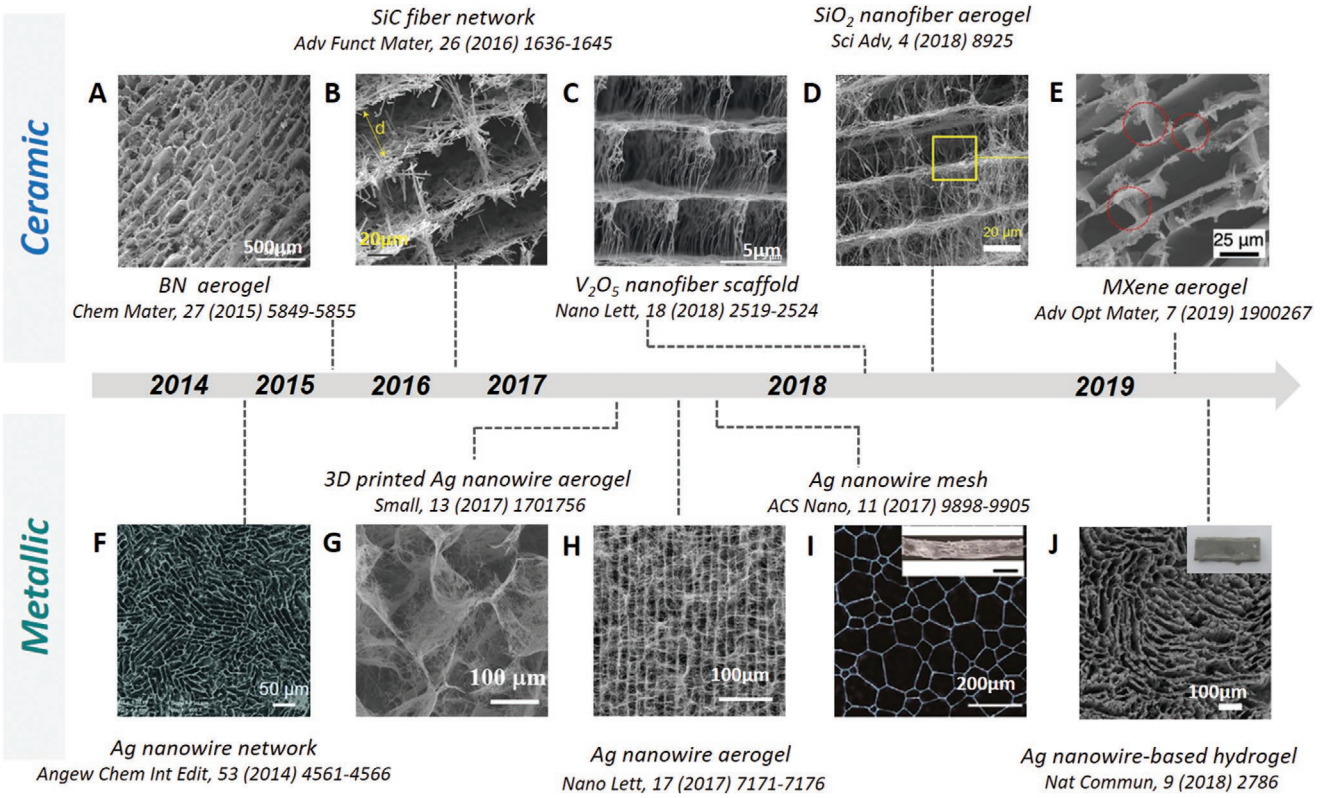

Figure 8. Timeline of the development of 3D aligned porous ceramic and metallic structures by freeze casting. Ceramic: (A) Reproduced with permission.[70] Copyright 2015, Wiley-VCH. (B) Reproduced with permission.[8b] Copyright 2016, Wiley-VCH. (C) Reproduced with permission.[71] Copyright 2018, American Chemical Society. (D) Reproduced with permission.[41] Copyright 2018, AAAS. (E) Reproduced with permission.[9c] Copyright 2019, Wiley-VCH. Metallic: (F) Reproduced with permission.[72] Copyright 2014, Wiley-VCH. (G) Reproduced with permission.[37b] Copyright 2017, Wiley-VCH. (H) Reproduced with permission.[8c] Copyright 2017, American Chemical Society. (I) Reproduced with permission.[10b] Copyright 2017, American Chemical Society. (J) Reproduced under the terms of the Creative Commons CC-BY license.[73] Copyright 2018, The Author(s), published by Springer Nature.

of BN nanosheets (BNNSs).[12b,70] The directional freeze casting of BNNSs demonstrates the utility of freeze-casting toward exploiting the anisotropic physical properties of BN to obtain highly functional materials for thermal interface applications.[12b,80b,c] MXenes, an emerging family of 2D transition metal carbides, carbonitrides and nitrides, have also been assembled in recent years into 3D aligned porous materials by freeze casting.[8d,9c] Additive-free, aligned, lamellar, and macroporous MXene aerogels were recently obtained by the construction of a set of MXenes ($Ti_3C_2T_x$, Ti_2CT_x, and Ti_3CNT_x) flakes by a bidirectional freeze-casting method.[9c] The obtained structures, in terms of lamellar spacing and the density of interlamellar bridges can be readily tailored by adjusting suspension parameters. As will be discussed in Section 5, the fabrication of such tailored MXene 3D structures offers valuable avenues toward the realization of materials with higher performance in applications of electromagnetic shielding and electrochemical storage.

3.4. Metallic Nanowires as Building Blocks

Low-density metal foams (LDMFs) are of interest toward many emerging applications in electronics, energy storage, catalyst supports, fuel cells, sensors, and medical devices. The use of nanowires to produce LDMFs offers a rational and effective pathway to highly conductive lightweight systems. However, the scope of the field of metal nanowires remains quite limited, and most studies have focused on the use of Ag nanowires,[8c,e,37b,40,72,73,82] with a smaller number of studies conducted into Cu nanowires[19,83] and Au nanowires.[84] Porous materials formed from the random assembly of AgNWs tend to suffer from poor mechanical attributes, motivating the use of freeze casting as means towards better weight-specific performance in ultralight AgNW scaffolds. Yu et al. conducted the first study of freeze cast AgNW structures, showing that ice templating can be used, without any additives, to achieve interconnected 2D networks of AgNWs forming aligned cell walls in a multiscale porous 3D scaffold.[72] This type of material offers a novel pathway toward unusually high conductivity to weight ratios. Following earlier studies, freeze- casting methods for the production of AgNW aerogels have been developed with a focus on further improving density-specific conductivity in these unique systems. Values of conductivity as high as 51 000 S m^{-1} have been achieved in this method for ultralight systems exhibiting densities as low as 4.8 mg cm^{-3}. A schematic illustration of freeze casting using AgNWs is given in Figure 9D–G.[8c] Analogous AgNW hydrogels, based on ice-templated aerogel scaffolds offers a route toward high-performance stretchable conductors.[73]

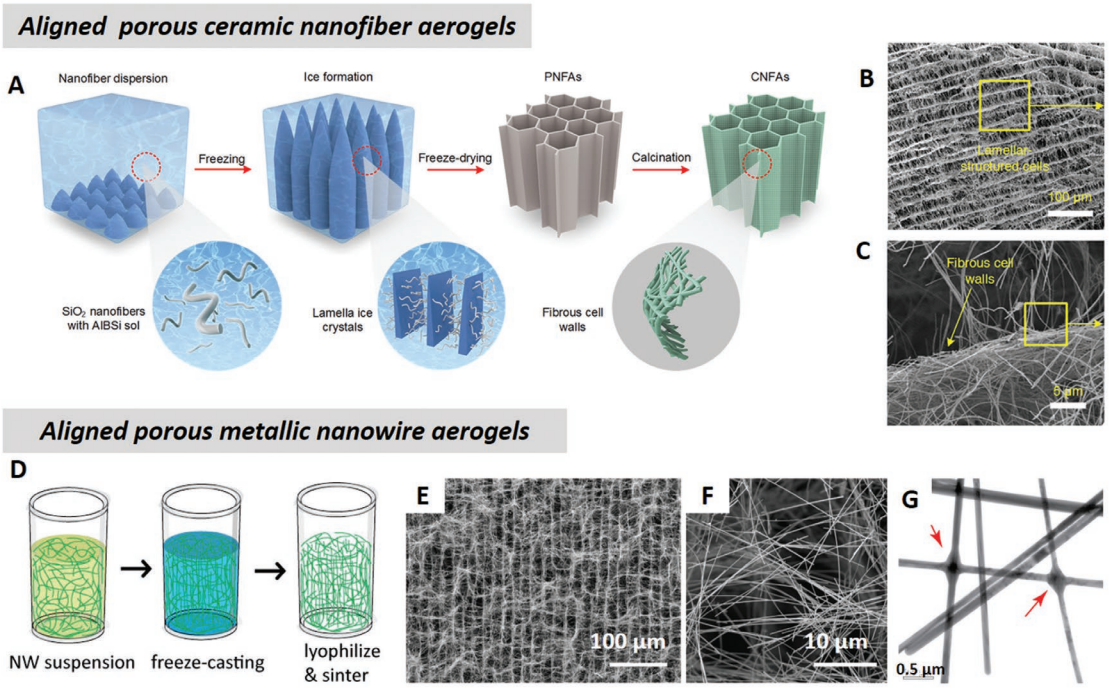

Figure 9. A) Schematic illustration of the fabrication of lamellar-structured ceramic nanofibrous aerogels. B,C) Microscopic structure of CNFAs at different magnifications. Reproduced with permission.[41] Copyright 2018, AAAS. D) Schematic illustration of the fabrication procedure of AgNW aerogel. E,F) SEM images of AgNW aerogel microstructures. G) TEM images of welded NW junctions. Reproduced with permission.[8c] Copyright 2017, American Chemical Society.

3.5. Polymer and Biomacromolecule as Building Blocks

Polymers and biomacromolecules represent versatile and abundantly available building blocks for the design and synthesis of biomimetic structures across multiple scales. As a means to achieve high levels of performance akin to those exhibited by natural structures, freeze casting techniques offer a pathway to control the assembly of these building blocks into aligned porous scaffolds (**Figure 10**). In particular, the use of biomacromolecules such as chitosan, cellulose, and silk fibroins is emerging in recent years as an effective approach toward the fabrication of bulk bioinspired materials offering a combination of biocompatibility, low environmental impact, and high performance in multiple applications.[15a,85]

Conventional freeze casting processes such as those outlined in Section 2 of this article have been applied to polymeric systems for decades. Generally, the fabrication of porous structures by freeze casting of polymers involves a solution of water or organic soluble polymers, which form a templated structure upon freezing, with the solvent removed by sublimation (**Figure 11**). In recent years, new methods for freeze casting of polymeric systems have been developed by integrating cross-linking steps to different processing stages. Freeze casting combined with photopolymerization has been utilized to produce aligned polymer scaffolds using precursor solutions of dispersed monomers, cross-linking agents, and photoinitiators.[23,88,92] As an example, shown in **Figure 12**A, a polyacrylamide (PAAm)-based aerogel was fabricated by radial freeze casting and in situ low temperature, light induced cross-linking, known as cryophotopolymerization. The resultant aerogel presents a biomimetic hierarchical structure with radially aligned channels, micropores, wrinkled internal surface, and molecular meshes (Figure 12B–E). This structure mimics tracheid cells found in conifer trees, which are remarkable for their ability to effectuate highly efficient water transport.[23] Another recent approach toward the enhancement of freeze-cast polymer scaffolds involves the crosslinking of polymers at elevated temperatures following the sublimation step, known as thermal curing (Figure 12F). In a recent study, such an approach facilitated the fabrication of bioinspired materials from phenolic and melamine resins with wood-like cellular microstructures (Figure 12G–I). Such wood-like freeze cast polymer scaffolds are able to achieve high levels of mechanical performance while exhibiting superior chemical stability, fire resistance, and thermal insulation.[93]

A further recent development in the freeze casting of polymeric solutions relates to the use of preceramic polymers to produce porous ceramic materials.[28c] By freeze casting organic solutions of Si-based polymers, including polycarbosilane,[86] polysiloxane,[94] or polysilazane,[27a,95] and subsequent pyrolysis, aligned porous polymer derived ceramics (PDCs) can be readily obtained in bulk porous forms. While the field of PDCs has seen growing interest in recent years, most forms produced from Si-polymer precursors tend to be thin films and powders. The processing of bulk PDC geometries is limited in its scope. Freeze casting of preceramic polymers offers a unique route toward the achievement of aligned porous SiC, SiOC, and other PDCs with typical primary dendrites structures (Figure 12J,K), which exhibit great utility in terms of functional properties including mechanical strength, chemical inertness,

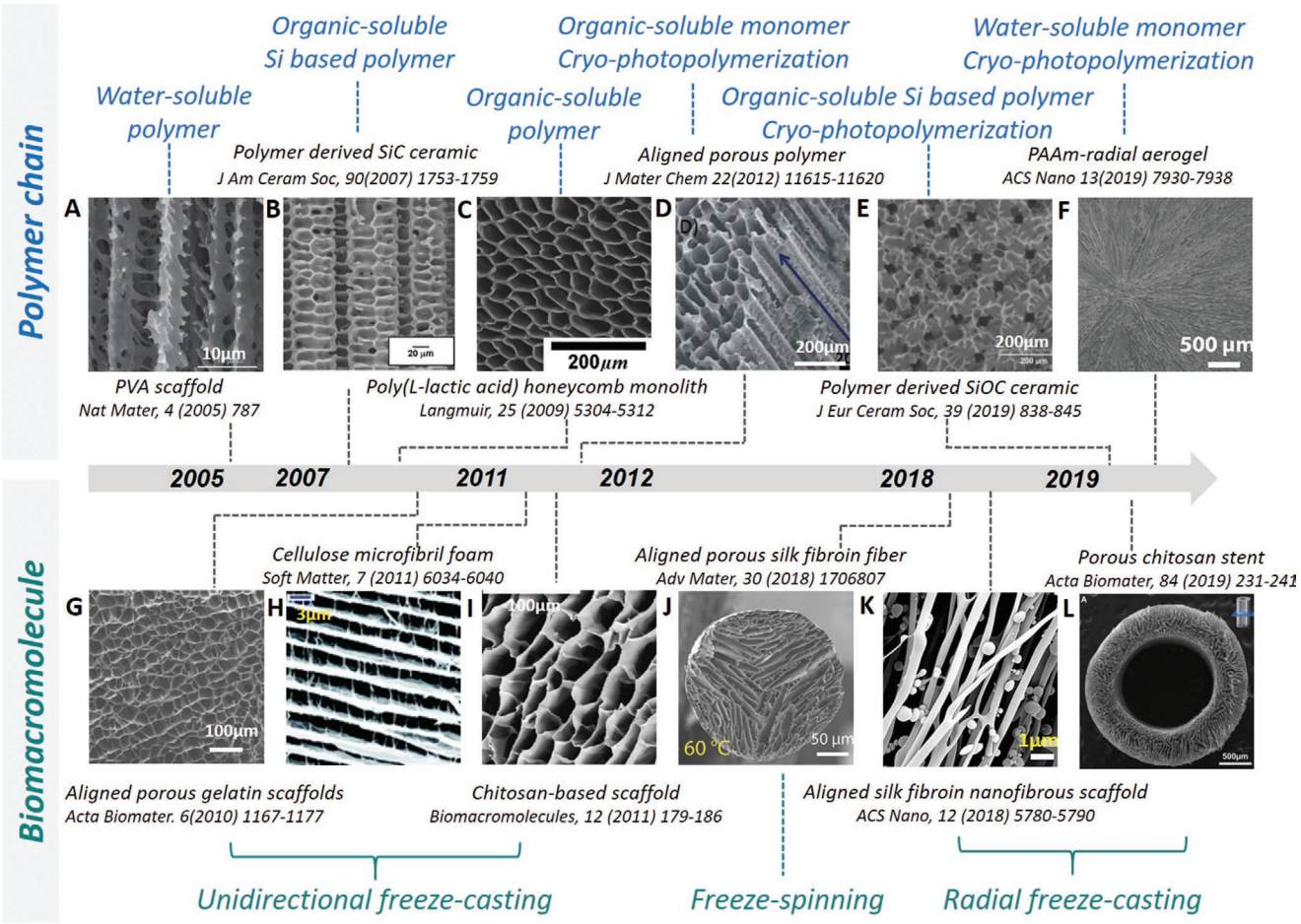

Figure 10. Timeline of developments relating to 3D scaffolds assembled with polymer chains and biomacromolecules by freeze casting. Polymer chains: A) Reproduced with permission.[1a] Copyright 2005, Springer Nature. B) Reproduced with permission.[86] Copyright 2007, Wiley-VCH. C) Reproduced with permission.[87] Copyright 2009, American Chemical Society. D) Reproduced with permission.[88] Copyright 2012, The Royal Society of Chemistry. E) Reproduced with permission.[27a] Copyright 2019, Elsevier. F) Reproduced with permission.[23] Copyright 2019, American Chemical Society. Biomacromolecule: G) Reproduced with permission.[89] Copyright 2019, Elsevier. H) Reproduced with permission.[90] Copyright 2011, Royal Society of Chemistry. I) Reproduced with permission.[91] Copyright 2011, American Chemical Society. J) Reproduced with permission.[30b] Copyright 2018, Wiley-VCH. K) Reproduced with permission.[15a] Copyright 2018, American Chemical Society. L) Reproduced with permission.[14] Copyright 2019, Elsevier.

and thermal stability. It can therefore be said that the freeze-casting of preceramic polymers presents a distinctive new route towards the production of versatile porous ceramics.

In general, partial cross-linking of the preceramic precursor in the initial solution is necessary to prevent pore structure from collapse during or after sublimation. However, control over the degree of polymerization in preceramic systems requires radical initiators which are mostly initiated thermally, rendering them unfit for use at low processing temperatures, affecting both solubility and viscosity of the solution required for directional solidification. An emerging concept of combining directional solidification of preceramic polymers with novel low-temperature photopolymerization steps opens up new approaches toward the fabrication of porous polymer-derived ceramics using precursors, which have either been unsuitable for freeze casting or have required a preliminary, tightly controlled cross-linking step before solidification (Figure 11). In a recent study, porous polysilazane-derived ceramic structures were generated through photopolymerization-assisted solidification templating, combining nonaqueous freeze casting of a liquid preceramic polymer with a photoinduced thiol-ene "click" reaction at low temperatures.[27a,92] Upon directional solidification of the solution consisting of the preceramic polymer, a quaternary thiol, a photo initiator, and pore-structuring agent, cryophotopolymerization was achieved by irradiation with visible light. The stability of the photopolymerized preceramic polymer scaffold is sufficiently high to impart structural integrity during the subsequent sublimation and pyrolysis processes. Such polymer derived ceramics with well-tailored aligned pore structures (Figure 12L,M) represent a new class of freeze-cast materials, with prospective applications as filters, bioscaffolds, and catalyst supports.

With the rapidly growing problem of environmental degradation due to the accumulation of waste plastics, the replacement of petroleum-based polymers with biomass derived materials is of great value. This is particularly important in the field of porous materials, as lightweight polymer foams are particular challenging to recover and dispose of effectively. Biomacromolecules

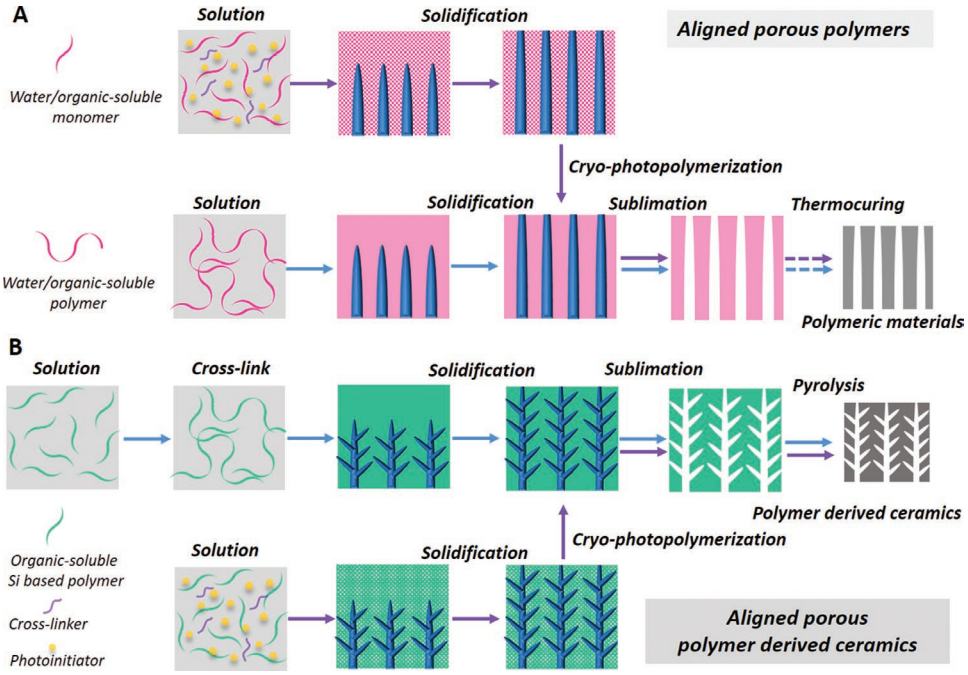

Figure 11. Freeze casting routes of aligned porous A) polymers and B) polymer-derived ceramics.

are defined as substances of biological origin exhibiting large molecular weight and complex structure. In recent years, biomacromolecule-based foams derived from renewable raw materials such as cellulose, chitosan and fibroin have been finding increasing applications with advantages, over petroleum-derived materials, including biocompatibility and biodegradability.

Over the past decade, freeze-cast scaffolds based on biomacromolecules have been made using cellulose,[9b,90,96] chitosan,[14,91,97] pullulan,[98] chitin,[99] collagen,[100] konjac glucomannan,[43a] amyloid fibril,[101] and silk fibroin[15a,30b,102] as building blocks, often including subsequent hybridizations[103] and their derived carbonaceous products.[43a,104] In freeze-casting processes, cellulose represents the most widely studied macromolecular building block. In a typical bioinspired approach, mimicking the cellular honeycomb structure of natural tree xylems, porous monoliths were fabricated from cellulose nanofibers (CNFs) by freeze casting.[9b] In this process, a viscous aqueous sol of chemically modified CNFs was subjected to unidirectional freezing to form a white cylindrical monolith, presenting an ordered microscale polygon-patterned morphology. The structure-directing function of chemically modified CNFs toward forming xylem-like structures can be achieved by controlling the chemical composition of the monoliths by introducing a variety of additives and surface grafting.

A second natural biomolecule commonly used in freeze-casting is chitosan, a low-cost crystalline polysaccharide readily derived from waste products in the seafood industry. Chitosan has been extensively studied as a building block in freeze-casting processes, particularly as chitosan scaffolds exhibit attractive properties such as robustness, shape-memory behavior, bioactivity, biodegradability, and nontoxicity. Because of these properties, chitosan freeze casting has been predominantly studied as a fabrication route for biomaterials such as bone supports and stents with further studies towards mechanical applications in foam form.[14,97c]

Fibroin, a protein found in silkworm silk, is another widely studied macromolecule of biological origin which, despite being significantly costlier relative to chitosan and cellulose, is attractive owing to its particularly high tensile strength. Freeze casting of fibroin is a logical route toward the obtainment of bioinspired, biomacromolecule-based porous materials with excellent strength to weight characteristics. Toward applications in biomedicine, 3D SiO_2-silk fibroin aerogels were synthesized through a one-pot aqueous based sol–gel hybridization of organosilane and silk fibroin biopolymer followed by unidirectional freeze casting and supercritical drying. The developed ultralight aerogels demonstrated a hierarchically organized porous structure with an interesting honeycomb micromorphology and microstructural alignment.[105]

4. Freeze Casting Materials in New Geometries

High production costs and poor machinability means that obtaining lightweight, functional, aligned porous scaffolds/aerogels in desired macroscopic forms necessitates the implementation of appropriate shaping techniques. This is essential toward realizing the attractive functional properties of aligned porous materials in applied engineering systems. Large, simple geometries are mostly achieved through the use of suitably shaped molds in the freeze-casting process. In particular, forming freeze-cast scaffolds into beads/microspheres, fibers, films/membranes/meshes and complex macrostructures requires the development of appropriate techniques.

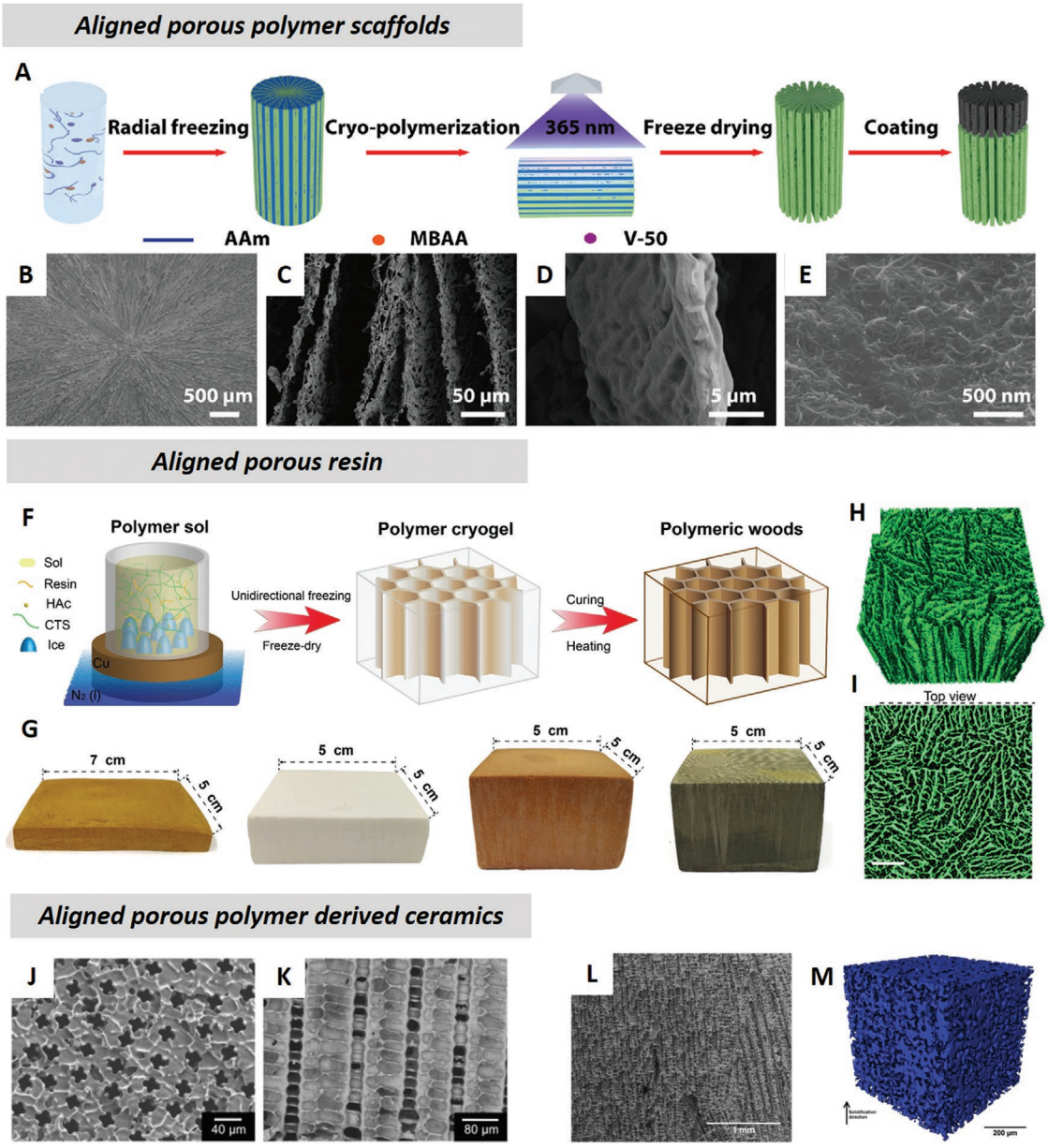

Figure 12. A) Radial freezing and in situ cryopolymerization of polyacrylamide aerogel. B–E) SEM images of PAAm radial aerogel at different magnifications. Reproduced with permission.[23] Copyright 2019, American Chemical Society. F) Fabrication scheme of bioinspired polymeric woods and G) composite woods based on PF and MF. H,I) 3D reconstruction of CPF wood from X-ray microtomography. Reproduced with permission.[93] Copyright 2018, AAAS. J) Primary dendrites seen from the transverse view perpendicular to the freezing direction and K) secondary dendrites seen from the longitudinal view parallel to the freezing. Reproduced with permission.[94d] Copyright 2017, Elsevier. L) Cross-section morphology and M) pore morphology of a porous polysilazane-derived ceramic. Reproduced with permission.[27a] Copyright 2019, Elsevier.

4.1. Aligned Porous Beads and Microspheres

Shaping freeze-cast 3D scaffolds into beads or microspheres enables their use in fluid environments for applications such as absorbents, drug/catalyst carriers, functional composite particles, and filtering membranes. In various examples from recently reported studies, beads or microspheres were made from freeze cast porous materials based on chitosan,[29a] SiC nanowire,[29i] CNT,[29d] graphene,[29e] and their hybrids.[29b,g]

A practical approach to the fabrication of freeze cast scaffolds in the form of microspheres involves the electrospraying of precursor suspensions directly into a cooled bath, usually of liquid nitrogen.[29e,g] A second approach for producing larger beads in smaller numbers involves the use of a syringe-like apparatus to generate drops of suspension, which too are dropped into a cooled liquid medium.[29b,c,f,i]

Of particular value, spheroidal scaffolds from freeze cast materials can be obtained with core–shell [29a,c] structures

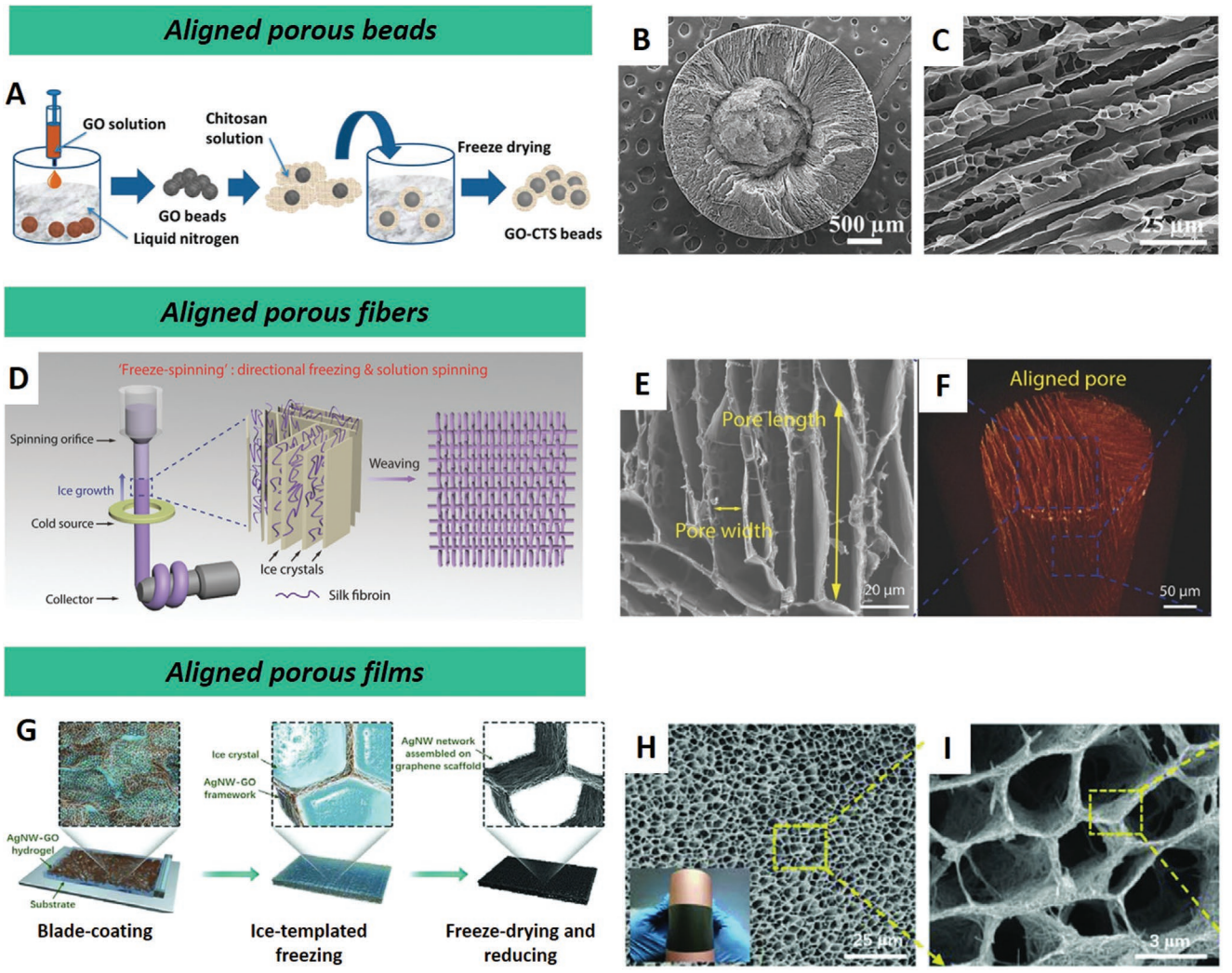

Figure 13. A–C) Process schematic and microstructures of GO-chitosan beads. Reproduced with permission.[29c] Copyright 2015, American Chemical Society. D) Schematic illustration of "freeze spinning" to realize continuous and large-scale fabrication of biomimetic fibers with aligned porous structures. E) Radial cross-sectional SEM image and F) X-ray computed microtomography images of aligned porous fibers. Reproduced with permission.[30b] Copyright 2018, Wiley-VCH. G) Schematic of the solution-based fabrication process of binary networks comprising Ag nanowires and graphene. H,I) Corresponding cross-sectional SEM images. Reproduced with permission.[32b] Copyright 2018, Wiley-VCH.

conferring distinct functionality. As a notable example, Ouyang et al. described inorganic–organic core–shell beads consisted of GO and chitosan formed by a two-step freeze-casting method for water treatment (**Figure 13**A).[29c] As illustrated in Figure 13B,C, in the GO/chitosan composite microspheres, the GO core is surrounded by long parallel channels ranging from the core to the surface of the chitosan shell. This distinctive structure allows rapid and extensive adsorption of heavy metal ions and cationic dyes. The aforementioned electrospraying combined with freeze-casting method was also applied to fabricate GO aerogel microspheres with a structure consisting of radially oriented microchannels.[29e] When this approach was extended to GO/chitosan aerogel microspheres, these channels assumed a honeycomb structure.[29g] High adsorption capacities and fast adsorption rates of heavy metal ions and cationic dyes as well as excellent recyclability, makes such porous microspheres promising candidates for efficient water treatment.

4.2. Aligned Porous Fibers

Integrating freeze-casting techniques with fiber production methods allows the synthesis of highly functional fibers for emerging applications including wearable electronics, lightweight electrical conductors, and highly insulating fabrics. The fabrication of fibers has drawn considerable attention as a means to harnessing the unique thermal, electrical, and mechanical properties of graphene in bulk form.[106] Important progress toward this end was reported by Xu and Gao,[64b] who used a aqueous liquid crystals of graphene oxide sheets in a wet spinning process to ultimately produce strong, flexible, directionally conductive graphene fibers. This process was subsequently developed further by integrating wet spinning with ice-templating to produce aligned porous fibers assembled from graphene oxide building blocks. The distinct core–shell structures thus obtained exhibit highly favorable

properties of low density, high strength, and excellent electrical conductivity.[30a]

Another strategy for producing cellular rGO wires is the combination of extrusion of GO emulsions with ice templating and thermal treatment.[8f] A GO emulsion usually involves a continuous aqueous solvent phase containing dispersed oil droplets. To enable successful extraction, the viscoelastic properties of a GO emulsion system can be controlled by adjusting the concentration of GO and oil, resulting in wires of viscous GO emulsions that maintain their shape (straight, curved, or spiral). Following thermal treatment, the rGO wires are several centimeters long and down to 200 mm in diameter. This processing route creates new opportunities for the fabrication of aligned porous graphene-based complex structures at the macroscale.

Further to graphene building blocks, recently, a continuous large-scale fabrication of silk fibroin fibers with aligned porous microstructures was achieved by combining processes of "directional freezing" and "solution spinning," namely "freeze-spinning" (Figure 13D).[30b] First, a wire is shaped by the extrusion of a well-dispersed viscous aqueous solution of silk fibroin. As the wire slowly passes through a cooled copper ring, ice crystals grow into a lamellar pattern within the wire, thus templating the ice morphology. When the extrusion speed is equal to the freezing speed, there forms a stable solid–liquid interface above the cold source. The frozen fiber is then collected and maintained at low temperatures to prevent melting. Subsequently, the collected frozen fiber is freeze-dried to conserve its porous microstructure. A roll of fiber can be obtained by this method and can be further woven into a textile. Having aligned porous microstructures (Figure 13E,F), such fibers show better strength and modulus relative to random pore structures, which enables these porous fibers to be woven into functional textiles. Although not yet commercially available, these light and strong polar bear inspired biomimetic fibers are of great promise toward highly insulating fabrics and clothing.

4.3. Aligned Porous Films, Membranes, and Meshes

Heterogeneous materials in the form of porous and infiltrated porous materials are of significant importance in diverse energy systems. The topology and connectivity of ion conducting and electron conducting phases play a key role in governing the mechanical and electrical performance in energy storage and conversion systems. Methods for the fabrication of films with tailorable pore structures, and their subsequent hybridization are of significant value in the design of supercapacitors as well as novel electrode systems for fuel cells and batteries. In recent years, the combined use of nanowires and graphene in electrodes has emerged as a promising approach in energy materials design and the use of freeze-casting techniques to obtain macroscopically flat porous structures from low-dimensional building blocks is ripe for further exploration.

Recently, graphene based films exhibiting dense layer-by-layer assembled structures have been developed using various methods such as coating and filtration assembly.[54a] However, such dense films lack the pore structures necessary to effectuate functionality in many energy materials. In particular, it is important to fabricate graphene film electrodes with connected pores that facilitate effective ionic transport pathways.[32]

Processes for the fabrication of porous graphene films are mostly similar to the fabrication of bulk freeze-cast graphene with the inclusion of an additional shaping step to produce thin layers prior to freezing and sublimation steps. The shaping of films is achieved either through filtration assembly,[32a] or through a blade coating method, using a viscous suspension,[32b] which is schematically illustrated in Figure 13G. Freeze cast porous graphene films (Figure 13H,I) commonly include secondary nanowire building blocks to facilitate electronic conduction, as this type of structure is predominantly of interest in electrode applications. Suspension properties in terms of solids loading, constituent ratios (GO/NWs) and viscosity govern the topology (phase connectivity) and porosity of the obtained electrodes and thus their overall performance. The key difference between the processing of freeze-cast films by blade coating or filtration assembly lies in the direction of the pores. In blade-coated graphene films, the pores are vertical, perpendicular to the plane of the film, while filtration assembly yields laminar pores in the plane of the film. A thin film containing perpendicular pores, can be considered as a mesh.

In order to produce porous free-standing graphene membranes with in-plane water transport channels via freeze-casting, an antifreeze assisted technique can be used by adding ethanol or methanol in GO suspension, which mitigates the kinetic instabilities in ice crystal growth and results in a more homogenous porosity between parallel graphene sheets.[10c]

4.4. Integrating Freeze Casting with Additive Manufacturing

The fabrication of 3D scaffolds in complex macroscopic geometries by freeze casting remains a significant challenge. Resolution limits of additive manufacturing processes limit their utility in forming fine interconnected pore structures. Integrating freeze casting with additive manufacturing processes offers a pathway towards the fabrication of porous scaffolds in diverse 3D geometries.

Freeze extrusion fabrication (FEF) has been used to create scaffolds with controlled porosity, using an approach akin to standard fused deposition modeling in which a 3D shape is built layer-by-layer by computer controlled extrusion and deposition of aqueous based colloidal pastes, followed by the solidification of the paste at low temperatures, with subsequent ice sublimation and sintering.[107] However, the formation of aligned micro pores is limited in this approach. Highly oriented pores can be obtained by a 3D ceramic/camphene-based coextrusion (3D-CoEx) technique (**Figure 14**A),[108] in which a continuous ceramic/camphene filament consisting of a pure camphene core and a frozen alumina/camphene shell is deposited by coextrusion. Subsequently, unidirectional macrochannels and interconnected micropores are created through removal of camphene.

Further to FEF and 3D-CoEx techniques, in recent years, unidirectional freeze casting and extrusion or inkjet-based additive manufacturing (Figure 14B) have been combined, allowing simultaneous printing and freezing, to produce porous ceramic,[37d] metallic,[37b] biomacromolecule,[109] and graphene

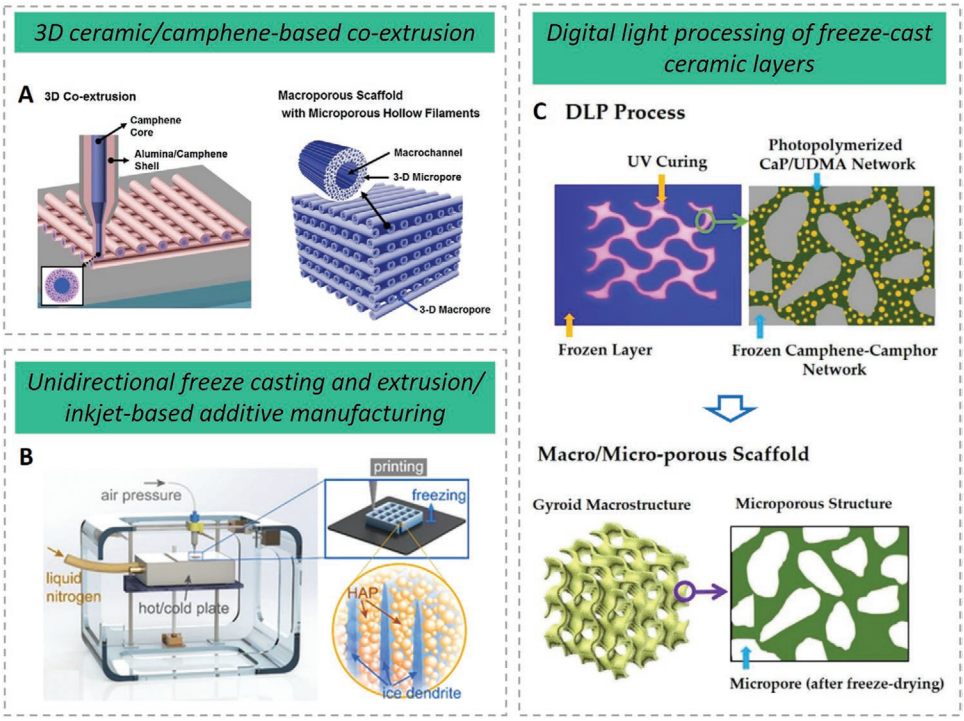

Figure 14. A) Schematic diagrams of 3D ceramic/camphene-based co-extrusion (3D-CoEx) for the production of macroporous ceramics consisting of highly microporous hollow filament. Reproduced with permission.[108c] Copyright 2015, Elsevier. B) Schematic of 3D printing combining freeze casting and extrusion/inkjet. Reproduced with permission.[37d] Copyright 2019, Wiley-VCH. C) Illustration of the manufacturing of a macroporous calcium phosphate (CaP) scaffold with a gyroid macrostructure comprised of microporous frameworks using DLP technique using a freeze-cast ceramic layer as the feedstock. Reproduced under the terms of the Creative Commons Attribution License.[111b] Copyright 2019, MDPI.

structures[37a] with interconnected pores across multiple length scales after being directly post-processed via lyophilization.

The additive manufacturing of graphene from graphene oxide inks has been the subject of several studies.[56,110] These inks, unlike ceramic slurries, contain very low solids contents, and generally consist predominantly of the solvent phase. This results in significant drying stress and shrinkage, which can be mitigated through freeze casting methods to yield stable highly porous structures, post printing, which can then be subjected to further processing such as sintering or infiltration with a second phase, including preceramic polymers.

A combination of freeze casting and additive manufacturing allows for fabrication of 3D graphene aerogel (GA) scaffolds with complex geometries/macrostructures and aligned pores. Recently graphene aerogels have been additively manufactured using a multinozzle drop-on-demand inkjet combined with freeze casting.[37a] In this process, the aqueous droplets solidify into ice crystals in the water-based GO suspension by contact with a cold sink (−25 °C). After post processing which consisted of immersing 3D parts into liquid nitrogen, freeze drying, and thermal annealing, functional graphene aerogels exhibiting honeycomb structures with aligned pores were obtained in controllable macroscopic geometries. As with other forms of graphene aerogels, these additively manufactured structures showed ultralight densities (0.5–10 mg cm^{-3}), significant electrical conductivity (≈15.4 S m^{-1}), and high compressibility. Another strategy for achieving ultralight hierarchical graphene materials is 3D printing of partially reduced graphene oxide (pr-GO) ink combined with freeze casting.[59] By simultaneously engineering 3D-printed macroscopic hollow structures and constructing an ice-crystal-induced cellular microstructure, graphene materials can achieve high stiffness and resilience.

Extrusion and inkjet-based additive manufacturing approaches are limited in their abilities to produce intricate geometries due to the simple geometry of filaments. To overcome this limitation, Kim et al. proposed photocurable ceramic slurries containing camphene-camphor as the porogen for use in digital light processing (DLP) techniques.[111] As illustrated in Figure 14C, thin layers of photocurable CaP suspensions containing diurethane dimethacrylate (UDMA) monomers could be solidified and photopolymerized by DLP.

4.5. Brick and Mortar Hybrid Composites

The fabrication of synthetic nanocomposite materials mimicking the structure of naturally occurring nacre is of great interest. Nacre, which in natural forms consists of aragonite platelets interspersed with a biopolymer phase, exhibits interesting mechanical properties including high hardness and fracture toughness. The use of freeze casting to produce nacre-like materials is realized using directional freezing as the lamellar structures that can be thus obtained offer an effective precursor to the fabrication of nacre-mimetic structures. In the fabrication of such systems, the freeze cast lamellar scaffold formed is infiltrated with a second phase,

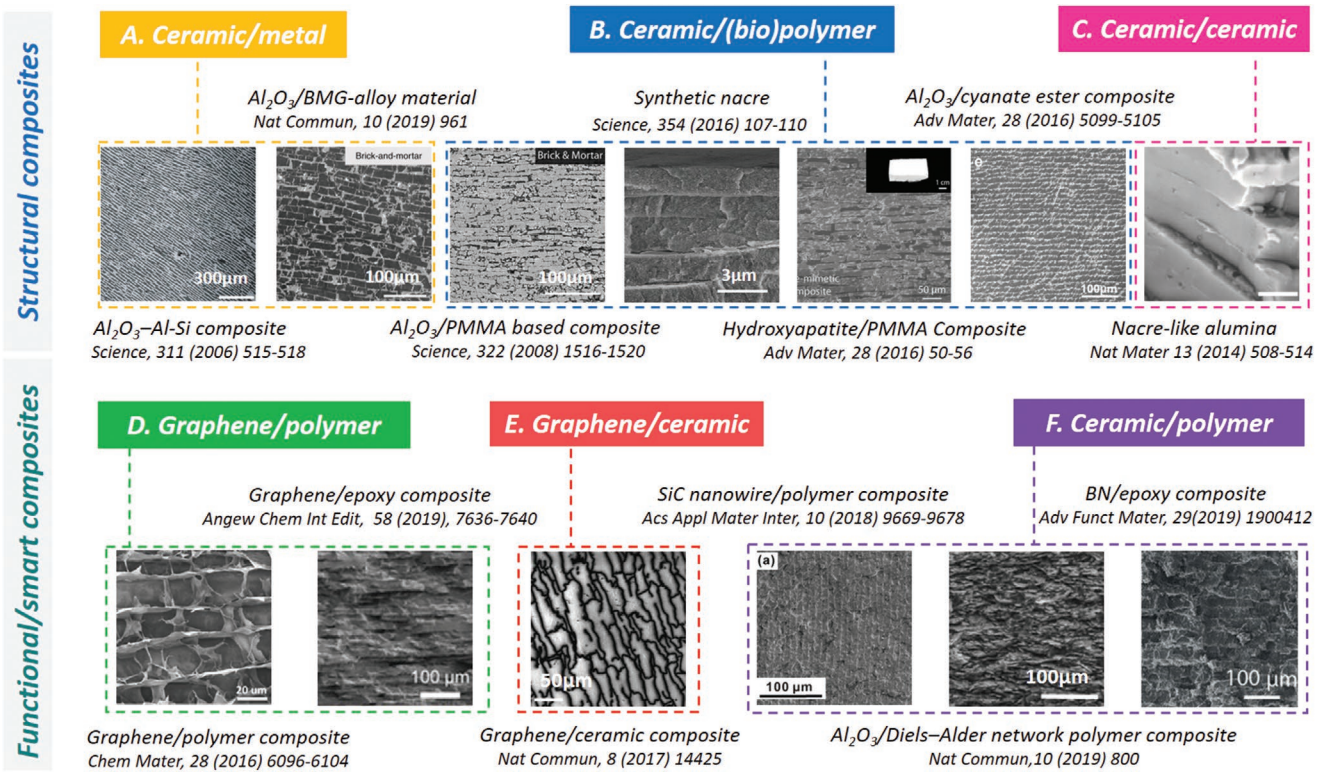

Figure 15. The development of brick and mortar hybrid composites. Structural composites: A) Left panel reproduced with permission.[1b] Copyright 2006, AAAS. Right panel reproduced under the terms of the Creative Commons CC-BY license.[44c] Copyright 2019, Springer Nature. B) From left to right: Reproduced with permission.[45c] Copyright 2008, AAAS. Reproduced with permission.[112a] Copyright 2016, AAAS. Reproduced with permission.[45b] Copyright 2016, Wiley-VCH. Reproduced with permission.[112b] Copyright 2016, Wiley-VCH. C) Reproduced with permission.[17] Copyright 2014, Springer Nature. Functional/smart composites: D) Left panel reproduced with permission.[62f] Copyright 2016, American Chemical Society. Right panel reproduced with permission.[117] Copyright 2019, Wiley-VCH. E) Reproduced under the terms of the Creative Commons CC-BY license.[42a] Copyright 2017, Springer Nature. F) Left to right: Reproduced with permission.[112c] Copyright 2018, American Chemical Society. Reproduced under the terms of the Creative Commons CC-BY license.[21] Copyright 2019, The Author(s), published by Springer Nature. Reproduced with permission.[12b] Copyright 2019, Wiley-VCH.

such as polymers, ceramics, or metals. So far, ceramic/polymer,[1b,45b,c,62j,79,112] ceramic/metals,[1b,44c,113] ceramic/ceramic,[17] metal/polymer,[72,73,114] macromolecule/polymer,[96j,k,115] graphene/polymer,[44a,b,45a,60a,b,62f,68,116] graphene/ceramic[42a] brick and mortar hybrid composites have been fabricated for structural, functional and smart applications (**Figure 15**).

The enhanced damage-resistance of brick and mortar composites stems from the presence of alternating layers with different properties, leading to load redistribution and reducing the stress concentration.[118] For this reason, the use of a ductile polymer as the minor binding phase alongside hard ceramic platelets is often the objective of nacre-mimetic synthesis. In typical freeze casting methods toward nacre-like materials, a layered ceramic scaffold is obtained as a first step. Such scaffolds have been produced using alumina and hydroxyapatite to date. Subsequently, the ductile phase is introduced to the freeze-cast scaffolds by a liquid infiltration approach. Ductile phases in freeze-cast synthetic nacres have included protein "glue,"[1b] polymethyl methacrylate,[45b,c] cyanate ester[112b] or metals.[1b,44c]

A second approach to form nacre-mimetic composites is the freeze casting of the ductile phase followed by mineralization of the pore spaces. This approach mimics the natural biological processes in molluscs through which nacre is generally formed. In one representative example, a chitosan scaffold in a laminar structure was formed by bidirectional freeze-casting, following freeze-drying the scaffold was converted to β-chitin by acetylation and an aragonite mineral phase was formed in the pores by solution infiltration and precipitation. Bonding was facilitated in this landmark study by the use of fibroin and hot pressing.[112a] In ceramics, improving toughness usually relies on the introduction of ductile metallic or polymeric phases, but this decreases the material's strength and stiffness as well as its high-temperature stability. Deville et al.[17] report a nacre-like ceramic without a ductile phase based on alumina platelets, alumina nanoparticles, and a silica–calcia liquid, formed by freezing suspensions under flow and field-assisted sintering approach. Such layered materials with submicrometer layer spacing present a unique combination of high strength (470 MPa), high toughness (17.3 MPa $m^{1/2}$), and high stiffness (290 GPa) and, having only mineral constituents as well as can retain their mechanical properties at high temperatures (600 °C).

In addition to structural functions, the freeze-casting based formation of nacre-like structures also serves to confer functional physical behavior in polymer matrix nanocomposites. Also termed inverse-nacre, formation of ultralight conductive nanowire (SiC or Ag) or nanosheet (graphene or BN) scaffolds by freeze casting and their subsequent infiltration

with polymer to form a ductile matrix results in a predominantly organic system in which superior properties can be attained including high conductivity,[44a,60a,72] excellent electromagnetic interference shielding,[68,119] and heat dissipation abilities.[12b,42c,44b,62f,j,80a-c,112c] Similarly, freeze-cast graphene scaffolds infiltrated with polymers or preceramic polymers can be used to produce self-healing and self-monitoring systems with inverse-nacre like structures.[42a,45a,117]

5. Emerging Applications of Freeze Cast Materials

The informed use of freeze-casting methods allows materials engineers to design cellular structures, both porous and dense, that are able to mimic the physical attributes found in diverse natural systems and harness these towards beneficial use in various applications. The scheme shown in **Figure 16** illustrates how freeze cast structures facilitate functional materials across multiple fields of applications.

5.1. Structural Applications

5.1.1. Damping and Superelasticity

The highly ordered porous structures of freeze-cast scaffolds facilitate very large recoverable compressive deformations relative to randomly porous systems, these deformations occur with varying levels of frictional energy dissipation, which depend on the structure and composition of the scaffolds. Consequently, the unique structures obtained by freeze casting offer new pathways toward high levels of weight-specific mechanical energy dissipation (damping) and large elastic deformations (superelasticity). The deformation and energy dissipation of cellular materials has a long been a subject of great interest towards the development of improved impact and vibration protection systems as well as acoustic insulation. As cells are compressed, energy is reversibly stored which allows for significant elastic deformations while friction of cell walls results in the dissipation of energy and thus damping. In porous foams, the total energy absorbed during a cycle of deformation and recovery E_{total} corresponds to the area contained in the stress–strain curve and the energy absorption efficiency is derived as: $E = E_{total}/\sigma_m$, where σ_m is the maximum stress.[120] Novel freeze casting approaches are of interest in energy dissipation for two main reasons. 1) The use of low dimensional building blocks such as graphene and ceramic nanofiber allows for very high strength to weight characteristics. 2) The ability to create well-ordered pore structures allows for increased energy absorption efficiency, high damping performance, and/or rapid elastic recovery.

Freeze casting has emerged as an effective technique for the fabrication of ceramic scaffolds for mechanical damping. The energy absorption efficiency and elastic response of

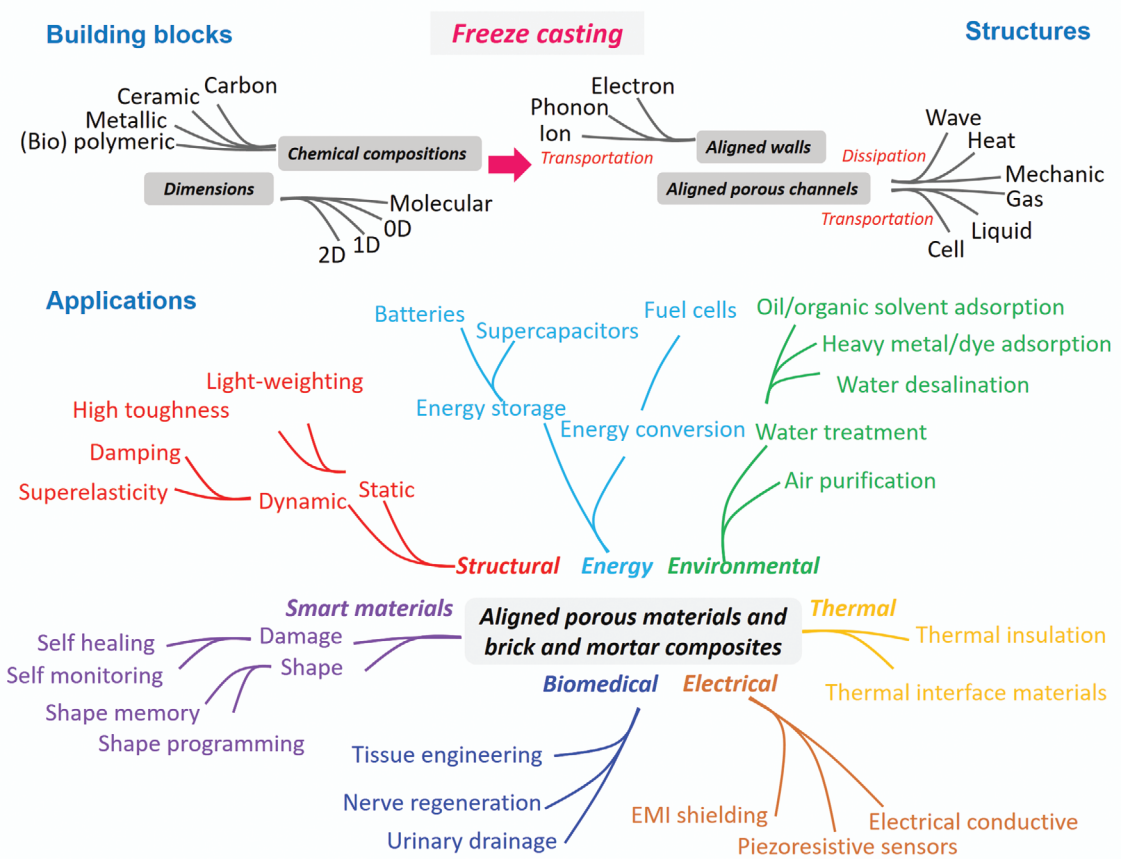

Figure 16. Emerging applications of freeze-cast materials.

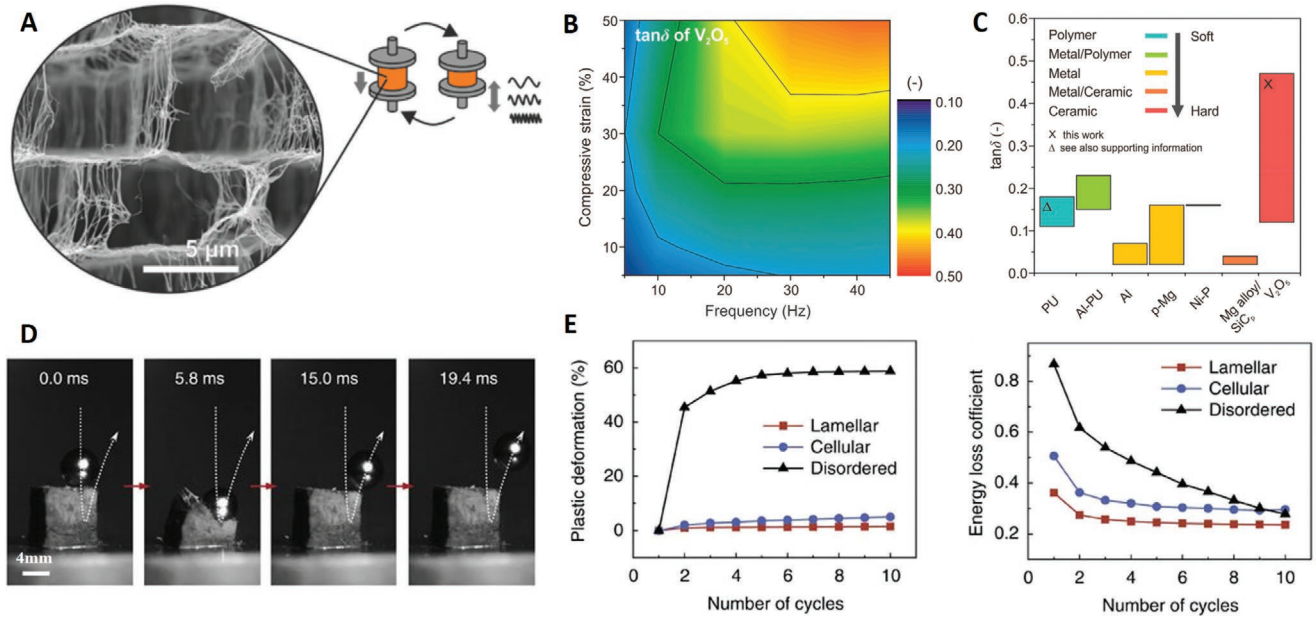

Figure 17. A) Hierarchically structured V_2O_5 scaffolds for mechanical dampers. B) Compressive-strain and frequency-dependent viscoelastic response of the V_2O_5 scaffold. C) Damping capacities of different types of foams. Reproduced with permission.[71] Copyright 2018, American Chemical Society. D) Real-time images from high-speed camera showing that C–G monolith can rebound a steel ball at large speed, in a spring-like fashion. E) Plastic deformation and energy loss coefficient of the three kinds of C–G monoliths during the first 10 compression cycles at a maximum strain of 80%. Reproduced under the terms of the Creative Commons CC-BY license.[22] Copyright 2016, The Author(s), published by Springer Nature.

a porous material can be greatly enhanced by imparting a structure of aligned pores, such as that found in freeze-cast structures.[8f,22,41,42b,58,62e,71] The orientation and geometries of pores imparted by freeze-casting govern dissipation and recovery during compressive strain. Knöller et al. have in recent years reported various biomimetic scaffold structures based on vanadium pentoxide nanofibers. At nanoscopic scales, V_2O_5, as other ceramic compounds, exhibits distinct mechanical behavior, showing flexibility that diverges from the brittle behavior found at larger scales. Coupled with their unique arrangement, ultralight V_2O_5 nanofiber based cellular networks fabricated by freeze casting have shown high damping capacity, exhibiting values of tan δ (loss factor, equal to the loss modulus divided by the storage modulus), of up to 0.47; damping performance which significantly exceeds existing materials(**Figure 17**A–C).[71]

Graphene aerogels formed by freeze casting, which as has been seen in this work are the subject of intensive investigations across diverse applications, are of interest also toward materials exhibiting enhanced energy absorption. Their extremely low density, superelasticity, and mechanical robustness render such systems highly suitable toward the dissipation of impact energy and acoustic insulation.[8f,58,62e]

Another promising carbon–graphene monolith with parallel, aligned, lamellar multiarch microstructure was obtained by a bidirectional freezing and annealing process.[22] An energy loss coefficient of only about 0.2 was achieved even with compressive strains up to 90%, and the monolith was able to rebound a steel ball (0.87 g, 100 times heavier than itself) at a high speed of 580 mms^{-1} (Figure 17D). Compared with open-cell foams with disordered pore structures, these lamellar C–G monoliths presented relatively little reduction in strength, permanent deformation and energy dissipation in cyclic compression. Such lamellar architectures with multiarch microstructure are particularly beneficial to tolerating large geometric deformations (Figure 17E).

5.1.2. High Fracture Toughness

A further mechanical attribute that can be attained in brick and mortar hybrid structures formed by infiltration of a freeze-cast scaffold is high fracture toughness. A high resistance to crack propagation as found in brick and mortar hybrid composites is reminiscent to that observed in the mother-of-pearl bearing molluscs from which they derive inspiration.[1b,17,45c,117]

5.2. Energy Storage and Conversion

As previously mentioned, the controlled heterogeneous structures that can be obtained by freeze-casting methods allow for the optimization of electronic, thermal, and ionic transport properties in energy materials, with significance in electrochemical conversion and storage systems. In batteries for example, for a given set of active phase and conductive materials, the relationships between structure and performance in electrodes is a very active field of research. Freeze casting offers new obtainable electrode structures and thus enables the advancement of this aspect of materials optimization. Toward thick electrodes with high active material loadings and improved volumetric energy density, aligned porous structured electrodes can provide effective ionic transport channels relative to traditional densely packed or random porous structures.[69,121] In freeze cast electrodes high levels of porosity further relieve the strain induced

by volume changes during charge/discharge cycles.[32b,121e,122] Freeze cast scaffolds are also promising as fillers for solid polymer electrolytes, which can significantly improve the mechanical properties and maximize ionic conductivity.[123]

The use of low-dimensional carbon, namely CNTs and graphene, in electrode systems offers high levels of performance owing to the excellent conductivity exhibited by these allotropes. Additionally, the utilization of ceramic nanoparticles in solid polymer electrolytes is a widely employed strategy to enhance ionic conductivity, thermal stability, mechanical strength, and electrochemical stability. To extract full benefit from these carbon structures in electrodes and ceramic fillers in electrolytes, their use as building blocks in freeze-casting processes is a logical step. To this end, freeze-casting techniques are investigated for the development of both novel carbon-based aligned porous electrodes and vertically aligned ceramics filled electrolytes to enhance performance in three types of batteries, namely Li-ion, Li-metal, and Li–S batteries.[36c,53,121a,c,e,123b,c,124]

In the field of Li-ion batteries (LIBs), a coassembly freeze-casting method was employed to construct low-tortuosity and mechanically robust electrodes.[69] Vertically aligned $LiFe_{0.7}Mn_{0.3}PO_4$ nanoplates (LFMP NPs) and graphene hybrid frameworks, driving a 2.5-fold increase in ion transfer and improved cycling performance rather than that of random structured electrodes (**Figure 18**A). In the sandwich framework, LFMP NPs are entrapped in the graphene wall in a "plate-on-sheet" contact mode, which prevents the detachment of NPs during cycling and forms electron transfer pathways in the electrode.

Lithium–sulfur (Li–S) batteries, based on metallic lithium as the anode and elemental sulfur as the cathode, are promising energy storage systems for next-generation electric vehicles due to their high theoretical capacity and low cost. However, the insulating attribute of sulfur, strain during charge/discharge processes, and the migration of dissolved polysulfides toward anodes during the discharge, remain as obstacles in the development of Li–S batteries. An effective approach to overcome these problems is the use of freeze casting to fabricate carbon-based supports, imparting increased electronic conductivity at the sulfur cathode while restraining the solubility of lithium polysulfides. Inspired by nacre structures found in abalone, a layered CNT matrix with compactly embedded sulfur was designed as the cathode for Li–S batteries using a unidirectional freeze-drying approach.[53] The compact lamellar configuration made possible through freeze-casting, with closely contacted neighboring CNT layers, facilitated a high sulfur loading (10 mg cm^{-2}) and areal capacity (11.0 mAh cm^{-2}) with significantly restrained polysulfide shuttling, resulting in a superior cyclic stability and an excellent rate performance for the produced batteries (Figure 18B).

The use of metallic lithium as an anode in next-generation batteries is hampered by limited charging/discharging rates and poor cycling performance. Using freeze-casting methods to assemble a vertically aligned porous architecture with a binary network of continuous silver nanowires on an interconnected 3D graphene skeleton as a host for Li-metal in composite anodes, can deliver improvements in both charging/discharging rates and long-term cycling performance for Li-metal batteries. These structures further confer the mechanical strength and toughness required to support massive Li deposition and buffer the internal stress fluctuations during repeated Li stripping/plating even under ultrafast charging/discharging rates (Figure 18C).[32b,122] Aside from vertical aligned porous electrodes, more recently, a layered holey carbon scaffold with enhanced thermal diffusivity and superior ion accessibility was developed to stabilize Li metal electrodes.[125] This novel Li anode exhibited a high coulombic efficiency and a long cycle life at a high current density of 4 mA cm^{-2}. In a cell where $LiFePO_4$ composite was used as the cathode, a high capacity of 90 mAh g^{-1} was achieved at 10 C with a high capacity retention of 92% after 1800 cycles.

A further proposed application for aligned porous materials is supercapacitors.[29f,32a,65b,126] 3D cellular graphene films as the active material in supercapacitors were fabricated by filtration assembly of partially reduced GO and a subsequent freeze-casting process.[32a] The structure and conductivity of freeze-cast graphene films facilitates good performance in terms of power density and energy density, with attained performance values of 7.8–14.3 kW kg^{-1} and 1.11 Wh L^{-1} respectively (Figure 18D,E).

Freeze casting techniques are increasingly studied toward implementation in high-performance fuel cells. As with energy storage systems, the structures offered by freeze casting confer effective ionic, electronic and mass transport properties. Structuring of fuel cell anodes by ice templating offers a pathway to minimize the use of expensive catalysts and enhance anode performance for diverse fuel conversion applications. As an example of such studies, Gutiérrez et al.[8a] reported 3D aligned porous MWCNTs structures hybridized with Pt nanoparticles assembled by freeze casting approach. The obtained microchannelled structures endow them with high electron conductivity with the value of 2.5 S cm^{-1}. These MWCNT-based structures were found to impart improved performance as anodes for a direct methanol fuel cell, enhancing the catalytic activity toward methanol oxidation through efficient fuel and product diffusion. The biomimetic pore structures conferred by freeze casting also offer methods to fabricate microbial fuel cells, with such systems exhibiting effective microbe mediated conversion of organic waste into hydrogen. The high surface area and effective mass/electron transport effectuated by nanocomposite freeze cast electrodes facilitate the adhesion and functionality of electroactive bacteria in such bioelectrochemical systems.[50c,61a]

5.3. Environmental Remediation

Aligned porous scaffolds formed by freeze-casting, especially those based on CNT, graphene, and macromolecular building blocks, exhibit promising prospects in the removal of pollutants from contaminated water and air for the following reasons. First, the porous structures formed by freeze casting offer excellent levels of specific surface area, comparable to nanopowders, without incurring the challenges of solids separation encountered with powder-form adsorbents. Second, the aligned pore networks in freeze cast materials are conducive to highly effective fluid transport relative to randomly porous materials, this allows for high throughput in filtration and adsorption applications with relevance to water treatment. Third, freeze-casting processes allow the obtainment of ordered

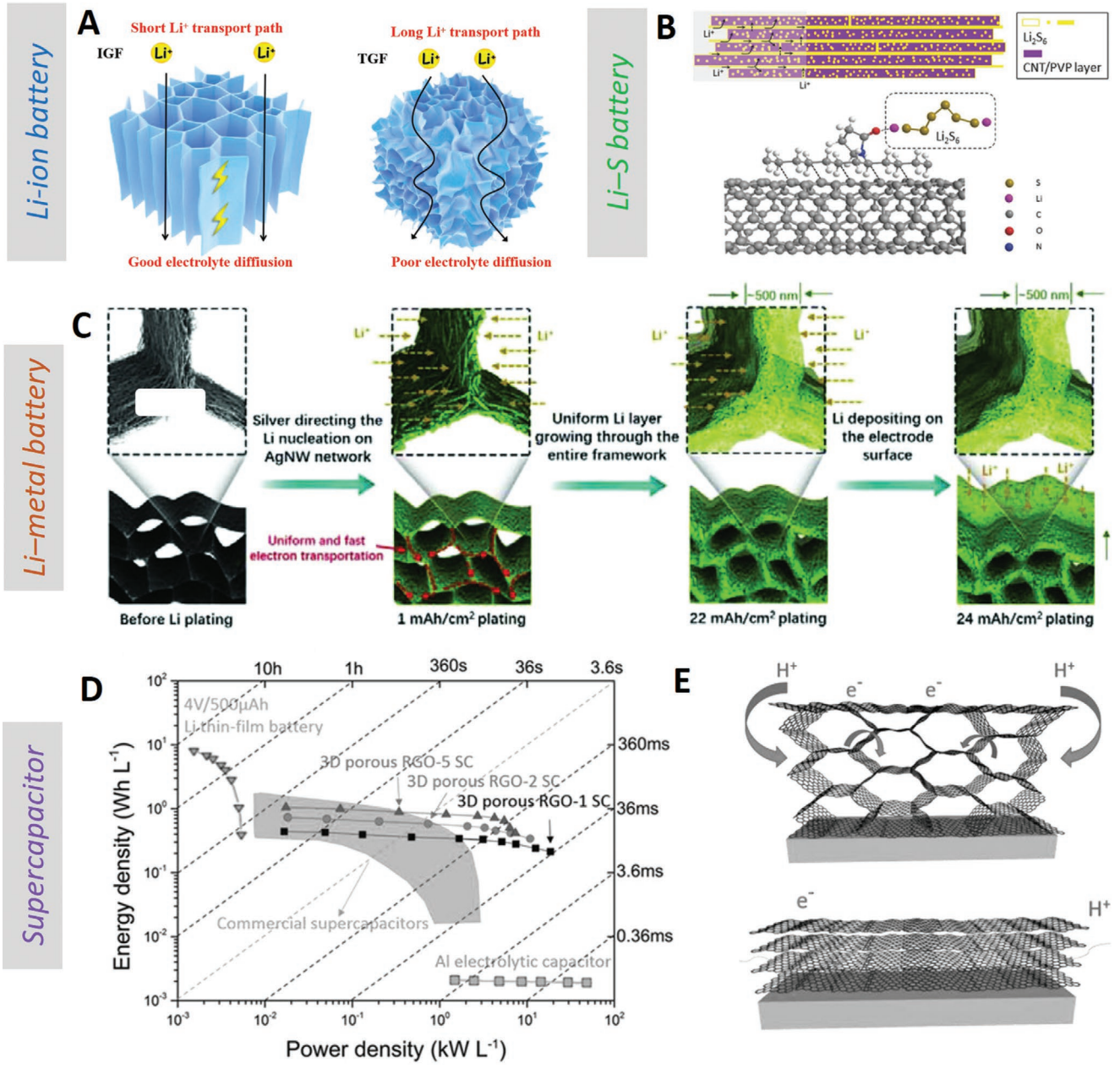

Figure 18. A) Illustration of Li-ion transfer and electrolyte diffusion in LFMP-IGF with vertical channels and disorder structure. Reproduced with permission.[69] Copyright 2019, Wiley-VCH. B) Schematic diagram of the NS electrode and the catholyte within. Reproduced under the terms of the Creative Commons Attribution License.[53] Copyright, The Authors, published by Wiley-VCH. C) Schematic illustration of the Li plating in the 3D-AGBN host at different states. Reproduced with permission.[32b] Copyright 2018, Wiley-VCH. D) Ragone plot of the volumetric power density versus energy density for 3D porous RGO supercapacitors compared to alternatives. E) Schematic illustration of ion and electron transport in a 3D porous RGO film and an RGO film. Reproduced with permission.[32a] Copyright 2016, Wiley-VCH.

porous structures from inert ceramic or carbon building blocks, allowing thermally and chemically stable systems that could otherwise not be obtained.[127] Based on the above advantages, aligned porous structures in forms such as microspheres, membranes, and scaffolds provide superior applications in removing contaminants such as dyes,[29a,c,g,67a] oil and organic solvents,[8f,15b,29e,i,42b,43b,60c,62l,103d,128] heavy metals[29g,62b] from water, water desalination,[10c,23,129] as well as air treatment.[43e,65c]

As an example, a vertical and radially aligned rGO aerogel with hydrophobic surface was shown to selectively absorb oil fouling contaminants within the order of few seconds.[15b] Benefiting from numerous narrowing capillary channels, organic solvents are particularly prone to be drawn into the pores of this rGO aerogel by capillary tension forces. In this study, a maximum absorption capacity of 374.7 g g^{-1} for carbon tetrachloride was achieved, a notable improvement compared

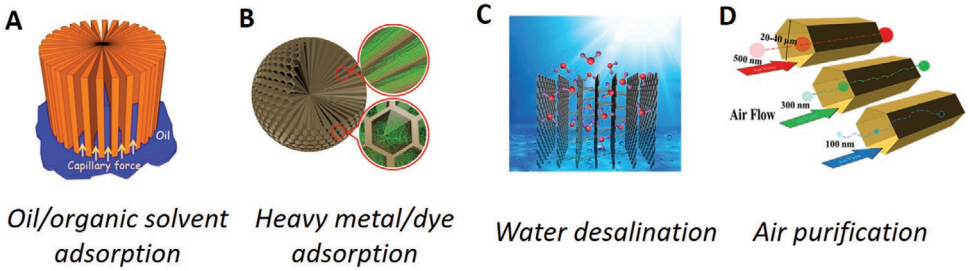

Figure 19. A) Illustration of a radially aligned rGO aerogel for oil/organic solvent absorption. Reproduced with permission.[15b] Copyright 2017, American Chemical Society. B) Illustration of GCAM with honeycomb-cobweb and radially oriented microchannel structures for heavy-metal/dye adsorption. Reproduced with permission.[29g] Copyright 2017, American Chemical Society. C) Illustration of the water-transport channel mechanism in vertically aligned graphene membrane for water desalination. Reproduced with permission.[10c] Copyright 2017, American Chemical Society. D) Schematics illustrating air purification of the wood-like aerogels for particles of different sizes. Reproduced with permission.[43e] Copyright 2019, American Chemical Society.

with conventional rGO aerogels (**Figure 19**A). In another work shown in Figure 19B, GO/chitosan aerogel microspheres (GCAMs) with radially oriented microchannel structures obtained through the integration of electrospraying with freeze-casting[29g] were applied successfully for water purification. The unique structure of such GCAMs shortens the internal diffusion path and assists rapid adsorption, while conserving a high adsorption capacity for heavy metal ions and dyes with good recyclability. The broad-spectrum and reusable adsorption performance imparts these GCAMs promising for highly efficient water treatment. In other work toward solar water treatment (Figure 19C), vertically aligned graphene sheet membranes, prepared by an antifreeze-assisted freezing technique were harnessed to enable solar driven water treatment by facilitating effective water transport and vapor release.[10c]

Aligned porous scaffolds are able to remove also gaseous contaminants in a manner analogous to contaminant removal from water (Figure 19D). For example, stable GO aerogels with the addition of tourmaline were found to be effective for particulate matter (PM) removal.[65c] The filtration efficiency of PM2.5 reaches 95.1% after 1 h adsorption of PM2.5, which is 2.5 times higher than that of traditional cotton and activated carbon filters and about 1.7 times higher than that of pure GO aerogel. Furthermore, the aerogel morphology can still maintain high stability, and the PM2.5 filtration efficiency is maintained even after repeated cycles of filtration and recycling.

5.4. Thermal Applications

5.4.1. Thermal Insulation Materials

Inorganic aerogels formed by sol–gel methods and supercritical drying techniques are widely known to exhibit highly effective thermal insulation. While thermally insulating aerogels were initially limited predominantly to materials based on silica and other ceramic building blocks, in recent years, as with other fields of application, studies into carbon and biomacromolecule nanostructured based freeze cast systems have delivered new performance benchmarks. Although conventional ceramic aerogels, such as SiO_2, Al_2O_3, ZrO_2, and SiC exhibit excellent heat resistance and low thermal conductivity, the common use of these aerogels has been plagued by their poor mechanical properties, namely brittleness, and safety concerns related to consequent dust release.[130] In aerogels produced through freeze casting methods, the use of low dimensional building blocks and the presence of aligned pores confers flexibility to the obtained porous materials allowing for recoverable deformation without failure and breakage of cell walls. By using freeze cast scaffolds in thermal insulation systems, high levels of performance can be obtained in both mechanical and thermal realms, thus overcoming the traditional limitations of brittleness in aerogels. This is particularly important for the development of advanced insulating materials for clothing, vehicles, and space systems.

Unlike conventional aerogels, aligned freeze cast pore structures give rise to anisotropic thermal insulation. The thermal insulation performance of a freeze cast material is significantly better in the direction orthogonal to the pore orientation due to a higher density of gas gaps. The thermal conductivity of a cellular monolith (λ) is determined by the sum of thermal convection (λ_{conv}), solid conduction (λ_{solid}), gas phase conduction (λ_{air}), and radiative heat transfer (λ_{rad}).[30b,62d] As illustrated in **Figure 20**A, thermal convection (λ_{conv}) is largely restricted in cellular scaffolds as air is constrained within individual micropores. Thermal conduction in the gas phase contained in pores is dependent on gas pressure and pore size (relative to the mean free path of gas molecules) and is generally significantly lower relative to solid phase conduction ($\lambda_{air} << \lambda_{solid}$). This means that for a given cell size, increasing the porosity of an aligned porous system reduces the overall thermal transport and improves its insulating properties. Freeze cast structures assembled from low dimensional building blocks such as nanowires or nanotubes further exhibit sub-micrometer pores within the ice-templated lamellar walls, which are often comparable in their size to the mean free path of gas molecules. Known as the Smoluchowski effect, when the characteristic length of the pore space is of similar magnitude to the mean free path the gas thermal conductivity is reduced.[131] This translates to yet higher levels of thermal insulation performance in multiscale porous freeze-cast scaffolds relative to single-scale materials of similar porosity.

Besides thermal convection and conduction, heat is transferred across pore spaces through radiation, mainly at infrared wavelengths. Carbonaceous materials are known to be efficient

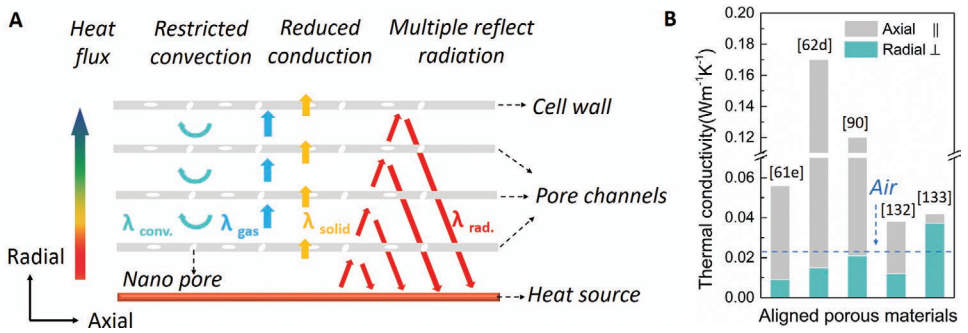

Figure 20. A) Contributions to thermal conductivity in the radial direction of aligned porous materials. B) Thermal conductivity values in axial and radial directions of typical aligned porous materials.

infrared absorbers and are therefore regularly used to reduce the radiative contribution in insulating materials. The presence of pores aligned perpendicular to the heat gradient results in a high density of solid–air interfaces and thus brings about a marked improvement in the reflectance of infrared radiation through a "multiple reflective effect" at a constant incident angle.[30b,62d]

Toward highly effective and mechanically robust thermal insulation systems, aligned porous structures assembled from diverse building blocks including silk fibroin fibers,[30b] anisotropic nanocellulose-based foams,[62d] polymeric woods,[93] graphene/polyimide foams,[61e,132] aramid nanofiber aerogels,[133] lamellar-structured ceramic nanofibrous aerogels[41] and ceramic microfiber networks[8b] have been developed by freeze casting methods showing highly effective thermal insulation performance in radial direction (Figure 20B). For example, Wicklein et al.[62d] reported lightweight (7.5 kg m^{-3}), highly porous (99.5%) foams with aligned tubular pores prepared through unidirectionally freezing colloidal suspensions of CNFs, GO, and sepiolite nanorods. The thermal conductivity in the radial orientation of CNF based foams is as low as 15 mW m^{-1} K^{-1}. Moreover, the mechanical properties of these foams showed considerable improvements relative to earlier cellulose based systems. Results from studies such as this provide substantial motivation to continue the development of high-performance thermal insulating materials based on sustainably produced low dimensional building blocks for the improvement of energy efficiency in the built environment. In silica- based ceramic nanofiber aerogel (CNFA) systems, which show improved mechanical performance relative to traditional SiO_2 aerogels, thermal conductivity values of 25 mW m^{-1} K^{-1}, were obtained alongside superelastic deformation characteristics.[41] These results demonstrate the promise of developing freeze-cast CNFAs as robust high-performance insulation materials.

The implementation of thermally insulating systems with aligned pores in textile form facilitates the development of thermal stealth materials and high performance clothing and protection systems for use in extreme environments. The fabrication of biomimetic aligned porous fibers, as discussed in the previous section of this article, facilitates the attainment of excellent thermal insulation properties.[30b]

5.4.2. Thermal Interface Materials

The development of electronic devices with higher on-chip power densities presents challenges in heat removal and motivates the development of new materials with high thermal dissipation behavior, known as thermal interface materials (TIMs), which serve to reduce thermal resistance between heat generating devices and cooling components (heat sinks). Although freeze-cast materials are more commonly associated with thermally insulating structures, with high void ratios, the use of ice-templating to fabricate aligned graphene or boron nitride sheets within polymer matrix composites has been found to effectuate highly efficient thermal conductivity while maintaining electrical insulation.

In the fabrication of TIMs based on highly thermally conductive 2D nanostructures, the use of ice templating serves to align platelets and ensure the formation of highly efficient thermally conductive pathways. Such pathways are not achievable with randomly dispersed 2D phases in polymer matrix (**Figure 21**A–C). The polymer phase serves to impart flexibility and electrical insulation to the overall composite. To date, 3D scaffolds containing low dimensional nanostructures of BN,[12b,80a–c,134] graphene,[42c,62f,135] SiC,[112c] carbon fiber,[136] and their hybrid materials[44b,62j,137] based 3D scaffolds have been studied as thermal interface materials and their thermal conductivity values are summarized in Figure 21D. As an example, Zeng et al.[80a] fabricated a 3D network of BNNSs by freeze casting and subsequent epoxy infiltration. The obtained composites exhibited a high thermal conductivity (2.85 W m^{-1} K^{-1}) at relatively low BNNSs loadings (9.29 vol%). In such freeze cast systems, the filler network, layer density, and thickness of the platelets play a key role in mitigating phonon scattering, and thus maintaining thermal conductance. In certain boron nitride composites, thermal conductance values of up to 6.07 W m^{-1} K^{-1} have been achieved.[12b] As shown in Figure 21E,F, the temperature difference is as large as 10 °C between a commercial silicone and BNNS/epoxy composite after being integrated as TIM in between a 20 W LED chip and a Cu heat sink, demonstrating the attractive capability of BNNS/epoxy composite in heat dissipation.

Further to boron nitride, thermally conducting structures have been designed by freeze casting using graphene, SiC

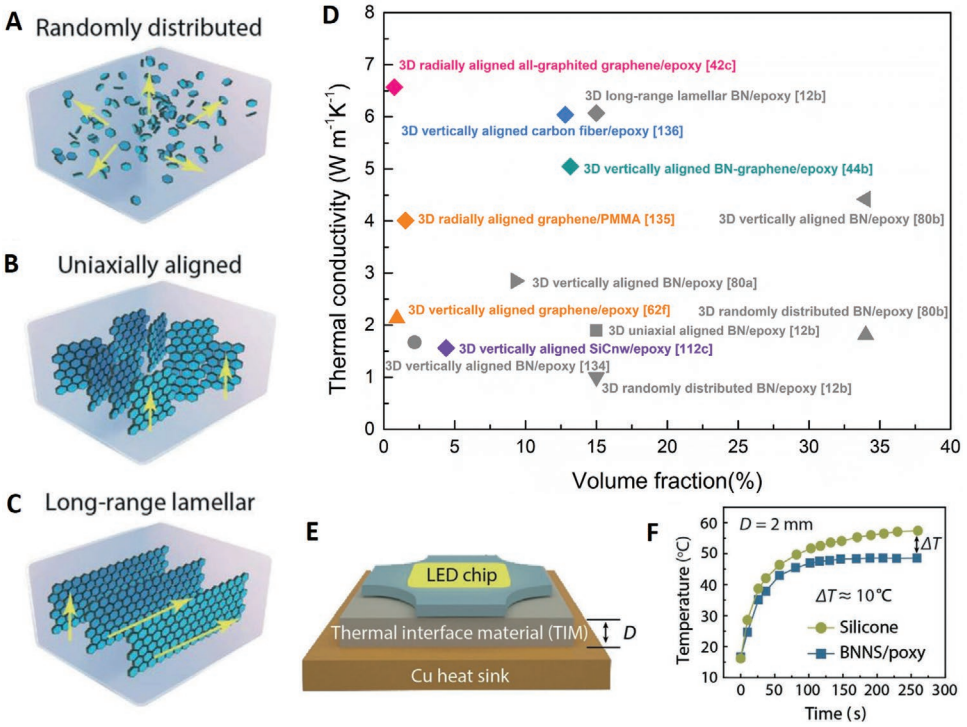

Figure 21. A–C) Schematic illustration of BNNS/epoxy composites with three different filler networks. D) Thermal conductivity of the typical thermal interface materials. E,F) Demonstration of BNNS/epoxy composite as a TIM. Reproduced with permission.[12b] Copyright 2019, Wiley-VCH.

nanowires and combined BN/rGO as scaffolds in conjunction with polymer matrices.[42c,44b,62f,112c,137b] These studies have shown that through careful design, effective phonon transport is achievable at low loadings of nanosheet phases.

5.5. Electrical Applications

5.5.1. Highly Conductive Materials

In certain applications such as electronics, energy storage, catalysis, fuel cells, and medical devices, where weight minimization is a key concern, there is an increasing demand for highly electrically conductive materials with very low specific densities. By aligning highly conductive nanomaterials, such as nanowires or graphene, freeze-casting processes offer a highly effective route to fabricate bulk materials exhibiting high electrical conductivity in ultra-lightweight forms.

For instance, ultralight conductive Ag nanowire aerogels with density ranging from ≈10 to 50 mg cm^{-3}, exhibited electrical conductivity from 1.5 to 5.1 × 10^4 S m^{-1}.[8c] As mentioned previously, such Ag nanowire scaffolds exhibit a high density of aligned nanowires with a much lower density of bridging nanowires. This combination results in optimized mechanical robustness and density specific conductivity. In the case of graphene scaffolds, an ultralight rGO cellular network with a low density of 1.5 mg cm^{-3}, was fabricated by freeze casting achieving a conductivity of 0.4 S cm^{-1}, which is one order of magnitude higher than that of a graphene elastomer with similar density.[8f] Similarly the use of nanowire or graphene networks formed by freeze casting can be used to fabricate polymer matrix composites with excellent electrical conductivity.[44a,60a]

In addition to the ultralow levels of density achievable in conductive freeze-cast scaffolds, this processing route can be utilized to fabricate systems with highly robust conductivity over large regimes of deformation. Ordered aerogels and hydrogels formed through freeze casting have been studied toward stretchable conductors that are resilient to extreme levels of cyclic deformation including stretching, twisting and bending.[72,73,79,116a]

5.5.2. Piezoresistive Materials

The strain-dependent electrical conductivity and the aforementioned superelasticity of anisotropic foams and aerogels,[8g,9b,66,67b,138] and nanocomposites[72,139] makes them suitable for applications as piezoresistive sensors. That is to say, materials exhibit strain-dependent impedance over large deformation regimes. Numerous studies have explored the use of freeze-cast scaffolds as strain sensors, using the deformation dependent conductivity of biomimetic aerogels and hydrogels formed from building blocks including graphene, SiO_2 nanofiber, AgNWs to gauge compressive or tensile deformation. For example, a biomimetic graphene aerogel[8g] with lamellae structure presents pressure-sensitive behavior. The conductivity of graphene aerogel depends on compressive strain, and it shows good cyclic performance due to the good mechanical properties of the graphene aerogel.

5.5.3. Electromagnetic Interference Shielding Materials

As diverse devices that emit electromagnetic radiation proliferate, and the frequencies utilized by these devices shift to higher regimes, it is increasingly important to provide electromagnetic shielding to ensure the function of electrical components. In particular achieving good shielding from GHz frequencies in compact, flexible, transparent, and low cost systems is an objective of numerous research efforts across multiple disciplines. The incorporation of highly conductive nanostructures such as graphene and CNTs into polymeric matrices provides a pathway toward highly effective and compact electromagnetic interference (EMI) shielding materials. In such shielding applications, radiation must be either reflected or absorbed to impart good EMI shielding effectiveness (EMI SE); thus, high electrical conductivity is essential. Foams and aerogels comprising nanowires, nanotubes or nanosheets combine both mechanisms to enhance EMI SE, by inducing multiple internal reflections inside the porous structure, resulting in additional scattering and absorption of EM radiation.

Freeze casting facilitates the optimized utilization of these effects as it enables the controlled alignment of heterogeneous nanostructures at low volume fractions in porous materials,[43c,d,62i,81b,140] aligned porous nanocomposites [114,141] and conductive polymer composites with 3D aligned porous fillers[68,119] as advanced electromagnetic interference shielding materials. That EMI SE divided by thickness of the aligned porous shielding materials as a function of density is summarized in **Figure 22**A. A lightweight ordered structure of graphene/SiC aerogels[62i] fabricated by the directional freeze-casting was found to exhibit a minimum reflection loss of −47.3 dB at 10.52 GHz for a thickness of 3 mm, with an effective bandwidth of reflection loss. In another study, Zeng et al.[43c] applied freeze-casting methods to synthesize composite aerogels containing rGO and lignin derived carbon with an ordered structure. The resulting materials exhibited very low densities, high elasticity and provided high EMI SE in the frequency regime 8.2–12.4 GHz (known as the X band). The mass specific shielding efficiency in such materials was found to be to 53 250 dB cm^2 g^{-1}, which represents a benchmark for such systems. Further studies have investigated alternative graphene-based composites, including polymer matrix systems.[68,119] In general, the alignment of graphene sheets in these ice templated materials is shown to enable multireflections and thus effective attenuation of incident high frequency radiation in versatile forms. Finally, it is worth noting that recently 2D MXene-based aligned porous structures have been emerging as alternative EMI shielding materials due to their electrical conductivity.[9c,81,140b] Koo and co-workers[140b] recently reported a 3D porous $Ti_3C_2T_x$/CNT aerogel fabricated via a bidirectional freezing casting for lightweight EMI shielding application. As illustrated in Figure 22B, the synergism of its high-conducting and lamellar porous structure contributed extensively to EMI SE value of 103.9 dB at 3 mm thickness at the X-band frequency.

5.6. Biological Applications

The development of novel high-performance porous scaffolds constitutes a key focal point in the realm of biomaterials. The function of porous scaffolds in biomedicine relates to tissue engineering and necessitates properties of mechanical strength and bioactivity. The enhancement of both of these attributes relies on the design of composition and pore structures. While at the atomic-scale numerous bioresorbable crystalline and amorphous material systems are under investigation for use in tissue engineering, the use of freeze-casting methods opens up new avenues of progress in the design of biomaterial scaffolds that support cell growth in bone and nerve regeneration.[105,142] The biomimetic structures that can be formed through freeze-casting can be tailored to mimic natural extracellular matrices (ECM) in terms of pore structure, chemical composition, and mechanical properties.

The use of unidirectional freeze casting to impart aligned porous structures has been conducted in various established biomaterial systems including bioactive polymers, ceramics, and bioglasses.[143] The cellular lamellar structures formed thusly are found to confer high strength, rapid bioresorption and effective cell intergrowth in these systems. In recent years novel building blocks have been applied in conjunction with freeze-casting to create bioactive scaffolds. Multiwall carbon nanotubes (MWCNTs) in particular have emerged as a candidate building block for the fabrication of biomaterial scaffolds. The strength and multiscale biomimetic porosity that arises through the ice-templating of carbon nanostructure

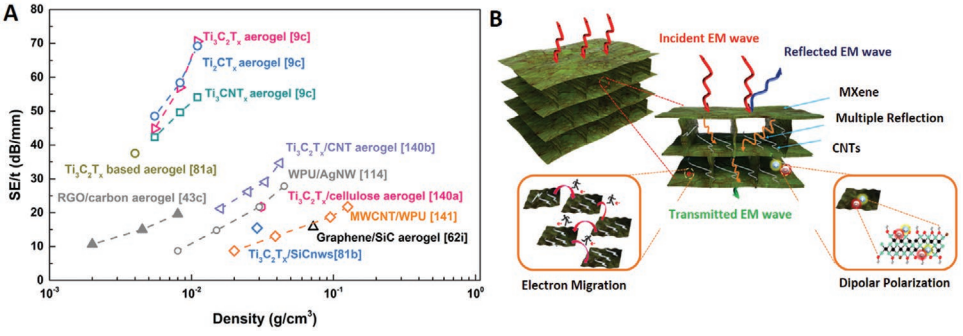

Figure 22. A) Summary of shielding performance of the aligned porous shielding materials in terms of that SE divided by thickness (t) as a function of density. B) Schematic representation of possible mechanism of EMI shielding in $Ti_3C_2T_x$ hybrid aerogel. Reproduced with permission.[140b] Copyright 2019, American Chemical Society.

suspensions results in high levels of performance.[2,50a,e,f] As an example, MWCNT-based scaffolds loaded with recombinant human bone morphogenetic protein 2 (rhBMP-2) and implanted in subcutaneous pockets in mice promoted effective ectopic bone formation.[50a] The high electrical conductivity of porous CNT structures facilitates a homogeneous mineralization by a "flow-through" electrodeposition process, and such scaffolds were also able to enhance osteoblast terminal differentiation.[47] In general, it is found that freeze cast scaffolds exhibiting pores sizes with similar dimensions to cells, and lower surface roughness, exhibit improved cytocompatibility.

Biocompatible polymers represent another domain of implantable biomaterials that benefit from freeze-casting techniques in their synthesis as functional 3D scaffolds.[15a,97a,100c,101] These materials have an important role to play in tissue engineering, in particular due to their excellent biocompatibility and biodegradability. The ability of freeze-casting techniques to produced well- controlled pore structures and interconnected microchannels here too enables the mimicry of extracellular matrices and thus enhance the capturing of cells and growth of tissue.[15a] A notable example in recent years in the freeze casting of chitosan for the fabrication of stents and drug delivery devices.[14]

5.7. Bioinspired Smart Materials

Living systems from all taxonomic kingdoms, are characterized by their remarkable ability to change position, rotate, elongate contract and otherwise move, or recover their shape following deformation. Movement and shape recovery in natural systems is facilitated by the presence of multiscale cellular, and/or fibrous structures such as those found in plant stems and muscle tissue.

In freeze cast materials, whether aerogels, hydrogels, or composites formed from infiltrated scaffolds, a cellular structure is formed, and in an analogous manner to biological systems can be used to facilitate versatile deformation, movement, and shape recovery behavior. As was examined in preceding sections, synthetic cellular structures akin to wood cork or other natural systems can be used to impart extensive elastic deformation and energy dissipation behavior. Nacre mimetic ice templated structures further give rise to high toughness. With careful control of the cellular structures formed by freeze-casting, the regular compartmentalized systems thus formed can be of use in the development of so called smart materials. This term here is used to refer to novel materials exhibiting controllable properties such as shape recovery, or shape memory, as well as controllable deformation.

The ordered aligned pore structures formed in freeze-casting processing are conducive to the rapid and repeatable recovery of macroscopic geometry over multiple deformation cycles.[60b,97b,144] In a recent study, it was shown an aligned porous chitosan scaffold could be compressed and folded randomly, and was restored to its original shape quickly by immersion in water. To develop this further, different functional nanoscale building blocks were integrated with chitosan scaffolds through a simple dip adsorption process. Importantly, the obtained macroscale assemblies still retain their shape-memory property and do not undergo structural collapse when they are subjected to cyclic compressional deformation.

Due to their robust mechanical properties and high electrical conductivity, 3D aligned porous graphene scaffolds are attractive alternatives for the fabrication of nacre-mimetic composites with shape memory,[60b,144a] self-healing,[45a] self-monitoring[42a,116b,144a] capabilities. For example, shape memory polymer–graphene composites can be deformed by bending twisting and folding and upon heating will recover to their original shapes. Moreover, electrical conductivity of freeze cast graphene networks can also be used to monitor the integrity of ceramic–graphene composites.[42a]

Recent work identified self-healing and shape programmability in nacre-mimetic composites obtained by infiltrating a thermally switchable Diels–Alder polymer into a bidirectional freeze-casted lamellar alumina scaffold. In addition to its capability of healing internal damage, the macroscopic shape of this smart nacre could be programmed permanently via plasticity and temporarily by a shape memory effect.[21]

6. Summary and Outlook

In naturally occurring porous and heterogeneous materials, an interplay of structural features at multiple scales can serve to impart high level of performance in diverse scenarios. Reproducing the functional structures that arise in nature is an effective pathway toward improved engineering materials. Over the past three decades, freeze-casting has emerged as an important and versatile processing approach toward high-performance materials in diverse fields of application. This approach is particularly effective toward the fabrication of biomimetic structures, which are often characterized by cellular structures and aligned pores. The use of solvent solidification to template suspended particles represents a distinct synthesis methodology, conferring effective transport properties and mechanical behavior that often mimic the high levels of functionality encountered in evolved biological systems.

Recent developments in the field of freeze casting notably include the use of novel low dimensional building blocks, in various combinations with additives and often in conjunction with controlled freezing methods that incorporate external fields to further direct the ice templating process. In particular, the use of carbon nanostructures and biopolymers to form functional freeze cast scaffolds represents a highly active realm of research with significance across an expanding range of applications ranging from battery electrodes to bone implants. As synthesis methods for low dimensional structures and other novel building blocks continue to develop, the range of freeze cast systems will further expand. It is envisaged that the ongoing uptake of freeze-casting methodologies to create bioinspired structures in the context of industrial materials processing will enable improved economic utilization of natural resources and waste materials as higher levels of functionality are extracted from naturally abundant constituents by their assembly across multiple scales.

Acknowledgements

This work was supported by The Startup Foundation for Introducing Talent of NUIST. Jiangsu Collaborative Innovation Center for Advanced Inorganic Function Composites.

Conflict of Interest

The authors declare no conflict of interest.

Keywords

composites, freeze casting, graphene, ice templating, porous materials

Received: November 1, 2019
Revised: December 30, 2019
Published online:

[1] a) H. Zhang, I. Hussain, M. Brust, M. F. Butler, S. P. Rannard, A. I. Cooper, *Nat. Mater.* **2005**, *4*, 787; b) S. Deville, E. Saiz, R. K. Nalla, A. P. Tomsia, *Science* **2006**, *311*, 515.

[2] M. C. Gutiérrez, Z. Y. García-Carvajal, M. J. Hortigüela, L. Yuste, F. Rojo, M. L. Ferrer, F. del Monte, *J. Mater. Chem.* **2007**, *17*, 2992.

[3] a) S. Deville, *Adv. Eng. Mater.* **2008**, *10*, 155; b) M. C. Gutiérrez, M. L. Ferrer, F. del Monte, *Chem. Mater.* **2008**, *20*, 634; c) U. G. K. Wegst, M. Schecter, A. E. Donius, P. M. Hunger, *Philos. Trans. R. Soc., A* **2010**, *368*, 2099; d) W. L. Li, K. Lu, J. Y. Walz, *Int. Mater. Rev.* **2012**, *57*, 37; e) Q. F. Cheng, C. J. Huang, A. P. Tomsia, *Adv. Mater.* **2017**, *29*, 1703155; f) K. L. Scotti, D. C. Dunand, *Prog. Mater. Sci.* **2018**, *94*, 243; g) S. Deville, *Freezing Colloids: Observations, Principles, Control, and Use: Applications in Materials Science, Life Science, Earth Science, Food Science, and Engineering*, Springer, Cham **2017**; h) H. Zhang, *Ice Templating and Freeze-Drying for Porous Materials and Their Applications*, Wiley, Weinheim, Germany **2018**.

[4] a) U. G. K. Wegst, H. Bai, E. Saiz, A. P. Tomsia, R. O. Ritchie, *Nat. Mater.* **2015**, *14*, 23; b) H. Zhang, A. I. Cooper, *Adv. Mater.* **2007**, *19*, 1529.

[5] a) I. Nelson, S. E. Naleway, *J. Mater. Res. Technol.* **2019**, *8*, 2372; b) S. Deville, *Scr. Mater.* **2018**, *147*, 119.

[6] T. Waschkies, R. Oberacker, M. J. Hoffmann, *Acta Mater.* **2011**, *59*, 5135.

[7] a) A. M. Anderson, M. G. Worster, *J. Fluid Mech.* **2014**, *758*, 786; b) B. Saint-Michel, M. Georgelin, S. Deville, A. Pocheau, *Langmuir* **2017**, *33*, 5617; c) J. You, Z. Wang, M. Grae Worster, *Acta Mater.* **2018**, *157*, 288; d) B. Saint-Michel, M. Georgelin, S. Deville, A. Pocheau, *Phys. Rev. E* **2019**, *99*, 052601.

[8] a) M. C. Gutiérrez, M. J. Hortigüela, J. M. Amarilla, R. Jiménez, M. L. Ferrer, F. del Monte, *J. Phys. Chem. C* **2007**, *111*, 5557; b) C. Ferraro, E. Garcia-Tuñon, V. G. Rocha, S. Barg, M. D. Fariñas, T. E. G. Alvarez-Arenas, G. Sernicola, F. Giuliani, E. Saiz, *Adv. Funct. Mater.* **2016**, *26*, 1636; c) F. Qian, P. C. Lan, M. C. Freyman, W. Chen, T. Y. Kou, T. Y. Olson, C. Zhu, M. A. Worsley, E. B. Duoss, C. M. Spadaccini, T. Baumann, T. Y. J. Han, *Nano Lett.* **2017**, *17*, 7171; d) Y. Hu, H. Zhuo, Q. Luo, Y. Wu, R. Wen, Z. Chen, L. Liu, L. Zhong, X. Peng, R. Sun, *J. Mater. Chem. A* **2019**, *7*, 10273; e) H. E. Romeo, C. E. Hoppe, M. A. López-Quintela, R. J. J. Williams, Y. Minaberry, M. Jobbágy, *J. Mater. Chem.* **2012**, *22*, 9195; f) S. Barg, F. M. Perez, N. Ni, P. do Vale Pereira, R. C. Maher, E. Garcia-Tuñon, S. Eslava, S. Agnoli, C. Mattevi, E. Saiz, *Nat. Commun.* **2014**, *5*, 4328; g) M. Yang, N. Zhao, Y. Cui, W. Gao, Q. Zhao, C. Gao, H. Bai, T. Xie, *ACS Nano* **2017**, *11*, 6817.

[9] a) A. Knöller, T. Runčevski, R. E. Dinnebier, J. Bill, Z. Burghard, *Sci. Rep.* **2017**, *7*, 42951; b) Z.-Z. Pan, H. Nishihara, S. Iwamura, T. Sekiguchi, A. Sato, A. Isogai, F. Kang, T. Kyotani, Q.-H. Yang, *ACS Nano* **2016**, *10*, 10689; c) M. Han, X. Yin, K. Hantanasirisakul, X. Li, A. Iqbal, C. B. Hatter, B. Anasori, C. M. Koo, T. Torita, Y. Soda, L. Zhang, L. Cheng, Y. Gogotsi, *Adv. Opt. Mater.* **2019**, *7*, 1900267.

[10] a) S. Deville, C. Viazzi, C. Guizard, *Langmuir* **2012**, *28*, 14892; b) S. Wu, L. Li, H. Xue, K. Liu, Q. Fan, G. Bai, J. Wang, *ACS Nano* **2017**, *11*, 9898; c) P. Zhang, J. Li, L. Lv, Y. Zhao, L. Qu, *ACS Nano* **2017**, *11*, 5087; d) S. Wu, C. Zhu, Z. He, H. Xue, Q. Fan, Y. Song, J. S. Francisco, X. C. Zeng, J. Wang, *Nat. Commun.* **2017**, *8*, 15154.

[11] A. Bahrami, U. Simon, N. Soltani, S. Zavareh, J. Schmidt, M. I. Pech-Canul, A. Gurlo, *Green Chem.* **2017**, *19*, 188.

[12] a) H. Bai, Y. Chen, B. Delattre, A. P. Tomsia, R. O. Ritchie, *Sci. Adv.* **2015**, *1*, 1500849; b) J. Han, G. Du, W. Gao, H. Bai, *Adv. Funct. Mater.* **2019**, *29*, 1900412.

[13] P. Niksiar, F. Y. Su, M. B. Frank, T. A. Ogden, S. E. Naleway, M. A. Meyers, J. McKittrick, M. M. Porter, *Ceramics* **2019**, *2*, 208.

[14] K. Yin, P. Divakar, U. G. K. Wegst, *Acta Biomater.* **2019**, *84*, 231.

[15] a) L. Fan, J.-L. Li, Z. Cai, X. Wang, *ACS Nano* **2018**, *12*, 5780; b) C. Wang, X. Chen, B. Wang, M. Huang, B. Wang, Y. Jiang, R. S. Ruoff, *ACS Nano* **2018**, *12*, 5816.

[16] F. Y. Su, J. R. Mok, J. McKittrick, *Ceramics* **2019**, *2*, 161.

[17] F. Bouville, E. Maire, S. Meille, B. Van de Moortèle, A. J. Stevenson, S. Deville, *Nat. Mater.* **2014**, *13*, 508.

[18] a) H.-D. Jung, S.-W. Yook, T.-S. Jang, Y. Li, H.-E. Kim, Y.-H. Koh, *Mater. Sci. Eng., C* **2013**, *33*, 59; b) L.-K. Yang, P. Shen, R.-F. Guo, Y.-L. Li, Q.-C. Jiang, *Scr. Mater.* **2019**, *167*, 101.

[19] Y. Tang, K. L. Yeo, Y. Chen, L. W. Yap, W. Xiong, W. Cheng, *J. Mater. Chem. A* **2013**, *1*, 6723.

[20] L. Lewis, S. G. Hatzikiriakos, W. Y. Hamad, M. J. MacLachlan, *ACS Macro Lett.* **2019**, *8*, 486.

[21] G. Du, A. Mao, J. Yu, J. Hou, N. Zhao, J. Han, Q. Zhao, W. Gao, T. Xie, H. Bai, *Nat. Commun.* **2019**, *10*, 800.

[22] H.-L. Gao, Y.-B. Zhu, L.-B. Mao, F.-C. Wang, X.-S. Luo, Y.-Y. Liu, Y. Lu, Z. Pan, J. Ge, W. Shen, Y.-R. Zheng, L. Xu, L.-J. Wang, W.-H. Xu, H.-A. Wu, S.-H. Yu, *Nat. Commun.* **2016**, *7*, 12920.

[23] W. Xu, Y. Xing, J. Liu, H. Wu, Y. Cui, D. Li, D. Guo, C. Li, A. Liu, H. Bai, *ACS Nano* **2019**, *13*, 7930.

[24] a) I. Nelson, T. A. Ogden, S. Al Khateeb, J. Graser, T. D. Sparks, J. J. Abbott, S. E. Naleway, *Adv. Eng. Mater.* **2019**, *21*, 1801092; b) M. M. Porter, P. Niksiar, J. McKittrick, *J. Am. Ceram. Soc.* **2016**, *99*, 1917; c) M. M. Porter, M. Yeh, J. Strawson, T. Goehring, S. Lujan, P. Siripasopsotorn, M. A. Meyers, J. McKittrick, *Mater. Sci. Eng., A* **2012**, *556*, 741; d) G. Gorgolis, C. Galiotis, *2D Mater.* **2017**, *4*, 032001; e) I. Nelson, L. Gardner, K. Carlson, S. E. Naleway, *Acta Mater.* **2019**, *173*, 106.

[25] a) Y. Tang, S. Qiu, Q. Miao, C. Wu, *J. Eur. Ceram. Soc.* **2016**, *36*, 1233; b) Y. Zhang, L. Hu, J. Han, *J. Am. Ceram. Soc.* **2009**, *92*, 1874; c) Y. F. Tang, K. Zhao, J. Q. Wei, Y. S. Qin, *J. Eur. Ceram. Soc.* **2010**, *30*, 1963.

[26] T. A. Ogden, M. Prisbrey, I. Nelson, B. Raeymaekers, S. E. Naleway, *Mater. Des.* **2019**, *164*, 107561.

[27] a) R. Obmann, S. Schörpf, C. Gorsche, R. Liska, T. Fey, T. Konegger, *J. Eur. Ceram. Soc.* **2019**, *39*, 838; b) M. Barrow, H. Zhang, *Soft Matter* **2013**, *9*, 2723.

[28] a) D. Chen, Y. Zhang, C. Ni, C. Ma, J. Yin, H. Bai, Y. Luo, F. Huang, T. Xie, Q. Zhao, *Mater. Horiz.* **2019**, *6*, 1013; b) W. F. Schroeder, R. J. J. Williams, C. E. Hoppe, H. E. Romeo, *J. Mater. Sci.* **2017**, *52*, 13669; c) N. M. Cativa, M. S. Alvarez Cerimedo, J. Puig, G. F. Arenas, F. Trabadelo, M. A. Ayude, M. A. Zensich, G. M. Morales, W. F. Schroeder, H. E. Romeo, C. E. Hoppe, *Mol. Syst. Des. Eng.* **2019**, *4*, 133.

[29] a) A. Ouyang, J. Liang, *RSC Adv.* **2014**, *4*, 25835; b) A. Ouyang, Q. Gong, J. Liang, *Adv. Eng. Mater.* **2015**, *17*, 460; c) A. Ouyang, C. H. Wang, S. T. Wu, E. Z. Shi, W. Q. Zhao, A. Y. Cao, D. H. Wu, *ACS Appl. Mater. Interfaces* **2015**, *7*, 14439; d) J. Wang, Q. Gong, D. Zhuang, J. Liang, *RSC Adv.* **2015**, *5*, 16870; e) S. C. Liao, T. L. Zhai, H. S. Xia, *J. Mater. Chem. A* **2016**, *4*, 1068; f) A. Ouyang, A. Y. Cao, S. Hu, Y. H. Li, R. Q. Xu, J. Q. Wei, H. W. Zhu, D. H. Wu, *ACS Appl. Mater. Interfaces* **2016**, *8*, 11179; g) R. M. Yu, Y. Z. Shi,

D. Z. Yang, Y. X. Liu, J. Qu, Z. Z. Yu, *ACS Appl. Mater. Interfaces* **2017**, *9*, 21809; h) X. Wang, W. Kong, W. Xie, L. Li, Y. Liu, X. Wu, J. Gao, *Chem. Eng. J.* **2012**, *197*, 509; i) Y. Yao, Y. Li, X. Zeng, N. Sun, R. Sun, J.-B. Xu, C.-P. Wong, *J. Mater. Chem. A* **2018**, *6*, 5984.

[30] a) Z. Xu, Y. Zhang, P. Li, C. Gao, *ACS Nano* **2012**, *6*, 7103; b) Y. Cui, H. Gong, Y. Wang, D. Li, H. Bai, *Adv. Mater.* **2018**, *30*, 1706807.

[31] X. Li, H. Wang, Q. Xu, S. Guo, J. Du, X. Liu, J. Weng, J. Xu, *Adv. Mater. Interfaces* **2018**, *5*, 1800256.

[32] a) Y. Shao, M. F. El-Kady, C. W. Lin, G. Zhu, K. L. Marsh, J. Y. Hwang, Q. Zhang, Y. Li, H. Wang, R. B. Kaner, *Adv. Mater.* **2016**, *28*, 6719; b) P. Xue, S. Liu, X. Shi, C. Sun, C. Lai, Y. Zhou, D. Sui, Y. Chen, J. Liang, *Adv. Mater.* **2018**, *30*, 1804165.

[33] L. Zhang, S. Ma, Y. Chen, Y. Wang, J. Ou, H. Uyama, M. Ye, *Anal. Chem.* **2019**, *91*, 2985.

[34] Q. Wang, X. Wang, F. Wan, K. Chen, Z. Niu, J. Chen, *Small* **2018**, *14*, 1800280.

[35] J. T. McCann, M. Marquez, Y. Xia, *J. Am. Chem. Soc.* **2006**, *128*, 1436.

[36] a) Y. Chen, J. Bunch, T. Li, Z. Mao, F. Chen, *J. Power Sources* **2012**, *213*, 93; b) Y. Chen, Y. Zhang, J. Baker, P. Majumdar, Z. Yang, M. Han, F. Chen, *ACS Appl. Mater. Interfaces* **2014**, *6*, 5130; c) Y. Hwa, E. Yi, H. Shen, Y. Sung, J. Kou, K. Chen, D. Y. Parkinson, M. M. Doeff, E. J. Cairns, *Nano Lett.* **2019**, *19*, 4731.

[37] a) Q. Zhang, F. Zhang, S. P. Medarametla, H. Li, C. Zhou, D. Lin, *Small* **2016**, *12*, 1702; b) P. Yan, E. Brown, Q. Su, J. Li, J. Wang, C. Xu, C. Zhou, D. Lin, *Small* **2017**, *13*, 1701756; c) V. C.-F. Li, C. K. Dunn, Z. Zhang, Y. Deng, H. J. Qi, *Sci. Rep.* **2017**, *7*, 8018; d) X. Song, H. Tetik, T. Jirakittsonthon, P. Parandoush, G. Yang, D. Lee, S. Ryu, S. Lei, M. L. Weiss, D. Lin, *Adv. Eng. Mater.* **2019**, *21*, 1800678; e) Y. Lin, F. Liu, G. Casano, R. Bhavsar, I. A. Kinloch, B. Derby, *Adv. Mater.* **2016**, *28*, 7993.

[38] Z. He, K. Liu, J. Wang, *Acc. Chem. Res.* **2018**, *51*, 1082.

[39] H. Geng, X. Liu, G. Shi, G. Bai, J. Ma, J. Chen, Z. Wu, Y. Song, H. Fang, J. Wang, *Angew. Chem., Int. Ed.* **2017**, *56*, 997.

[40] T. M. Fears, J. A. Hammons, J. D. Sain, M. H. Nielsen, T. Braun, S. O. Kucheyev, *APL Mater.* **2018**, *6*, 091103.

[41] Y. Si, X. Wang, L. Dou, J. Yu, B. Ding, *Sci. Adv.* **2018**, *4*, aas8925.

[42] a) O. T. Picot, V. G. Rocha, C. Ferraro, N. Ni, E. D'Elia, S. Meille, J. Chevalier, T. Saunders, T. Peijs, M. J. Reece, E. Saiz, *Nat. Commun.* **2017**, *8*, 14425; b) L. Qiu, B. Huang, Z. He, Y. Wang, Z. Tian, J. Z. Liu, K. Wang, J. Song, T. R. Gengenbach, D. Li, *Adv. Mater.* **2017**, *29*, 201701553; c) X.-H. Li, P. Liu, X. Li, F. An, P. Min, K.-N. Liao, Z.-Z. Yu, *Carbon* **2018**, *140*, 624.

[43] a) Y. Si, X. Wang, C. Yan, L. Yang, J. Yu, B. Ding, *Adv. Mater.* **2016**, *28*, 9512; b) C. Li, Z. Y. Wu, H. W. Liang, J. F. Chen, S. H. Yu, *Small* **2017**, *13*, 1700453; c) Z. Zeng, C. Wang, Y. Zhang, P. Wang, S. I. Seyed Shahabadi, Y. Pei, M. Chen, X. Lu, *ACS Appl. Mater. Interfaces* **2018**, *10*, 8205; d) Z. Zeng, Y. Zhang, X. Y. D. Ma, S. I. S. Shahabadi, B. Che, P. Wang, X. Lu, *Carbon* **2018**, *140*, 227; e) Z. Zeng, X. Y. D. Ma, Y. Zhang, Z. Wang, B. F. Ng, M. P. Wan, X. Lu, *ACS Sustainable Chem. Eng.* **2019**, *7*, 6959.

[44] a) Z. Y. Wang, X. Shen, N. M. Han, X. Liu, Y. Wu, W. J. Ye, J. K. Kim, *Chem. Mater.* **2016**, *28*, 6731; b) Y. Yao, J. Sun, X. Zeng, R. Sun, J.-B. Xu, C.-P. Wong, *Small* **2018**, *14*, 1704044; c) A. Wat, J. I. Lee, C. W. Ryu, B. Gludovatz, J. Kim, A. P. Tomsia, T. Ishikawa, J. Schmitz, A. Meyer, M. Alfreider, D. Kiener, E. S. Park, R. O. Ritchie, *Nat. Commun.* **2019**, *10*, 961.

[45] a) E. D'Elia, S. Barg, N. Ni, V. G. Rocha, E. Saiz, *Adv. Mater.* **2015**, *27*, 4788; b) H. Bai, F. Walsh, B. Gludovatz, B. Delattre, C. Huang, Y. Chen, A. P. Tomsia, R. O. Ritchie, *Adv. Mater.* **2016**, *28*, 50; c) E. Munch, M. E. Launey, D. H. Alsem, E. Saiz, A. P. Tomsia, R. O. Ritchie, *Science* **2008**, *322*, 1516.

[46] P. Gannon, S. Sofie, M. Deibert, R. Smith, V. Gorokhovsky, *J. Appl. Electrochem.* **2009**, *39*, 497.

[47] S. Nardecchia, M. C. Serrano, M. C. Gutiérrez, M. T. Portolés, M. L. Ferrer, F. del Monte, *Adv. Funct. Mater.* **2012**, *22*, 4411.

[48] M. Klotz, M. Weber, S. Deville, D. Oison, I. Iatsunskyi, E. Coy, M. Bechelany, *Front. Mater.* **2018**, *5*, 28.

[49] Z. Li, Z. Liu, H. Sun, C. Gao, *Chem. Rev.* **2015**, *115*, 7046.

[50] a) A. Abarrategi, M. C. Gutiérrez, C. Moreno-Vicente, M. J. Hortigüela, V. Ramos, J. L. López-Lacomba, M. L. Ferrer, F. del Monte, *Biomaterials* **2008**, *29*, 94; b) M. J. Hortigüela, M. C. Gutiérrez, I. Aranaz, M. Jobbágy, A. Abarrategi, C. Moreno-Vicente, A. Civantos, V. Ramos, J. L. López-Lacomba, M. L. Ferrer, F. del Monte, *J. Mater. Chem.* **2008**, *18*, 5933; c) K. Katuri, M. L. Ferrer, M. C. Gutiérrez, R. Jiménez, F. del Monte, D. Leech, *Energy Environ. Sci.* **2011**, *4*, 4201; d) A. Fonseca-García, J. D. Mota-Morales, I. A. Quintero-Ortega, Z. Y. García-Carvajal, V. Martínez-López, E. Ruvalcaba, C. Landa-Solís, L. Solis, C. Ibarra, M. C. Gutiérrez, M. Terrones, I. C. Sanchez, F. Monte, M. C. Velasquillo, G. Luna-Bárcenas, *J. Biomed. Mater. Res., Part A* **2014**, *102*, 3341; e) M. C. Serrano, S. Nardecchia, C. García-Rama, M. L. Ferrer, J. E. Collazos-Castro, F. del Monte, M. C. Gutiérrez, *Biomaterials* **2014**, *35*, 1543; f) S. Nardecchia, M. C. Serrano, M. C. Gutiérrez, M. L. Ferrer, F. d. Monte, *J. Mater. Chem. B* **2013**, *1*, 3064.

[51] S.-M. Kwon, H.-S. Kim, H.-J. Jin, *Polymer* **2009**, *50*, 2786.

[52] J. Zhong, J. Meng, X. Gui, T. Hu, N. Xie, X. Lu, Z. Yang, N. Koratkar, *Carbon* **2014**, *77*, 637.

[53] Z.-Z. Pan, W. Lv, Y.-B. He, Y. Zhao, G. Zhou, L. Dong, S. Niu, C. Zhang, R. Lyu, C. Wang, H. Shi, W. Zhang, F. Kang, H. Nishihara, Q.-H. Yang, *Adv. Sci.* **2018**, *5*, 1800384.

[54] a) C. Cheng, S. Li, A. Thomas, N. A. Kotov, R. Haag, *Chem. Rev.* **2017**, *117*, 1826; b) J. Mao, J. Iocozzia, J. Huang, K. Meng, Y. Lai, Z. Lin, *Energy Environ. Sci.* **2018**, *11*, 772; c) B. Qiu, M. Xing, J. Zhang, *Chem. Soc. Rev.* **2018**, *47*, 2165.

[55] a) C. Zhu, T. Y.-J. Han, E. B. Duoss, A. M. Golobic, J. D. Kuntz, C. M. Spadaccini, M. A. Worsley, *Nat. Commun.* **2015**, *6*, 6962; b) F. Guo, Y. Jiang, Z. Xu, Y. Xiao, B. Fang, Y. Liu, W. Gao, P. Zhao, H. Wang, C. Gao, *Nat. Commun.* **2018**, *9*, 881; c) Y. Q. Jiang, Z. Xu, T. Q. Huang, Y. J. Liu, F. Guo, J. B. Xi, W. W. Gao, C. Gao, *Adv. Funct. Mater.* **2018**, *28*, 1707024; d) S. D. Lacey, D. J. Kirsch, Y. Li, J. T. Morgenstern, B. C. Zarket, Y. Yao, J. Dai, L. Q. Garcia, B. Liu, T. Gao, S. Xu, S. R. Raghavan, J. W. Connell, Y. Lin, L. Hu, *Adv. Mater.* **2018**, *30*, 1705651; e) Z. Qi, J. Ye, W. Chen, J. Biener, E. B. Duoss, C. M. Spadaccini, M. A. Worsley, C. Zhu, *Adv. Mater. Technol.* **2018**, *3*, 1800053; f) X. Tang, H. Zhou, Z. Cai, D. Cheng, P. He, P. Xie, D. Zhang, T. Fan, *ACS Nano* **2018**, *12*, 3502; g) Q. Zhang, F. Zhang, X. Xu, C. Zhou, D. Lin, *ACS Nano* **2018**, *12*, 1096.

[56] R. M. Hensleigh, H. Cui, J. S. Oakdale, J. C. Ye, P. G. Campbell, E. B. Duoss, C. M. Spadaccini, X. Zheng, M. A. Worsley, *Mater. Horiz.* **2018**, *5*, 1035.

[57] V. J. L., P. A. J., M. Stephen, *Adv. Mater.* **2009**, *21*, 2180.

[58] L. Qiu, J. Z. Liu, S. L. Y. Chang, Y. Wu, D. Li, *Nat. Commun.* **2012**, *3*, 1241.

[59] M. Peng, Z. Wen, L. Xie, J. Cheng, Z. Jia, D. Shi, H. Zeng, B. Zhao, Z. Liang, T. Li, L. Jiang, *Adv. Mater.* **2019**, *31*, 1902930.

[60] a) J. Kim, N. M. Han, J. Kim, J. Lee, J.-K. Kim, S. Jeon, *ACS Appl. Mater. Interfaces* **2018**, *10*, 37507; b) C. Huang, J. Peng, Y. Cheng, Q. Zhao, Y. Du, S. Dou, A. P. Tomsia, H. D. Wagner, L. Jiang, Q. Cheng, *J. Mater. Chem. A* **2019**, *7*, 2787; c) H. Y. Mi, X. Jing, A. L. Politowicz, E. Chen, H. X. Huang, L. S. Turng, *Carbon* **2018**, *132*, 199.

[61] a) Z. He, J. Liu, Y. Qiao, C. M. Li, T. T. Y. Tan, *Nano Lett.* **2012**, *12*, 4738; b) M. C. Serrano, J. Patino, C. Garcia-Rama, M. L. Ferrer, J. L. G. Fierro, A. Tamayo, J. E. Collazos-Castro, F. del Monte, M. C. Gutierrez, *J. Mater. Chem. B* **2014**, *2*, 5698; c) S. Han, X. Wang, Y. Huang, Y. Tang, Y. Ai, J. Jiang, D. Wu, *RSC Adv.* **2015**, *5*, 98399; d) Y. Huang, D. Wu, J. Jiang, Y. Mai, F. Zhang, H. Pan,

X. Feng, *Nano Energy* **2015**, *12*, 287; e) Q. Peng, Y. Qin, X. Zhao, X. Sun, Q. Chen, F. Xu, Z. Lin, Y. Yuan, Y. Li, J. Li, W. Yin, C. Gao, F. Zhang, X. He, Y. Li, *ACS Appl. Mater. Interfaces* **2017**, *9*, 44010.

[62] a) L. Estevez, A. Kelarakis, Q. Gong, E. H. Da'as, E. P. Giannelis, *J. Am. Chem. Soc.* **2011**, *133*, 6122; b) X. Mi, G. Huang, W. Xie, W. Wang, Y. Liu, J. Gao, *Carbon* **2012**, *50*, 4856; c) X. Xie, Y. Zhou, H. Bi, K. Yin, S. Wan, L. Sun, *Sci. Rep.* **2013**, *3*, 2117; d) B. Wicklein, A. Kocjan, G. Salazar-Alvarez, F. Carosio, G. Camino, M. Antonietti, L. Bergström, *Nat. Nanotechnol.* **2015**, *10*, 277; e) N. Ni, S. Barg, E. Garcia-Tunon, F. M. Perez, M. Miranda, C. Lu, C. Mattevi, E. Saiz, *Sci. Rep.* **2015**, *5*, 13712; f) G. Lian, C. C. Tuan, L. Y. Li, S. L. Jiao, Q. L. Wang, K. S. Moon, D. L. Cui, C. P. Wong, *Chem. Mater.* **2016**, *28*, 6096; g) W. W. Gao, N. F. Zhao, W. Q. Yao, Z. Xu, H. Bai, C. Gao, *RSC Adv.* **2017**, *7*, 33600; h) Z. Y. Wang, N. M. Han, Y. Wu, X. Liu, X. Shen, Q. B. Zheng, J. K. Kim, *Carbon* **2017**, *123*, 385; i) Y. Jiang, Y. Chen, Y. J. Liu, G. X. Sui, *Chem. Eng. J.* **2018**, *337*, 522; j) J. Yang, L.-S. Tang, L. Bai, R.-Y. Bao, Z. Liu, B.-H. Xie, M.-B. Yang, W. Yang, *ACS Sustainable Chem. Eng.* **2018**, *6*, 6761; k) P. Min, J. Liu, X. Li, F. An, P. Liu, Y. Shen, N. Koratkar, Z.-Z. Yu, *Adv. Funct. Mater.* **2018**, *28*, 1805365; l) S. Long, Y. Feng, F. He, S. He, H. Hong, X. Yang, L. Zheng, J. Liu, L. Gan, M. Long, *Carbon* **2020**, *158*, 137.

[63] N. Zhao, M. Yang, Q. Zhao, W. Gao, T. Xie, H. Bai, *ACS Nano* **2017**, *11*, 4777.

[64] a) B. Yao, J. Chen, L. Huang, Q. Zhou, G. Shi, *Adv. Mater.* **2016**, *28*, 1623; b) Z. Xu, C. Gao, *Nat. Commun.* **2011**, *2*, 571.

[65] a) P. K. Sahoo, B. Panigrahy, D. Thakur, D. Bahadur, *New J. Chem.* **2017**, *41*, 7861; b) P. K. Sahoo, N. Kumar, S. Thiyagarajan, D. Thakur, H. S. Panda, *ACS Sustainable Chem. Eng.* **2018**, *6*, 7475; c) S. Zhang, J. Sun, D. Hu, C. Xiao, Q. Zhuo, J. Wang, C. Qin, L. Dai, *J. Mater. Chem. A* **2018**, *6*, 16139.

[66] X. Peng, K. Wu, Y. Hu, H. Zhuo, Z. Chen, S. Jing, Q. Liu, C. Liu, L. Zhong, *J. Mater. Chem. A* **2018**, *6*, 23550.

[67] a) J. L. Xiao, W. Y. Lv, Y. H. Song, Q. Zheng, *Chem. Eng. J.* **2018**, *338*, 202; b) M. Wang, C. Shao, S. Zhou, J. Yang, F. Xu, *Cellulose* **2018**, *25*, 7329.

[68] S. Zhao, H.-B. Zhang, J.-Q. Luo, Q.-W. Wang, B. Xu, S. Hong, Z.-Z. Yu, *ACS Nano* **2018**, *12*, 11193.

[69] Z. Zhao, M. Sun, W. Chen, Y. Liu, L. Zhang, N. Dongfang, Y. Ruan, J. Zhang, P. Wang, L. Dong, Y. Xia, H. Lu, *Adv. Funct. Mater.* **2019**, *29*, 1809196.

[70] X. L. Zeng, L. Ye, S. H. Yu, R. Sun, J. B. Xu, C. P. Wong, *Chem. Mater.* **2015**, *27*, 5849.

[71] A. Knöller, S. Kilper, A. M. Diem, M. Widenmeyer, T. Runčevski, R. E. Dinnebier, J. Bill, Z. Burghard, *Nano Lett.* **2018**, *18*, 2519.

[72] H.-L. Gao, L. Xu, F. Long, Z. Pan, Y.-X. Du, Y. Lu, J. Ge, S.-H. Yu, *Angew. Chem., Int. Ed.* **2014**, *53*, 4561.

[73] P. Song, H. Qin, H.-L. Gao, H.-P. Cong, S.-H. Yu, *Nat. Commun.* **2018**, *9*, 2786.

[74] A. Du, H. Wang, B. Zhou, C. Zhang, X. Wu, Y. Ge, T. Niu, X. Ji, T. Zhang, Z. Zhang, G. Wu, J. Shen, *Chem. Mater.* **2018**, *30*, 6849.

[75] G. Zu, J. Shen, L. Zou, W. Wang, Y. Lian, Z. Zhang, A. Du, *Chem. Mater.* **2013**, *25*, 4757.

[76] L. Su, H. Wang, M. Niu, X. Fan, M. Ma, Z. Shi, S.-W. Guo, *ACS Nano* **2018**, *12*, 3103.

[77] X. Xu, Q. Zhang, M. Hao, Y. Hu, Z. Lin, L. Peng, T. Wang, X. Ren, C. Wang, Z. Zhao, C. Wan, H. Fei, L. Wang, J. Zhu, H. Sun, W. Chen, T. Du, B. Deng, G. J. Cheng, I. Shakir, C. Dames, T. S. Fisher, X. Zhang, H. Li, Y. Huang, X. Duan, *Science* **2019**, *363*, 723.

[78] M. Niederberger, *Adv. Funct. Mater.* **2017**, *27*, 1703647.

[79] Y. Si, L. Wang, X. Wang, N. Tang, J. Yu, B. Ding, *Adv. Mater.* **2017**, *29*, 1700339.

[80] a) X. Zeng, Y. Yao, Z. Gong, F. Wang, R. Sun, J. Xu, C.-P. Wong, *Small* **2015**, *11*, 6205; b) J. Hu, Y. Huang, Y. Yao, G. Pan, J. Sun, X. Zeng, R. Sun, J.-B. Xu, B. Song, C.-P. Wong, *ACS Appl. Mater. Interfaces* **2017**, *9*, 13544; c) X. Hou, Y. Chen, L. Lv, W. Dai, S. Zhao, Z. Wang, L. Fu, C.-T. Lin, N. Jiang, J. Yu, *ACS Appl. Nano Mater.* **2019**, *2*, 360; d) M. A. Kashfipour, R. S. Dent, N. Mehra, X. Yang, J. Gu, J. Zhu, *Compos. Sci. Technol.* **2019**, *182*, 107715.

[81] a) R. Bian, G. He, W. Zhi, S. Xiang, T. Wang, D. Cai, *J. Mater. Chem. C* **2019**, *7*, 474; b) X. Li, X. Yin, H. Xu, M. Han, M. Li, S. Liang, L. Cheng, L. Zhang, *ACS Appl. Mater. Interfaces* **2018**, *10*, 34524.

[82] L. Zhang, X. Liu, A. Deb, G. Feng, *ACS Sustainable Chem. Eng.* **2019**, *7*, 19910.

[83] a) Y. Tang, S. Gong, Y. Chen, L. W. Yap, W. Cheng, *ACS Nano* **2014**, *8*, 5707; b) S. M. Jung, D. J. Preston, H. Y. Jung, Z. Deng, E. N. Wang, J. Kong, *Adv. Mater.* **2016**, *28*, 1413.

[84] F. Qian, A. Troksa, T. M. Fears, M. H. Nielsen, A. J. Nelson, T. F. Baumann, S. O. Kucheyev, T. Y.-J. Han, M. Bagge-Hansen, *Nano Lett.* **2020**, *20*, 131.

[85] M. Li, L. Zong, W. Yang, X. Li, J. You, X. Wu, Z. Li, C. Li, *Adv. Funct. Mater.* **2019**, *29*, 1901798.

[86] B.-H. Yoon, E.-J. Lee, H.-E. Kim, Y.-H. Koh, *J. Am. Ceram. Soc.* **2007**, *90*, 1753.

[87] J.-W. Kim, K. Taki, S. Nagamine, M. Ohshima, *Langmuir* **2009**, *25*, 5304.

[88] M. Barrow, A. Eltmimi, A. Ahmed, P. Myers, H. Zhang, *J. Mater. Chem.* **2012**, *22*, 11615.

[89] X. Wu, Y. Liu, X. Li, P. Wen, Y. Zhang, Y. Long, X. Wang, Y. Guo, F. Xing, J. Gao, *Acta Biomater.* **2010**, *6*, 1167.

[90] J. Lee, Y. Deng, *Soft Matter* **2011**, *7*, 6034.

[91] M. J. Hortigüela, I. Aranaz, M. C. Gutiérrez, M. L. Ferrer, F. del Monte, *Biomacromolecules* **2011**, *12*, 179.

[92] X. Wang, F. Schmidt, A. Gurlo, *J. Eur. Ceram. Soc.* **2020**, *40*, 315.

[93] Z.-L. Yu, N. Yang, L.-C. Zhou, Z.-Y. Ma, Y.-B. Zhu, Y.-Y. Lu, B. Qin, W.-Y. Xing, T. Ma, S.-C. Li, H.-L. Gao, H.-A. Wu, S.-H. Yu, *Sci. Adv.* **2018**, *4*, aat7223.

[94] a) M. Naviroj, S. M. Miller, P. Colombo, K. T. Faber, *J. Eur. Ceram. Soc.* **2015**, *35*, 2225; b) H. Zhang, P. D'Angelo Nunes, M. Wilhelm, K. Rezwan, *J. Eur. Ceram. Soc.* **2016**, *36*, 51; c) M. Naviroj, P. W. Voorhees, K. T. Faber, *J. Mater. Res.* **2017**, *32*, 3372; d) M. Naviroj, M. M. Wang, M. T. Johnson, K. T. Faber, *Scr. Mater.* **2017**, *130*, 32; e) N. Soltani, U. Simon, A. Bahrami, X. Wang, S. Selve, J. D. Epping, M. I. Pech-Canul, M. F. Bekheet, A. Gurlo, *J. Eur. Ceram. Soc.* **2017**, *37*, 4809; f) H. Zhang, C. L. Fidelis, M. Wilhelm, Z. Xie, K. Rezwan, *Mater. Des.* **2017**, *134*, 207; g) D. Schumacher, M. Wilhelm, K. Rezwan, *Mater. Des.* **2018**, *160*, 1295.

[95] G. Mikl, R. Obmann, S. Schörpf, R. Liska, T. Konegger, *Adv. Eng. Mater.* **2019**, *21*, 1900052.

[96] a) R. Dash, Y. Li, A. J. Ragauskas, *Carbohydr. Polym.* **2012**, *88*, 789; b) T. Köhnke, A. Lin, T. Elder, H. Theliander, A. J. Ragauskas, *Green Chem.* **2012**, *14*, 1864; c) P. Munier, K. Gordeyeva, L. Bergström, A. B. Fall, *Biomacromolecules* **2016**, *17*, 1875; d) X. Zhang, H. Wang, Z. Cai, N. Yan, M. Liu, Y. Yu, *ACS Sustainable Chem. Eng.* **2019**, *7*, 332; e) Y. Chen, D. Fan, S. Lyu, G. Li, F. Jiang, S. Wang, *ACS Sustainable Chem. Eng.* **2019**, *7*, 1381; f) X. Zhang, M. Liu, H. Wang, N. Yan, Z. Cai, Y. Yu, *Carbohydr. Polym.* **2019**, *208*, 232; g) T. Nissilä, S. S. Karhula, S. Saarakkala, K. Oksman, *Compos. Sci. Technol.* **2018**, *155*, 64; h) S. Gupta, F. Martoïa, L. Orgéas, P. J. J. Dumont, *Appl. Sci.* **2018**, *8*, 2463; i) M. Chau, K. J. De France, B. Kopera, V. R. Machado, S. Rosenfeldt, L. Reyes, K. J. W. Chan, S. Förster, E. D. Cranston, T. Hoare, E. Kumacheva, *Chem. Mater.* **2016**, *28*, 3406; j) C. Wang, Z.-Z. Pan, W. Lv, B. Liu, J. Wei, X. Lv, Y. Luo, H. Nishihara, Q.-H. Yang, *Small* **2019**, *15*, 1805363; k) Y. Cao, L. Lewis, W. Y. Hamad, M. J. MacLachlan, *Adv. Mater.* **2019**, *31*, 1808186.

[97] a) N. L. Francis, P. M. Hunger, A. E. Donius, B. W. Riblett, A. Zavaliangos, U. G. K. Wegst, M. A. Wheatley, *J. Biomed. Mater. Res., Part A* **2013**, *101*, 3493; b) H.-L. Gao, Y. Lu, L.-B. Mao, D. An, L. Xu, J.-T. Gu, F. Long, S.-H. Yu, *Mater. Horiz.* **2014**, *1*, 69; c) D. Wang, F. Romer, L. Connell, C. Walter, E. Saiz, S. Yue, P. D. Lee, D. S. McPhail, J. V. Hanna, J. R. Jones, *J. Mater. Chem. B* **2015**, *3*, 7560; d) Y. H. Wang, M. Wakisaka, *Carbohydr. Polym.* **2015**, *122*, 18; e) M. Nieto-Suárez, M. A. López-Quintela, M. Lazzari, *Carbohydr. Polym.* **2016**, *141*, 175.

[98] a) F. Deuber, S. Mousavi, M. Hofer, C. Adlhart, *ChemistrySelect* **2016**, *1*, 5595; b) F. Deuber, S. Mousavi, L. Federer, C. Adlhart, *Adv. Mater. Interfaces* **2017**, *4*, 1700065; c) F. Deuber, S. Mousavi, L. Federer, M. Hofer, C. Adlhart, *ACS Appl. Mater. Interfaces* **2018**, *10*, 9069.

[99] Y. Zhou, S. Fu, Y. Pu, S. Pan, A. J. Ragauskas, *Carbohydr. Polym.* **2014**, *112*, 277.

[100] a) P. Divakar, K. Yin, U. G. K. Wegst, *J. Mech. Behav. Biomed. Mater.* **2019**, *90*, 350; b) L. Mohee, G. S. Offeddu, A. Husmann, M. L. Oyen, R. E. Cameron, *Acta Biomater.* **2019**, *83*, 189; c) C. Rieu, C. Parisi, G. Mosser, B. Haye, T. Coradin, F. M. Fernandes, L. Trichet, *ACS Appl. Mater. Interfaces* **2019**, *11*, 14672.

[101] G. Nyström, W.-K. Fong, R. Mezzenga, *Biomacromolecules* **2017**, *18*, 2858.

[102] a) M. C. T. Asuncion, J. C.-H. Goh, S.-L. Toh, *Mater. Sci. Eng., C* **2016**, *67*, 646; b) B. B. Mandal, E. S. Gil, B. Panilaitis, D. L. Kaplan, *Macromol. Biosci.* **2013**, *13*, 48.

[103] a) S. Aliramaji, A. Zamanian, M. Mozafari, *Mater. Sci. Eng., C* **2017**, *70*, 736; b) K. Gao, Y. Guo, Q. Niu, L. Han, L. Zhang, Y. Zhang, L. Wang, *Cellulose* **2018**, *25*, 429; c) J. Q. Han, Y. Y. Yue, Q. L. Wu, C. B. Huang, H. Pan, X. X. Zhan, C. T. Mei, X. W. Xu, *Cellulose* **2017**, *24*, 4433; d) J. Yang, Y. F. Xia, P. Xu, B. B. Chen, *Cellulose* **2018**, *25*, 3533; e) A. E. Donius, A. Liu, L. A. Berglund, U. G. K. Wegst, *J. Mech. Behav. Biomed. Mater.* **2014**, *37*, 88; f) J. Li, J. Li, H. Meng, S. Xie, B. Zhang, L. Li, H. Ma, J. Zhang, M. Yu, *J. Mater. Chem. A* **2014**, *2*, 2934; g) N. L. Francis, P. M. Hunger, A. E. Donius, U. G. K. Wegst, M. A. Wheatley, *J. Tissue Eng. Regener. Med.* **2017**, *11*, 285.

[104] C. Li, Y.-W. Ding, B.-C. Hu, Z.-Y. Wu, H.-L. Gao, H.-W. Liang, J.-F. Chen, S.-H. Yu, *Adv. Mater.* **2020**, *32*, 1904331;

[105] H. Maleki, M. A. Shahbazi, S. Montes, S. H. Hosseini, M. R. Eskandari, S. Zaunschirm, T. Verwanger, S. Mathur, B. Milow, B. Krammer, N. Husing, *ACS Appl. Mater. Interfaces* **2019**, *11*, 17256.

[106] Z. Xu, C. Gao, *Mater. Today* **2015**, *18*, 480.

[107] a) T. Huang, M. S. Mason, G. E. Hilmas, M. C. Leu, *Virtual Phys. Prototyping* **2006**, *1*, 93; b) T. S. Huang, M. N. Rahaman, N. D. Doiphode, M. C. Leu, B. S. Bal, D. E. Day, X. Liu, *Mater. Sci. Eng., C* **2011**, *31*, 1482; c) N. D. Doiphode, T. Huang, M. C. Leu, M. N. Rahaman, D. E. Day, *J. Mater. Sci.: Mater. Med.* **2011**, *22*, 515.

[108] a) Y.-W. Moon, K.-H. Shin, Y.-H. Koh, S.-W. Yook, C.-M. Han, H.-E. Kim, *J. Am. Ceram. Soc.* **2012**, *95*, 1803; b) Y.-W. Moon, K.-H. Shin, Y.-H. Koh, H.-D. Jung, H.-E. Kim, *J. Am. Ceram. Soc.* **2014**, *97*, 32; c) Y.-W. Moon, I.-J. Choi, Y.-H. Koh, H.-E. Kim, *J. Eur. Ceram. Soc.* **2015**, *35*, 4623; d) I.-J. Choi, Y.-W. Moon, Y.-H. Koh, H.-E. Kim, *J. Am. Ceram. Soc.* **2016**, *99*, 395.

[109] D. Kam, M. Chasnitsky, C. Nowogrodski, I. Braslavsky, T. Abitbol, S. Magdassi, O. Shoseyov, *Colloids Interfaces* **2019**, *3*, 46.

[110] a) E. García-Tuñon, S. Barg, J. Franco, R. Bell, S. Eslava, E. D'Elia, R. C. Maher, F. Guitian, E. Saiz, *Adv. Mater.* **2015**, *27*, 1688; b) J. Sha, Y. Li, R. Villegas Salvatierra, T. Wang, P. Dong, Y. Ji, S.-K. Lee, C. Zhang, J. Zhang, R. H. Smith, P. M. Ajayan, J. Lou, N. Zhao, J. M. Tour, *ACS Nano* **2017**, *11*, 6860.

[111] a) J.-B. Lee, W.-Y. Maeng, Y.-H. Koh, H.-E. Kim, *Ceram. Int.* **2019**, *45*, 21321; b) J.-W. Kim, J.-B. Lee, Y.-H. Koh, H.-E. Kim, *Materials* **2019**, *12*, 2893; c) Y.-H. Lee, J.-B. Lee, W.-Y. Maeng, Y.-H. Koh, H.-E. Kim, *J. Eur. Ceram. Soc.* **2019**, *39*, 4358.

[112] a) L.-B. Mao, H.-L. Gao, H.-B. Yao, L. Liu, H. Cölfen, G. Liu, S.-M. Chen, S.-K. Li, Y.-X. Yan, Y.-Y. Liu, S.-H. Yu, *Science* **2016**, *354*, 107; b) H. W. Zhao, Y. H. Yue, L. Guo, J. T. Wu, Y. W. Zhang, X. D. Li, S. C. Mao, X. D. Han, *Adv. Mater.* **2016**, *28*, 5099; c) Y. M. Yao, X. D. Zhu, X. L. Zeng, R. Sun, J. B. Xu, C. P. Wong, *ACS Appl. Mater. Interfaces* **2018**, *10*, 9669; d) M. T. Abba, P. M. Hunger, S. R. Kalidindi, U. G. K. Wegst, *J. Mech. Behav. Biomed. Mater.* **2016**, *55*, 140.

[113] a) J. I. Lee, A. Wat, J. Kim, C. W. Ryu, H. J. Chang, E. S. Park, R. O. Ritchie, *Scr. Mater.* **2019**, *172*, 159; b) M. J. Garnier, D. C. Dunand, *Mater. Sci. Eng., A* **2019**, *743*, 190.

[114] Z. Zeng, M. Chen, Y. Pei, S. I. Seyed Shahabadi, B. Che, P. Wang, X. Lu, *ACS Appl. Mater. Interfaces* **2017**, *9*, 32211.

[115] T. Zhai, Q. Zheng, Z. Cai, L.-S. Turng, H. Xia, S. Gong, *ACS Appl. Mater. Interfaces* **2015**, *7*, 7436.

[116] a) L. Qiu, D. Liu, Y. Wang, C. Cheng, K. Zhou, J. Ding, V.-T. Truong, D. Li, *Adv. Mater.* **2014**, *26*, 3333; b) J. Peng, C. Huang, C. Cao, E. Saiz, Y. Du, S. Dou, A. P. Tomsia, H. D. Wagner, L. Jiang, Q. Cheng, *Matter* **2020**, *2*, 220.

[117] C. Huang, J. Peng, S. Wan, Y. Du, S. Dou, H. D. Wagner, A. P. Tomsia, L. Jiang, Q. Cheng, *Angew. Chem., Int. Ed.* **2019**, *58*, 7636.

[118] a) S. Pimenta, P. Robinson, *Compos. Sci. Technol.* **2014**, *104*, 111; b) J. Henry, S. Pimenta, *J. Mech. Phys. Solids* **2018**, *118*, 322.

[119] X.-H. Li, X. Li, K.-N. Liao, P. Min, T. Liu, A. Dasari, Z.-Z. Yu, *ACS Appl. Mater. Interfaces* **2016**, *8*, 33230.

[120] S. J. Yeo, M. J. Oh, P. J. Yoo, *Adv. Mater.* **2019**, *31*, 1803670.

[121] a) R. Amin, B. Delattre, A. P. Tomsia, Y.-M. Chiang, *ACS Appl. Energy Mater.* **2018**, *1*, 4976; b) W. K. Jung, C. Baek, J.-H. Kim, S. Moon, D. S. Kim, Y. H. Jung, D. K. Kim, *Mater. Des.* **2018**, *139*, 89; c) C. Huang, M. Dontigny, K. Zaghib, P. S. Grant, *J. Mater. Chem. A* **2019**, *7*, 21421; d) Y. Yu, H. Zhang, X. Yang, J. Gou, X. Tong, X. Li, H. Zhang, *Energy Storage Mater.* **2019**, *19*, 88; e) X. Zhang, Z. Ju, L. M. Housel, L. Wang, Y. Zhu, G. Singh, N. Sadique, K. J. Takeuchi, E. S. Takeuchi, A. C. Marschilok, G. Yu, *Nano Lett.* **2019**, *19*, 8255.

[122] Y.-C. Yin, Z.-L. Yu, Z.-Y. Ma, S.-H. Yu, H.-B. Yao, F. Zhou, T. Ma, T.-W. Zhang, Y.-Y. Lu, *Natl. Sci. Rev.* **2019**, *6*, 247.

[123] a) H. Zhai, P. Xu, M. Ning, Q. Cheng, J. Mandal, Y. Yang, *Nano Lett.* **2017**, *17*, 3182; b) W. Tang, S. Tang, X. Guan, X. Zhang, Q. Xiang, J. Luo, *Adv. Funct. Mater.* **2019**, *29*, 1900648; c) X. Wang, H. Zhai, B. Qie, Q. Cheng, A. Li, J. Borovilas, B. Xu, C. Shi, T. Jin, X. Liao, Y. Li, X. He, S. Du, Y. Fu, M. Dontigny, K. Zaghib, Y. Yang, *Nano Energy* **2019**, *60*, 205; d) X. Yang, Q. Sun, C. Zhao, X. Gao, K. R. Adair, Y. Liu, J. Luo, X. Lin, J. Liang, H. Huang, L. Zhang, R. Yang, S. Lu, R. Li, X. Sun, *Nano Energy* **2019**, *61*, 567.

[124] S. Zavareh, A. Hilger, K. Hirselandt, O. Goerke, I. Manke, J. Banhart, A. Gurlo, *J. Ceram. Soc. Jpn.* **2016**, *124*, 1067.

[125] D. Cao, Q. Zhang, A. M. Hafez, Y. Jiao, Y. Ma, H. Li, Z. Cheng, C. Niu, H. Zhu, *Small Methods* **2019**, *3*, 1800539.

[126] J. Kong, G. Xiong, Z. Bo, X. Lu, K. Yi, W. Kuang, S. Yang, H. Yang, S. Tian, J. Yan, K. Cen, *ChemElectroChem* **2019**, *6*, 2788.

[127] a) N. Yousefi, X. Lu, M. Elimelech, N. Tufenkji, *Nat. Nanotechnol.* **2019**, *14*, 107; b) K. C. Lai, L. Y. Lee, B. Y. Z. Hiew, S. Thangalazhy-Gopakumar, S. Gan, *J. Environ. Sci.* **2019**, *79*, 174.

[128] a) T. Liu, M. Huang, X. Li, C. Wang, C.-X. Gui, Z.-Z. Yu, *Carbon* **2016**, *100*, 456; b) R. J. Zhang, R. R. Hu, X. M. Li, Z. Zhen, Z. H. Xu, N. Li, L. M. He, H. W. Zhu, *Adv. Funct. Mater.* **2018**, *28*, 1705879.

[129] Q. Zhang, G. Yi, Z. Fu, H. Yu, S. Chen, X. Quan, *ACS Nano* **2019**, *13*, 13196.

[130] a) X. Wu, G. Shao, X. Shen, S. Cui, X. Chen, *Chem. Eng. J.* **2017**, *330*, 1022; b) X. Wu, G. Shao, S. Cui, L. Wang, X. Shen, *Ceram. Int.*

2016, *42*, 874; c) X. Wu, G. Shao, S. Liu, X. Shen, S. Cui, X. Chen, *Powder Technol.* **2017**, *312*, 1; d) Y. Kong, X. Shen, S. Cui, M. Fan, *Ceram. Int.* **2014**, *40*, 8265.

[131] a) Y. Gan, F. Hernandez, D. Hanaor, R. Annabattula, M. Kamlah, P. Pereslavtsev, *Fusion Sci. Technol.* **2014**, *66*, 83; b) W. Dai, S. Pupeschi, D. Hanaor, Y. Gan, *Fusion Eng. Des.* **2017**, *118*, 45; c) W. Dai, D. Hanaor, Y. Gan, *Int. J. Therm. Sci.* **2019**, *142*, 266.

[132] Y. Qin, Q. Peng, Y. Zhu, X. Zhao, Z. Lin, X. He, Y. Li, *Nanoscale Adv.* **2019**, *1*, 4895.

[133] C. Xie, L. He, Y. Shi, Z.-X. Guo, T. Qiu, X. Tuo, *ACS Nano* **2019**, *13*, 7811.

[134] X. Wang, P. Wu, *ACS Appl. Mater. Interfaces* **2019**, *11*, 28943.

[135] Z. Bo, H. Zhu, C. Ying, H. Yang, S. Wu, J. Kong, S. Yang, X. Wei, J. Yan, K. Cen, *Nanoscale* **2019**, *11*, 21249.

[136] X. Hou, Y. Chen, W. Dai, Z. Wang, H. Li, C.-T. Lin, K. Nishimura, N. Jiang, J. Yu, *Chem. Eng. J.* **2019**, *375*, 121921.

[137] a) J. Yang, L.-S. Tang, R.-Y. Bao, L. Bai, Z.-Y. Liu, W. Yang, B.-H. Xie, M.-B. Yang, *J. Mater. Chem. A* **2016**, *4*, 18841; b) F. An, X. Li, P. Min, H. Li, Z. Dai, Z.-Z. Yu, *Carbon* **2018**, *126*, 119; c) D. An, S. Cheng, Z. Zhang, C. Jiang, H. Fang, J. Li, Y. Liu, C.-P. Wong, *Carbon* **2019**, *155*, 258.

[138] a) J. Kuang, L. Liu, Y. Gao, D. Zhou, Z. Chen, B. Han, Z. Zhang, *Nanoscale* **2013**, *5*, 12171; b) C. Li, M. Ding, B. Zhang, X. Qiao, C.-Y. Liu, *Nanoscale* **2018**, *10*, 18291; c) W. Huang, K. Dai, Y. Zhai, H. Liu, P. Zhan, J. Gao, G. Zheng, C. Liu, C. Shen, *ACS Appl. Mater. Interfaces* **2017**, *9*, 42266.

[139] Z. Zeng, S. I. Seyed Shahabadi, B. Che, Y. Zhang, C. Zhao, X. Lu, *Nanoscale* **2017**, *9*, 17396.

[140] a) Y. Jiang, X. Xie, Y. Chen, Y. Liu, R. Yang, G. Sui, *J. Mater. Chem. C* **2018**, *6*, 8679; b) P. Sambyal, A. Iqbal, J. Hong, H. Kim, M.-K. Kim, S. M. Hong, M. Han, Y. Gogotsi, C. M. Koo, *ACS Appl. Mater. Interfaces* **2019**, *11*, 38046.

[141] Z. Zeng, H. Jin, M. Chen, W. Li, L. Zhou, Z. Zhang, *Adv. Funct. Mater.* **2016**, *26*, 303.

[142] L. H. Wang, Y. Y. Qiu, H. J. Lv, Y. Si, L. F. Liu, Q. Zhang, J. P. Cao, J. Y. Yu, X. R. Li, B. Ding, *Adv. Funct. Mater.* **2019**, *29*, 1901407.

[143] a) L. M. Henning, S. Zavareh, P. H. Kamm, M. Höner, H. Fischer, J. Banhart, F. Schmidt, A. Gurlo, *Adv. Eng. Mater.* **2017**, *19*, 1700129; b) S. Deville, E. Saiz, A. P. Tomsia, *Biomaterials* **2006**, *27*, 5480.

[144] a) E. D'Elia, H. S. Ahmed, E. Feilden, E. Saiz, *Appl. Mater. Today* **2019**, *15*, 185; b) S. Kang, T.-H. Kang, B. S. Kim, J. Oh, S. Park, I. S. Choi, J. Lee, J. G. Son, *Composites, Part B* **2019**, *162*, 580; c) C. Li, L. Qiu, B. Zhang, D. Li, C.-Y. Liu, *Adv. Mater.* **2016**, *28*, 1510.